Technical Report

TR-11-03

Corrosion studies with high burnup light water reactor fuel

Release of nuclides into simulated groundwater during accumulated contact time of up to two years

Hans-Urs Zwicky, Zwicky Consulting GmbH

Jeanett Low, Ella Ekeroth, Studsvik Nuclear AB

March 2011

Svensk Kärnbränslehantering AB
Swedish Nuclear Fuel
and Waste Management Co

Box 250, SE-101 24 Stockholm
Phone +46 8 459 84 00

ISSN 1404-0344
SKB TR-11-03

Corrosion studies with high burnup light water reactor fuel

Release of nuclides into simulated groundwater during accumulated contact time of up to two years

Hans-Urs Zwicky, Zwicky Consulting GmbH

Jeanett Low, Ella Ekeroth, Studsvik Nuclear AB

March 2011

Summary

In the framework of comprehensive research work supporting the development of a Swedish concept for the disposal of highly radioactive waste and spent fuel, Studsvik has performed a significant number of spent fuel corrosion studies under a variety of different conditions. These experiments, performed between 1990 and 2002, covered a burnup range from 27 to 49 MWd/kgU, which was typical for fuel to be disposed at that time. As part of this work, the so called Series 11 tests were performed under oxidising conditions in synthetic groundwater with fuel samples from a rod irradiated in the Ringhals 1 Boiling Water Reactor (BWR). In the meantime, Swedish utilities tend to increase the discharge burnup of fuel operated in their reactors. This means that knowledge of spent fuel corrosion performance has to be extended to higher burnup as well. Therefore, a series of experiments has been started at Studsvik, aiming at extending the data base acquired in the Series 11 corrosion tests to higher burnup fuel.

Fuel burnup leads to complex and significant changes in the composition and properties of the fuel. The transformed microstructure, which is referred to as the high burnup structure or rim structure in the outer region of the fuel, consists of small grains of submicron size and a high concentration of pores of typical diameter 1 to 2 μm. This structure forms in UO_2 fuel at a local burnup above 50 MWd/kgU, as long as the temperature is below 1,000–1,100°C. The high burnup at the pellet periphery is the consequence of plutonium build-up by neutron capture in ^{238}U followed by fission of the formed plutonium. The amount of fission products in the fuel increases more or less linearly with burnup, in contrast to alpha emitting actinides that increase above average. As burnup across a spent fuel pellet is not uniform, but increases towards the periphery, the radiation field is also larger at the pellet surface. At the same time, it is easier for water to access the pellet surface than the bulk of the pellet in leaching experiments. Thus, formation of oxidising species and radicals by radiolysis is expected to be disproportionately high as well. Therefore, when discussing high burnup fuel dissolution, the effect of the increased radiation field with burnup, as well as of the influence of the smaller grain size and increased porosity at the rim are mentioned as factors which contribute to increased dissolution rates. A third factor, increased fission product and actinide doping with burnup, has been discussed extensively in connection with increased resistance to air oxidation of the fuel.

Samples from four different fuel rods, all operated in Pressurised Water Reactors (PWR), are used in the new series of corrosion experiments. They cover a burnup range from 58 to 75 MWd/kgU. The nuclide inventory of all four samples was determined by means of a combination of experimental nuclide analysis and sample specific modelling calculations. More than 40 different nuclides were analysed by isotope dilution analysis using Inductively Coupled Plasma Mass Spectrometry (ICP-MS), as well as other ICP-MS and gamma spectrometric methods. The content of roughly all fission products and actinides was also calculated separately for each sample.

The experiments are performed under oxidising conditions in synthetic groundwater at ambient temperature. In order to make results as comparable as possible to those of the Series 11 experiments, the same procedure and the same leachant is used. At least nine consecutive contact periods of one and three weeks and two, three, six and twelve months are planned. The present report covers the first five contact periods up to a cumulative contact time of one year for all four samples and in addition the sixth period up to a cumulative contact time of two years for two of the samples. The samples, kept in position by a platinum wire spiral, are exposed to synthetic groundwater in a Pyrex flask. After the contact period, water samples are taken for different analyses and for pH and carbonate determination. The fuel sample is placed in a new flask with fresh synthetic groundwater for the next contact period.

Release fractions are calculated by dividing the total amount of a nuclide of concern in the analysed solution by the total amount in the corroded fuel sample. Cumulative release fractions are the sum of release fractions up to a certain cumulative contact time. Release rates are calculated by dividing release fractions by the length of the contact period of concern.

Caesium and rubidium were released to a significantly larger extent in the high burnup samples, compared to the Series 11 experiments. This is probably more a consequence of different operating conditions than of burnup. Under PWR conditions, the temperature of the fuel is higher, which causes a higher portion of mobile fission products to diffuse to grain boundaries, to pellet-pellet interfaces and to the pellet cladding gap, from where they are more readily released than nuclides retained in the fuel matrix.

A marked opposite effect is observed for molybdenum and technetium. These elements are part of the group of elements that form alloy particles or the so called ε-phase. Formation of these particles is influenced by the inventory that increases with burnup and by the temperature of the fuel. Lower release is observed in high burnup PWR fuel samples, compared to Series 11 results.

Based on apparent uranium release, it can be concluded that the stabilising effect of the increased content of dopant nuclides, i.e. fission product and actinide atoms in the UO_2 matrix of the spent fuel, more than compensates the potentially adverse effects of radiolysis and of smaller grains and higher porosity. The $^{236}U/^{235}U$ ratio in the leachant indicates that uranium is not preferentially released from the peripheral part of the pellets.

Some potential differences in corrosion performance of the different fuel types might not just be a function of burnup, but caused by differences in fuel fabrication and, even more important, in fuel operation. Nevertheless, it can be concluded that corrosion performance of high burnup PWR fuel under oxidising conditions is well comparable to the performance of BWR fuel with lower burnup.

Sammanfattning

Inom ramen för det omfattande forskningsarbetet, till stöd för utvecklingen av det svenska slutförvarskonceptet av radioaktivt avfall och bestrålat kärnbränsle, har Studsvik utfört ett stort antal bränslelakningsstudier under olika förhållanden. I de experiment som utfördes mellan 1990 och 2002 användes bränsle med en utbränning mellan 27 till 49 MWd/kgU. Detta var ett typiskt utbränningsspann för slutförvaret vid den tidsperioden. En del av den lakningsstudien kallas serie 11 och experimenten utfördes under oxiderande förhållanden i syntetiskt grundvatten med bränsleprover från en bestrålad bränsletav från BWR-reaktorn Ringhals 1. Sedan dess har de svenska kärnkraftsproducenterna ökat utbränningen hos kärnbränslet, det innebär att kunskapen för lakning av bränsle med högre utbränning måste fördjupas. En ny experimentserie har startats på Studsvik där försök med bränsle med högre utbränning skall utöka databasen från lakningsförsöken i serie 11.

Den högre utbränningen leder till komplexa och signifikanta förändringar i sammansättning och egenskaper hos bränslet. Den perifera delen av bränslet får en förändrad mikrostruktur, den kallas högutbränningsstruktur eller rimeffekt och består av korn mindre än 1 μm och har en hög koncenation av porer som är en till två mikrometer i diameter. Denna struktur bildas i UO_2-bränslet vid en lokal utbränning större än 50 MWd/kgU och så länge som temperaturen är lägre än 1 000–1 100°C. Den höga utbränningen i kutsens perifera område är en konsekvens av uppbyggnaden av plutonium genom neutroninfångning av ^{238}U följt av fission av det bildade plutoniumet. Mängden fissionsprodukter i bränslet ökar i princip linjärt med utbränningen, däremot ökar mängden alfastrålande nuklider mer än proportionellt. Kutsens utbränning sett över ett tvärsitt är inte konstant, den ökar mot periferin, strålfältet är också högre vid ytan. Det också är en större tillgänglighet för laklösningen att nå kutsytan än bränslebulken vid lakningsexperiment. Dessutom förväntas produktionen av oxiderande ämnen och radikaler genom radiolys av vatten vara hög. Effekten av ökande strålfält med ökande utbränning liksom inverkan av en mindre kornstorlek och ökad porositet i randzonen är faktorer som kan bidra till ökande upplösningshastigheter av högutbränt bränsle. En tredje faktor, att fissionsprodukterna och aktiniddopingen som ökar med utbränningen gett ett ökat oxidationsmotstånd av bränsle i luft, har diskuterats mycket.

Bränsleprover från fyra olika bränslestavar, där samtliga har varit i drift i tryckvattenreaktorer (PWR), har använts i en ny serie lakningsexperiment. Proverna omfattar ett utbränningsspann från 58 till 75 MWd/kgU. Nuklidinventariet hos de fyra proverna har bestämts genom en kombination av experimentella nuklidanalyser och provspecifika modelleringsberäkningar. Fler än 40 olika nuklider har analyserats genom isotoputspädningsmetodik genom att använda Induktiv Kopplat Plasma Mass Spektrometri (ICP-MS) liksom andra ICP-MS och gammaspektrometriska metoder. Innehållet av i princip alla fissionsprodukter och aktinider har beräknats separat för varje bränsleprov.

Experimenten är utförda under oxiderande miljö i syntetiskt grundvatten vid rumstemperatur. Laknigsförfarande och laklösningssammansättning är desamma som för serie 11 för att få så jämförbara resultat som möjligt. Minst nio konsekutiva kontakperioder uppgående till en och tre veckor samt två, tre, sex och tolv månader är planerade. Denna rapport täcker de fösta fem kontaktperioderna till och med en kumulativ kontakttid på ett år för alla fyra proven och dessutom tillkommer en kumulativ kontakttid på två år för två av proven. Respektive bränsleprov hålls på plats med en platinatrådspiral och exponeras för syntetiskt grundvatten i en pyrexglaskolv. Efter en kontaktperiod tas laklösningsprover för nuklidanalys och för att bestämma pH och karbonathalt i lösningen. Bränsleprovet placeras i en ny glaskolv med färskt syntetiskt grundvatten för nästa kontaktperiod.

Utsläppsfraktionen beräknas genom att dividera det totala innehållet av en nuklid i den analyserade laklösningen med den totala mängden av nukliden i bränsleprovet som lakats. Den kumulativa utsläppsfraktionen är summan av utsläppsfraktionerna till och med en viss kumulativ kontaktperiod. Utsläppshastigheterna beräknas genom att dividera utsläppsfraktionen med längden på kontaktperioden som avses.

Cesium och rubidium lakades ut i betydligt större omfattning för bränsleprov med hög utbränning jämfört med serie 11 experimenten. Det är sannolikt en konsekvens av olika driftförhållanden snarare än en effekt av utbränning. Under PWR-förhållanden är temperaturen i bränslet högre vilket leder

till att en högre andel rörliga fissionsproduter kan diffundera till korngränser, kuts-kuts gränsytor och till gapet mellan kuts och kapsling där de är mer lättillgängliga för lakning än för nuklider som hålls kvar i bränslematrisen.

Motsatt effekt har observerats för molybden och teknetium vilket är utmärkande. Dessa ämnen är del av en grupp element som bildar metalliska partiklar, även kallade ε-partiklar. Bildandet av dessa partiklar påverkas av inventariet som ökar med utbränningen samt av temperaturen hos bränslet. Högutbrända PWR-bränsleprov visar att utsläppet av dessa element minskar med ökande utbränning jämfört med resultaten från serie 11.

Baserat på det uppmätta uranutsläppet, kan slutsatsen dras att den stabiliserande effekten av ett ökande innehåll av dopade nuklider, d.v.s. fissionsprodukter och aktinidatomer i UO_2 matrisen hos bestrålat bränsle, mer än kompenserar för de potentiellt ogynsamma effekterna av radiolys, mindre korn och högre porositet. $^{236}U/^{235}U$ förhållandet i laklösningen indikerar att uran inte företrädesvis lakas från den perifera delen av bränslekutsen.

Skillander i bränslelakningsbeteende mellan olika bränsletyper är inte bara en funktion av utbränning, utan också orsakade av skillnader i bränsletillverkning och inte minst skillander i driftförhållanden. Icke desto mindre kan slutsatsen dras att lakningsegenskaperna för högutbrända PWR-bränslen under oxiderande förhållanden är jämförbara med lakningsegenskaperna för BWR-bränslen med lägre utbrännng.

Contents

1 Introduction

The majority of Light Water Reactor (LWR) fuels are solid UO_2, enriched in ^{235}U (typically in the range 3 to 5%). In the reactor, ^{235}U is consumed ("burned") by nuclear fission and transformed into fission products. At the same time, higher actinides are produced through neutron capture and decay reactions. Thus, spent fuel is largely UO_2 with a small fraction of other actinides and fission products. The majority of these nuclides are dispersed or in solid solution in the UO_2 matrix /Kleykamp 1985/.

In order to evaluate the so-called source term for the safety assessment of deep geological repositories, it is important to characterise the dissolution behaviour of the spent fuel matrix and of important radionuclides. The rate of dissolution of spent fuel depends on a variety of factors such as the composition of the spent fuel itself and of the groundwater, as well as the redox conditions under which the dissolution takes place. Fuel radiation causes radiolysis of water and reactive species are formed of which H_2O_2 was shown to be of highest importance /Ekeroth et al. 2006/.

In the framework of comprehensive research work supporting the development of a Swedish concept for the disposal of highly radioactive waste and spent fuel, Studsvik has performed a significant number of spent fuel corrosion studies under a variety of different conditions. These experiments, performed between 1990 and 2002, covered a burnup range of 27 to 49 MWd/kgU, which was typical for fuel to be disposed at that time. Some of the results, amongst others those of the so called Series 11 tests performed under oxidising conditions in synthetic groundwater with BWR fuel samples from a rod irradiated in the Ringhals 1 Boiling Water Reactor (BWR), were documented in /Forsyth 1997/.

In the meantime, Swedish utilities tend to increase the discharge burnup of fuel operated in their reactors. This means that knowledge of spent fuel corrosion performance has to be extended to higher burnup as well. Therefore, a series of experiments has been started at Studsvik, aiming at extending the data base acquired in the Series 11 corrosion tests to higher burnup fuel.

Fuel burnup leads to complex and significant changes in the composition and properties of the fuel. The transformed microstructure, which is referred to as the high burnup structure (HBS) or rim structure in the outer region of the fuel, consists of small grains of submicron size and a high concentration of pores of typical diameter 1 to 2 μm. This structure forms in UO_2 fuel at a local burnup above 50 MWd/kgU, as long as the temperature is below 1,000–1,100°C. The high burnup at the pellet periphery is the consequence of plutonium build-up by neutron capture in ^{238}U followed by fission of the formed plutonium.

The chemical composition and microstructure of nuclear fuel have been studied extensively /Kleykamp 1985, 1988, Johnson and Shoesmith 1988/. Only a short summary is given below. Fission products which are stable in metallic form (Mo, Ru, Pd, Tc, Rh) tend to form metallic alloy particles, often referred to as 4d-alloy particles or ε-particles. Fission products which are stable as oxides but incompatible with the UO_2 matrix (Rb, Cs, Ba, Zr, Nb, Mo, Te, Sr) separate into precipitates sometimes referred to as grey phases. Elements that form stable oxides in solid solution with the UO_2 matrix include actinides (Np, Pu, Am, Cm), lanthanides (La, Ce, Pr, Nd, Pm, Sm, Eu, Gd) and Y as well as Sr, Zr, Ba, Te and Nb within the limits of their solubility in UO_2 and to the extent that they have not precipitated in perovskite-type oxides.

As mentioned above, the burnup across a spent fuel pellet is not uniform, but increases significantly towards the periphery. Consequently, the content of fission products and of minor actinides and thus the radiation field is also larger at the pellet surface. The difference in local burnup at the periphery and in the pellet centre increases disproportionately with burnup. Due to different thermal expansion coefficients, a gap is formed between the pellet and the cladding, when a fuel rod is cooled down from operating temperature. This cold gap allows for water to access the pellet surface easier than the bulk of the pellet in leaching experiments. Thus, formation of oxidising species and radicals by radiolysis is expected to be disproportionately high as well. Therefore, when discussing high burnup fuel dissolution, the effect of the increased radiation field with burnup, as well as of the influence of the smaller grain size and increased porosity at the rim are mentioned as factors which contribute to increased dissolution rates. A third factor, which is the increase of fission product and actinide doping in high burnup fuel, has been discussed extensively in connection with increased resistance to

air oxidation of the fuel /Einziger et al. 1992, Thomas et al. 1993, Hanson 1998, Cobos et al. 1998/, but only recently in connection with fuel dissolution /Hanson and Stout 2004, Hanson et al. 2004, Hanson 2005, 2008, He et al. 2007/.

In the Series 11 experiments mentioned above, the cumulative fractional release increased slightly, almost linearly, with burnup up to values of 40–45 MWd/kgU, but afterwards decreased. Therefore, a series of experiments has been started at Studsvik, aiming at extending the data base acquired in the series 11 corrosion tests to higher burnup fuel. Preliminary results of corrosion tests with high burnup Pressurised Water Reactor (PWR) fuel under oxidising conditions in synthetic groundwater for a cumulative contact time of 182 days have been published in /Ekeroth et al. 2009/. This report presents final data acquired up to a cumulative contact time of one year for two samples and two years for another two samples. The results are compared to corresponding Series 11 data.

2 Materials and methods

2.1 Fuel rod data

All fuel rods of concern were operated in Pressurised Water Reactors (PWR). This choice is, amongst others, also due to the fact that there is no BWR fuel of burnup higher than 50 MWd/kgU in Sweden. Pre-irradiation data and a summary of the operating history are compiled in Table 2-1.

Fuel rod 4I8-Q12/171-30027-34 was manufactured by ASEA Atom AB (later ABB Atom, now Westinghouse Electric Company Sweden AB). It was operated in position Q12 of fuel assembly 4I8 in the Ringhals 3 reactor for five annual cycles between 1989 and 1994 to a calculated average rod burnup of 52.2 MWd/kgU.

Rod 3V5-Q13 was fabricated by Siemens (now AREVA) and operated in position Q13 of assembly 3V5 in the Ringhals 3 reactor for five annual cycles between July 2000 and May 2005 to a calculated rod average burnup of 60 MWd/kgU.

Fuel rod SUT-00477 was manufactured by Framatome ANP (now AREVA) and operated in position E14 of fuel assembly 50T in the Ringhals 4 reactor for five annual cycles between September 1998 and end of July 2003 to a calculated rod average burnup of 62.8 MWd/kgU.

The fuel rod AM2-K12 was fabricated by Westinghouse and irradiated in the U.S. nuclear power plant North Anna within an experimental high burnup program. It had a somewhat untypical irradiation history. During three cycles, it was located in position K12 of assembly AM2, which started operation in July 1987 during Cycle 7 of North Anna 1. In March 1989, the assembly was unloaded for detailed inspections, before it was reinserted in March 1991 into North Anna 1 for Cycles 9 and 10 until September 1994. Finally, the rod was extracted from assembly AM2 and put into position E06 of assembly 3A4 for Cycle 14 of North Anna 2 (October 1999–March 2001). The rod reached a calculated average burnup of 70.2 MWd/kgU.

Approximate cycle-specific linear heat generating rates (LHGR) were estimated for the four sample locations on the basis of rated power and the power histories relative to rated power shown in Figure 2-1 to Figure 2-4. The results are compiled in Table 2-2. The length of the cycles for rod AM2-K12 was approximately 18 months, whereas the other three rods were operated on a twelve month cycle basis.

Krypton and xenon release to the free rod volume, relative to the produced amount calculated by ORIGEN, are compiled in Table 2-3, together with the isotopic composition of the released krypton and xenon. Fission gas release (FGR) in the three rods operated in Ringhals reactors seem to be correlated to the linear heat generating rate during the last two cycles of operation. In the last cycle, the LHGR was roughly the same, but in the second but last cycle, the highest rate is related to the highest fission gas release. Rod AM2-K12 was operated under different conditions, compared to the three Ringhals rods. In addition, high burnup effects have significantly contributed to higher FGR /Manzel and Walker 2000/.

Table 2-1. Fuel rod data.

Sample designation (Studsvik)	**4I8-Q12/ 171-30027-…**	**3V5-Q13:…**	**SUT3-00477:…**	**AM2-K12:…**
Leaching	**..–32**	**…:212**	**…:472**	**…:122**
Isotope inventory	**..–34**	**…:213**	**…:473**	**…:124**
Fabricated by	ASEA Atom	Siemens	Framatome	Westinghouse
Initial enrichment [wt% U-235]	3.6	3.8	3.7	4.0
External cladding diameter [mm]	9.5	9.55	9.49	9.5
Internal cladding diameter [mm]	8.36	8.33	8.36	8.357
Cladding wall thickness [mm]	0.57	0.61	0.56	0.572
Pellet diameter [mm]	(8.193)	8.165	8.19	8.192
Pellet length [mm]	10	9.8	12.97	9.83
Initial pellet density [g/cm^3]	10.50	10.45	10.45	10.44
Initial pellet/cladding diametral gap [mm]	0.167	0.165	0.17	0.165
Total fuel column length [mm]		3,658	3,657.6	3,657
Plenum length [mm]		169.8	180.9	174.2
Total rod length (nominal, BOB[1], incl. end plugs) [mm]	3,836.4	3,853		3,854.1
Total rod length (EOB[2], incl. end plugs) [mm]	3,855	3,870	3,867.1	3,885.4
Fill gas pressure [MPa]	2.5	2.52	2	1.9
Cladding material	ZIRLO™	Duplex-D4	M5™	ZIRLO™
Reactor	Ringhals 3	Ringhals 3	Ringhals 4	North Anna 1/2
Assembly/rod position	4I8/Q12	3V5/Q13	50T/E14	AM2/K12; 3A4/E06
Irradiation period	1989–1994-06-16	2000-07-12–2005-05-25	1998-09-13–2003-07-31	1987-07-01–2001-03-12
Core position (Cycle #/Position)	7/8B		16/3L	
	8/8L		17/9G	
	9/5K		18/10E	
	10/7R		19/7N	
	11/8H		20/8H	
Rod average BU (calculated) [MWd/kgU]	52.2	60.0	62.8	70.2
Isotope analysis sample position (from lower rod end) [mm]	2,963–2,969	1,039–1,044	3,275–3,289	970–975
Corrosion sample position (from lower rod end) [mm]	2,937–2,957	1,019–1,039	3,255–3,275	945–965
Local burnup (gammascan) [MWd/kgU]	57.9	65	62.7±3.0	78
Rod puncturing /Thanger A 2008, pers. comm./	94-12-13	06-02-02	03-11-27	02-08-07
Date of 1st cut /Thanger A 2008, pers. comm./	95-02-06	06-02-04	03-12-19	02-08-15
Date of sample cutting	07-11-30	07-03-14	08-01-04	07-03-16
Start date of leaching experiment	08-03-04	07-03-20	08-03-04	07-03-20

1 “beginning of bombardment”; pre-irradiation length.

2 “end of bombardment”; length after end of irradiation.

Table 2-2. Approximate average local linear heat generation rate.

Rod		**4I8-Q12**	**3V5-Q13**	**SUT3-00477**	**AM2-K12**
Rated power [W/gU]		38.9	38.8	38.4	39.5
Average LHGR [kW/m]		18.3	18.3	18.1	18.6
Approximate LHGR during cycle	#1	20.1	24.3	19.3	24.3
	#2	22.0	24.3	24.4	23.4
	#3	19.2	20.3	22.6	6.7
	#4	6.0	11.0	17.2	14.8
	#5	15.4	15.3	15.4	

Table 2-3. Release of fission gases relative to calculated produced amount, and isotopic composition of released krypton and xenon.

Rod		4I8-Q12	3V5-Q13	SUT3-00477	AM2-K12
Reference		/Jonsson and Källström 1995/	/Janzon Sjöstedt 2006/	/Zwicky 2004/	/Källström 2002/
Fission gas release [%]	Kr	0.94	2.6	2.3	5.04
	Xe	0.94	2.7	2.4	4.85
Isotopic composition of Kr [%]	^{80}Kr	0.013	0.003	0.001	0.016
	^{82}Kr	0.212	0.240	0.39	0.265
	^{83}Kr	9.192	8.277	8.31	7.41
	^{84}Kr	33.93	34.771	34.72	36.4
	^{85}Kr	5.89	5.796	5.93	3.48
	^{86}Kr	50.76	50.912	50.66	52.4
Isotopic composition of Xe [%]	^{128}Xe	0.06	0.064	0.07	0.073
	^{129}Xe	0.003	0.003	0.01	0.004
	^{130}Xe	0.213	0.229	0.24	0.245
	^{131}Xe	5.941	5.209	5.01	4.57
	^{132}Xe	23.11	23.534	23.65	24.2
	^{134}Xe	27.65	27.626	27.58	28.0
	^{136}Xe	43.02	43.337	43.45	42.9

2.2 Sample cutting

The first time the fuel gets into contact with air after operation is when the rod is punctured for determining internal pressure and free volume. At Studsvik, full-length LWR rods are normally cut into about four segments shortly after puncturing. The dates of these operations are compiled in Table 2-1.

Three samples were cut out of each rod:

- Fuel corrosion sample, consisting of a segment, cut at mid-pellet height, containing one complete and two half pellets.
- Sample for determining the nuclide inventory, consisting of about half a pellet (two pellet halves from rod SUT3-00477).
- Sample for fuel density measurement, if required[1], consisting of about half a pellet.

The location and local burnup, based on gamma scanning, of the corrosion samples can be found in Table 2-1. Instead of the complete sample designation given in the table, only the designation of the rod is used in the report.

2.3 Determination of nuclide inventory

The nuclide inventory of all four samples was determined by means of a combination of experimental nuclide analysis and sample specific modelling calculations.

2.3.1 CASMO calculations

Detailed nuclide inventories were calculated for all four samples by Studsvik Scandpower. The work was documented in /Børresen 2008/ and /Børresen 2009/. A summary of the two reports is included below.

[1] Finally not included in project scope.

Power histories

Studsvik Scandpower disposes of all necessary information for modelling fuel operated in Ringhals reactors. They obtained detailed operating histories of the three samples from rods 3V5-Q13, SUT3-00477 and 4I8-Q12 from CASMO-4 / SIMULATE-3 core follow calculations.

SNF calculations, using the SIMULATE-3 restart files as input, were set up for each of the three cases to obtain the detailed power histories of the given nodes, through all of the cycles. Based on these detailed power histories from SIMULATE-3/SNF, new, simplified power histories with 14–15 time-steps were generated for use in the final CASMO-4 calculations from which the isotopic inventories were determined. The SIMULATE-3 and simplified nodal power histories are shown in Figure 2-1, Figure 2-2 and Figure 2-3. The relative powers (P_{rel}) are nodal values normalised so that:

$$P_{rated} \sum \left(\Delta T \cdot P_{rel} \right) = Burnup_{Node}^{S3}$$

P_{rated} : Rated power in kW/gU

ΔT : Time step length (days)

In the case of the sample from rod AM2-K12 irradiated in the North Anna reactors, Studsvik Scandpower did not have access to core follow data. Therefore, the nuclide inventory was calculated in a more generic way, nevertheless based on rather detailed information on the power history. Due to the special operating history and in particular the long cooling time before the last cycle, the detailed history of North Anna cycles 7, 9 and 10 is not very important for the final results. In the last cycle, North Anna cycle 14, power was rather constant except for a gradual reduction near the end of the cycle. The practical power history for CASMO-4 calculations was developed by performing SNF calculations, using data for a similar PWR fuel rod. The reference SNF model was set up with a total of 55 time steps. The results were compared to a simplified SNF calculation with ten time steps only. The results of the two calculations were nearly identical. Thus, the final CASMO-4 calculations were performed with the 10 step power history illustrated in Figure 2-4.

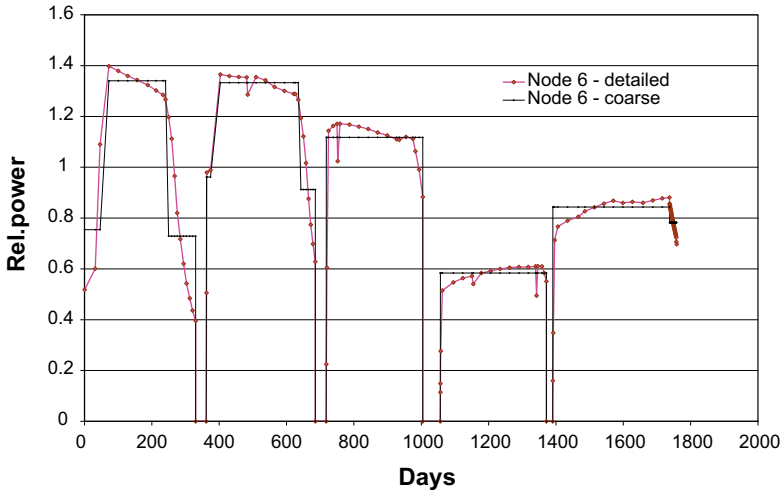

Figure 2-1. *Nodal power history of sample R3-3V5 – detailed (SIMULATE-3) and coarse (for CASMO-4).*

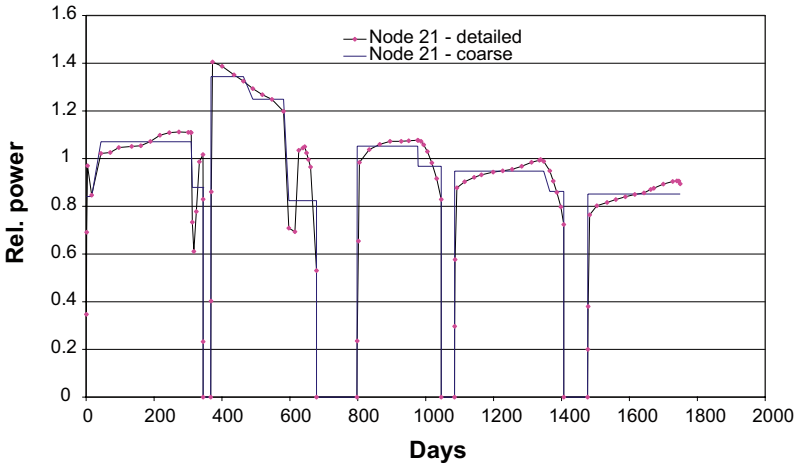

Figure 2-2. *Nodal power history of sample R4-50T – detailed (SIMULATE-3) and coarse (for CASMO-4).*

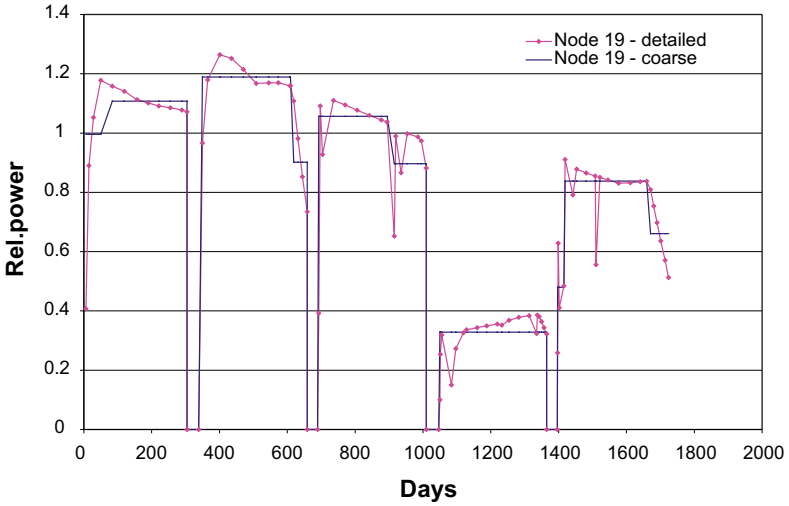

Figure 2-3. *Nodal power history of sample R3-4I8 – detailed (SIMULATE-3) and coarse (for CASMO-4).*

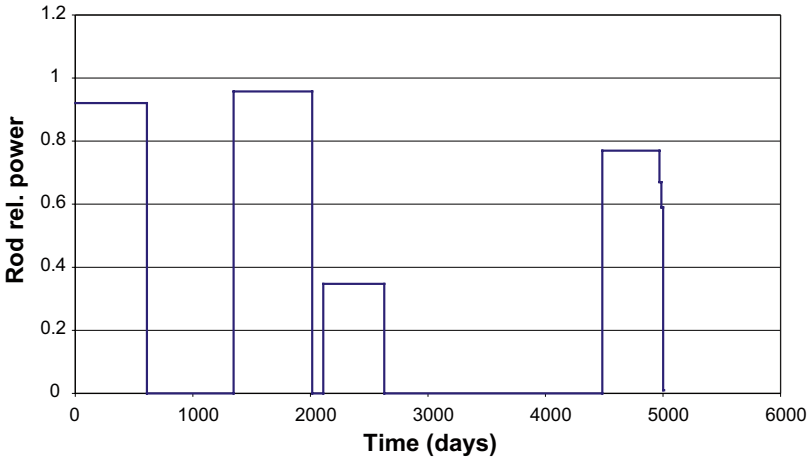

Figure 2-4. *Nodal power history of sample AM2-K12 applied in CASMO-4 calculations.*

Calculations

The CASMO-4/SIMULATE-3 core follow calculations are based on data consistent with those used at Ringhals 3 and Ringhals 4. The CASMO-4 model uses a reduced UO_2 density to account for pellet dishing, amongst others.

As mentioned above, the core follow calculations for Ringhals 3 and 4 were used to generate the complete power histories of the nodes where the samples from the Ringhals rods were located. Then, two optional methods were investigated for generation of the sample isotopic concentrations. The results shown here are without decay since the final date of measurement is unknown.

1. Using the SNF program with sample (fuel pin) isotope data tables from CASMO-4 and detailed power histories from the SIMULATE-3 restart files. Decay calculations up to a given date may be performed with SNF. The SNF isotopes are limited to radioactive isotopes of importance in source term calculations.
2. Using CASMO-4 calculations for the selected nodes, coarse power histories and no decay. This option is preferred by Studsvik Nuclear since the data are presented in a way consistent with earlier analyses and also include more isotopes than those present in the SNF program.

The CASMO-4 calculations for option 1 were run at nominal power density. A new calculation option to save SNF isotope tables for the selected fuel pins was utilised.

An example of ratios of pin-isotopic concentrations to (standard) node isotopic concentrations is shown in Figure 2-5. In this case, the ratios vary from about 0.93 to about 1.10.

Another set of CASMO-4 calculations was performed for option 2. Here, variable power densities according to the coarse power histories illustrated above were used. Isotopic data as a function of burnup, for a small range of final burnups, were saved for the selected fuel pins.

Option 1 accounts for the power histories in a more detailed manner than option 2, however, the differences in results between the two methods are limited to short lived isotopes. This is illustrated in Figure 2-6 that shows ratios of isotopic actinide concentrations using the coarse history (15 steps) over concentrations obtained with the detailed history (112 steps) for the sample from Ringhals 4. It is obvious that short-lived nuclides are underpredicted with the coarse power history. This is also the case for short-lived fission products. These short-lived isotopes are, however, not of interest in this project. Thus, it was concluded that option 2 is acceptable.

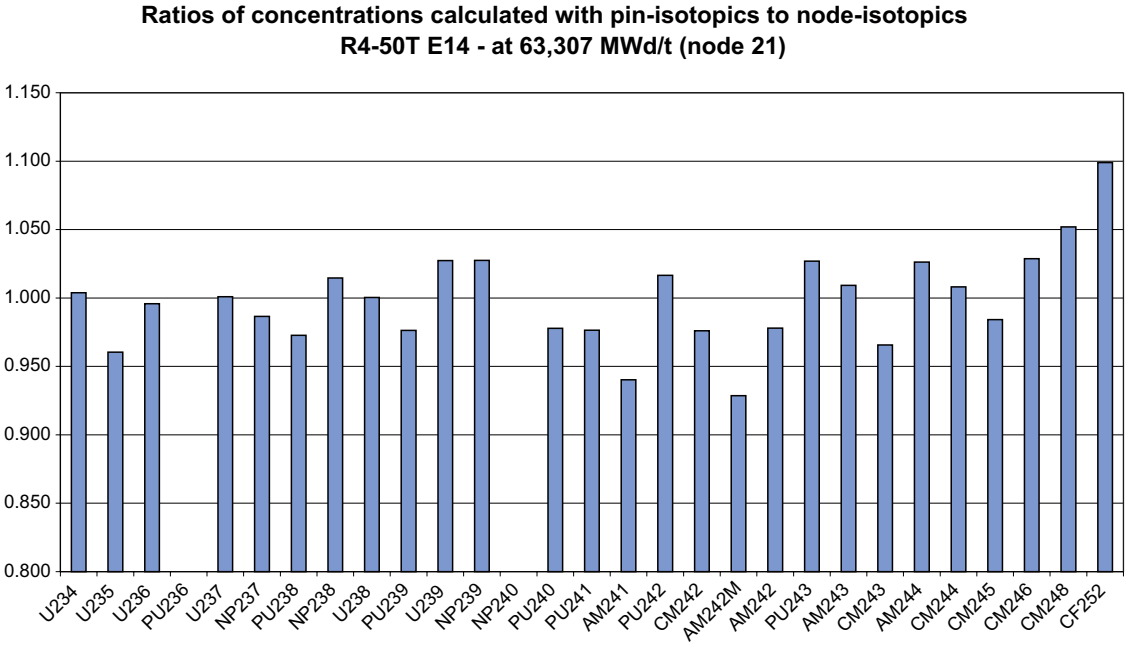

Figure 2-5. *Example of ratios of pin-isotopic to node isotopic concentrations (CASMO-4).*

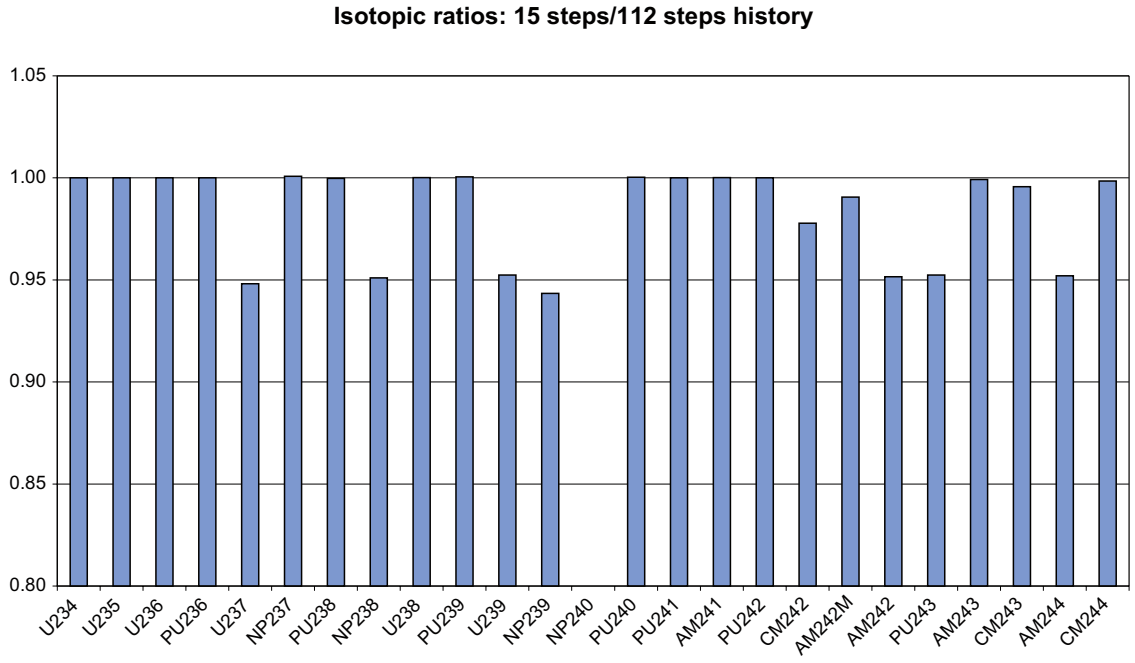

Figure 2-6. *Effect of coarse versus detailed power history, actinides (SNF calculations).*

2.3.2 Axial gamma scans

Method

All rod segments of concern had been scanned in the framework of the post-irradiation examinations within the original projects. These scans were re-evaluated in order to determine the inventory of gamma emitting nuclides.

A high purity germanium detector behind a 0.5 mm tungsten collimator was used for the measurements. Axial gamma scanning was performed applying the technique of closely spaced point measurements.

The efficiency file for the detector and collimator system was calibrated to give photon energy independent activity values for a fuel rod with an outer diameter of 9.5 mm with no extra absorber. Activities were decay corrected to the respective reference date, corresponding to the end of irradiation.

A well characterised reference rod was scanned together with the corresponding rod segments. By comparing the apparent ^{137}Cs activity measured for the reference rod with the decay-corrected ^{137}Cs activity known from the characterisation of the rod, a correction factor to be applied on all apparent activities was determined. Dead time correction of the system was checked by following the signal from a ^{60}Co source placed close to the detector.

Rod 4I8-Q12 had been scanned in February 1995. Unfortunately, this measurement had not been documented sufficiently well in order to allow re-evaluation. The rod segment of concern was therefore scanned again before cutting the samples for the fuel corrosion experiment. Only ^{137}Cs, ^{134}Cs and ^{154}Eu, the last two with rather large uncertainty, could be assessed. Moreover, the measurement was impacted by a drift of the measured signals, probably caused by an error in the geometry of the measurement set-up. By comparing the shape of the measured ^{137}Cs profile with the shape in the original scan, a correction function could be established that allowed evaluating the data.

When the ^{103}Ru, ^{106}Ru and ^{144}Ce contents based on the gamma scan of rod 3V5-Q13 were compared to calculated values, it was obvious that the experimentally determined values were by far too low. The reason for the discrepancy could not be found. Therefore, these values are not reported.

The absolute activity was determined according to the following general formula:

$$a = \bar{a} \cdot c \cdot \frac{1}{f(E_\gamma)} \cdot g \cdot d$$

With

a: Absolute activity [Bq/mm]

$\bar{a}$: Apparent (measured) activity [Bq/mm]

f: Absorption factor

E_γ: Energy peak

g: Geometry factor

d: Dead time correction factor

c: ^{137}Cs reference rod correction: $c = \frac{a_{RR}(t_{ref})}{\bar{a}_{RR}(t_{ref})}$

a_{RR}: Activity of reference rod

$\bar{a}_{RR}$: Apparent (measured) activity of reference rod

t_{ref}: Time at end of irradiation of the rod

Measurements

A segment from rod F3F6 was used as reference rod in all measurements. Rod data and measurement parameters are compiled in Table 2-4.

Table 2-4. Rod data and measurement parameters.

Rod	4I8-Q12	AM2-K12	SUT-00477	3V5-Q13	F3F6
End of irradiation[yymmdd]	940616	010312	030731	050525	930605
Scanning date [yyddmm]	071120	020824	040117	060309	
Fuel density [g/cm^3]	10.50	10.44	10.45	10.45	10.51
Pellet diameter [mm]	8.193	8.192	8.19	8.165	8.190
Cladding inner diameter [mm]	8.36	8.357	8.36	8.33	8.36
Cladding outer diameter [mm]	9.5	9.5	9.49	9.55	9.62
Collimator window [mm]	0.5	0.5	0.5	0.5	
Extra absorber	None	None	30 mm Al	20 mm Al	
Step width [mm]	0.3	0.25	0.25	0.25	
Accumulation time [s]	15	8	10	10	
Geometry factor	1	1	1	1	
Absorption factor	1	1	1	1	
^{137}Cs reference rod correction	1.10	0.90	1.77	1.76	

For estimating the total uncertainty, the following contributions were taken into account:

- Statistical error of the gamma spectrometry measurement, determined by calculating the standard deviation of the mean value based on the single data points, excluding pellet-pellet interfaces.
- Statistical error of ^{137}Cs measurement in the reference rod (1.0%).
- Uncertainty of ^{137}Cs content in reference rod (2.0%).
- Uncertainty of decay corrections (0.1%).
- Uncertainty of efficiency calibration relative to 661 keV line of ^{137}Cs.

Transformation into amount ^{n}X relative to ^{238}U

The gamma scan results were transformed into amount of nuclide ^{n}X in weight percent relative to ^{238}U according to the following procedure:

- The average activity per length unit [Bq/mm] was calculated from the gamma scan data. Values from pellet-pellet interfaces were excluded.
- Based on the basic formula for radioactivity ($A = \lambda N$), the amount of nuclide ^{n}X per length unit [µg/mm] was calculated.
- The amount of ^{238}U per length unit [µg/mm] of unirradiated fuel was determined, based on pre-irradiation data (density, stoichiometry, enrichment).
- The residual ^{238}U per length unit at the end of bombardment (in percentage of initial amount of ^{238}U) was estimated based on CASMO calculations, neglecting the irradiation-induced change of the fuel stack length, which uses to be less than 1%.
- The amount of nuclide ^{n}X in weight percent relative to ^{238}U was calculated by dividing the amount of nuclide ^{n}X per length unit by the amount of ^{238}U per length unit.

The error includes the error of the activity measurement and a relative error of 2% for the amount of ^{238}U per length unit.

2.3.3 Chemical analyses

Dissolution

The samples were placed in a glass flask together with 90 ml of 8 *M* HNO_3 (Suprapure) and kept at 65°C for 6 h. Evaporation of liquid was avoided by means of an air-cooled reflux cooler. Nitrogen was bubbled through the liquid in order to stir it. The fuel matrix together with all fission products of interest went into solution. The cladding and the metallic fission product inclusions remained undissolved.

In the order of 0.1–0.4 g of the original fuel solution was diluted into 100 ml of HNO_3 (7.5 *M*) in the hotcell. 20 ml of this solution were transferred to the laboratory. An appropriate aliquot was diluted with 100 ml HNO_3 (0.16 *M*) to a target uranium concentration of about 5 ppm. The uranium concentration was determined by Scintrex analysis. The Scintrex[2] UA-3 is a uranium analyser, measuring the characteristic fluorescence of the uranyl ion in solution after irradiation with a very short pulse of ultraviolet light from a nitrogen laser. 40 g of this mother solution is then mixed with all necessary spike solutions.

The HPLC-ICP-MS instrument

The HPLC-ICP-MS instrument is shown in Figure 2-7. A DIONEX SP Gradient High Performance Liquid Chromatography (HPLC) system and Autosampler Dionex AS with an IonPac CG10 (4·50 mm) guard and an IonPac CS10 (4·250 mm) analytical column was used for the separations. Chromeleon Xpress, CHX-1 software was used to control the autosampler, injector and HPLC pump. The eluents were directly injected into a Perkin Elmer Elan 6100 DRC II Inductively Coupled Plasma Mass Spectrometer (ICP-MS), installed in a glove box. The ICP-MS instrument is controlled by Perkin Elmer Chromera software. The Chromera software was also used for the collection and evaluation of the chromatograms. Peak areas were used for the evaluation.

ICP-MS analysis based on one-point calibration

In this mode of analysis, count rates from an aliquot of the mother solution that is diluted as appropriate were compared to count rates from multi-element standard solutions. The first step in the evaluation of the data consisted of normalising all count rates to each other by means of added internal standards (^{115}In, ^{209}Bi). Blank corrections were performed by means of measurements of a pure diluted HNO_3 solution (0.16 *M*) preceding the analysis of each sample and standard solution.

[2] SCINTREX UA-3 Uranium Analyser, SCINTREX, Snidercroft Road, Concord Ontario Canada L4K 1B5.

Figure 2-7. *The HPLC-ICP-MS instrument.*

Average values were then compared to the corresponding average values measured in the standard solutions. Based on the known concentration of the nuclide in the standard, the concentration of the nuclide in the sample was calculated.

This mode of analysis is restricted to isotopes without any isobaric overlap. ^{99}Tc, ^{133}Cs, ^{135}Cs, ^{139}La, ^{237}Np as well as ^{244}Cm and ^{246}Cm were determined by analysis based on one-point calibration. In addition, some nuclides analysed by Isotope Dilution Analysis (IDA) were assessed by one-point calibration analysis as well. The error estimation of one-point calibration analysis was amongst others based on a comparison with the IDA results for interference-free nuclides determined by both methods.

Isotope dilution analysis

Basis

IDA is based on the addition of a known amount of an enriched isotope ("spike") to a sample. Isotopic ratios between the added isotope and the isotope to be analysed are determined by mass spectrometry in the mixture of spike and sample, in the sample and, if not already known, in the spike. The amount of the isotope to be determined in the sample can be calculated according to the Equation 2-5 derived below:

a = spike isotope
b = isotope to be analysed
R_s *= isotope ratio (a/b) in sample*
R_{Sp} *= isotope ratio in spike*
R_M *= isotope ratio in mixture*
N_a^S *= number of isotope a in sample*
N_a^{Sp} *= number of isotope a in spike*
N_b^S *= number of isotope b in sample*
N_b^{Sp} *= number of isotope b in spike*

$$R_s = \frac{N_a^S}{N_b^S} \tag{2-1}$$

$$R_{sp} = \frac{N_a^{Sp}}{N_b^{Sp}} \tag{2-2}$$

$$R_M = \frac{N_a^S + N_a^{Sp}}{N_b^S + N_b^{Sp}} \tag{2-3}$$

By transforming Equation 2-3, the following Equation 2-4 can be derived:

$$N_b^S = \frac{N_a^{Sp} - R_M \times N_b^{Sp}}{R_M - R_s} \tag{2-4}$$

N_b^{SP} can be substituted by means of Equation 2-2, which leads to Equation 2-5:

$$N_b^S = N_a^{Sp} \times \frac{1 - \frac{R_M}{R_{Sp}}}{R_M - R_s} \tag{2-5}$$

Once the amount of isotope *b* in the sample has been determined, all other isotopes of the same element can easily be determined by means of the isotopic ratios measured by mass spectrometry.

Spiking

R_S, the isotope ratio in the sample, is given. R_{Sp}, the ratio in the spike is fixed as well, once the appropriate standard is chosen for a series of analyses. R_M, the isotope ratio in the mixture, on the other hand can be influenced by the amount of spike solution that is blended with the sample aliquot. Two aspects have to be taken into account when choosing the appropriate R_M value: counting statistics, influencing the uncertainty of the isotopic ratio, and the factor that determines the contribution of the uncertainty in R_M by error propagation to the overall error of the analysis.

The approximate amount of the isotopes to be analysed in the sample as well as the corresponding R_S values were estimated based on the result of semi-quantitative analyses and on CASMO calculations. After choosing an appropriate R_M value, the number of spike isotopes to be added to an aliquot of the mother solution was calculated based on Equation 2-5.

Identities of spike isotopes and of isotopes to be analysed, as well as their abundance in the corresponding spike solutions, are shown in Table 2-5.

Table 2-5. Abundances of spike isotope and isotope to be analysed in spike solutions.

Spike Isotope	Abundance [%]	Isotope to be analysed	Abundance [%]
^{233}U	98.043	^{238}U	0.804
^{242}Pu	99.903	^{239}Pu	0.0826
^{243}Am	99.966(1) 99.967(2)	^{241}Am	0.031(1) 0.030(2)
^{133}Cs	100.00	^{137}Cs	–
^{140}Ce	99.30	^{142}Ce	0.70
^{148}Nd	91.60	^{146}Nd	2.50
^{154}Sm	99.02	^{152}Sm	0.473
^{151}Eu	99.24	^{153}Eu	0.76
^{155}Gd	91.6	^{156}Gd	6.34

Reference date: April 12, 1984.
Calculated for February 2007.

IDA without separation

Uranium isotopes were determined by IDA based on ICP-MS without separation. Aliquots of spiked and unspiked solutions were diluted as appropriate in order to avoid too large dead time corrections. The measurements were performed in the peak jump mode.

HPLC-ICP-MS

Plutonium and americium isotopes were determined by IDA based on HPLC-ICP-MS, with an elution program separating the two elements from each other and from interfering elements, e.g. uranium. Aliquots of spiked and unspiked solutions were diluted as appropriate.

In a separate run, the lanthanides cerium, neodymium, samarium, europium and gadolinium were determined, applying the corresponding elution method.

Caesium was determined in a separate run as well, applying a dedicated elution method.

Data evaluation

Count rates measured in the analysis of uranium, performed without any separation, were blank corrected. The count rates from the unspiked and spiked samples of mass 238 were corrected for the contribution of ^{238}Pu, based on the count rate for mass 239 and the ratio of ^{238}Pu and ^{239}Pu determined in the plutonium analysis. The abundance of uranium isotopes in the unspiked sample was determined by normalising the corresponding count rates of five individual measurements to 100%, followed by calculating an average value for each individual isotope. R_S was determined based on the corresponding abundances; R_M was calculated directly from the corresponding count rates. The number of ^{238}U atoms was calculated according to Equation 2-5. For all other isotopes, the number of atoms in the sample was calculated by means of the corresponding abundances, based on the number of atoms of the isotope to be analysed.

The number of atoms of all other isotopes in the sample was determined accordingly, based on peak areas determined after HPLC separation.

The number of atoms in the sample was transformed into micrograms. Finally, the amount of nuclide ${}^{n}X$ in weight percent relative to ^{238}U was calculated by dividing the corresponding amount by the amount of ^{238}U.

Estimation of uncertainty

The uncertainty of the number of counts in a pulse counting system like ICP-MS is given by the square root of the number of counts, neglecting the contribution of the background signal. When applying the rules of error propagation on the simple Equation 2-6 for the ratio of two isotopes of interest, it can be demonstrated that the precision of the ratio is limited by the size of the smaller peak (Equation 2-7).

$$r = \frac{a}{b} \tag{2-6}$$

with

r = isotopic ratio

a, b = number of counts

$$\frac{s_r}{r} = \sqrt{\frac{1}{a} + \frac{1}{b}} \tag{2-7}$$

with

S_r *= error of r*

Experience from routine analysis has shown that it is normally not possible to achieve a lower relative standard deviation of *r* than about 0.1%, even if sufficient counts are available. If the number of counts in the smaller of the two peaks is significantly larger than 10^6, the contribution of counting statistics is negligible. This is normally the case in HPLC-ICP-MS analyses. In ICP-MS analyses in peak jump mode, numbers of counts may be smaller. With 10^5 counts in the smaller peak, the contribution of counting statistics to the relative error of *r* is still below 0.5%. On the other hand, additional factors like instrument instability limit the achievable accuracy. A possibility of assessing this scatter is calculating the relative standard deviation of the five and three abundance values of individual isotopes, respectively, in the unspiked samples that were determined by normalising the count rates of individual measurements to 100%. For each isotopic ratio, s_r calculated by error propagation from the standard deviation of abundance values was compared to a value based on Equation 2-7. The larger of the two values was then used in the overall error estimation.

The equation for calculating the error of the number of atoms of the isotope to be analysed in the sample (Equation 2-8) is derived from Equation 2-5 according to the general rules of error propagation.

$$s_{N_b^S} = N_b^S \times \sqrt{\left(\frac{s_{N_a^{Sp}}}{N_a^{Sp}}\right)^2 + \left(\frac{R_S - R_{Sp}}{R_{Sp} - R_M}\right)^2 \times \left(\frac{s_{R_M}}{R_M - R_S}\right)^2 + \left(\frac{s_{R_S}}{R_M - R_S}\right)^2 + \left(\frac{R_M}{R_{Sp} - R_M}\right)^2 \times \left(\frac{s_{R_{Sp}}}{R_{Sp}}\right)^2} \tag{2-8}$$

with

S_i *= absolute error of i*

For all other isotopes, Equation 2-9 is applied:

$$s_{N_x} = N_x \times \sqrt{\left(\frac{s_{N_b^s}}{N_b^s}\right)^2 + \left(\frac{s_r}{r}\right)^2} \tag{2-9}$$

The relative error of the number of added spike atoms $\left(\frac{s_{N_a^{Sp}}}{N_a^{Sp}}\right)$ and the relative error of R_{Sp} $\left(\frac{s_{R_{Sp}}}{R_{Sp}}\right)$ used in the calculations are estimated as shown in Table 2-6.

Table 2-6. Uncertainties of input data used in IDA calculations.

Parameter		Relative Error (Comment)
N_a^{Sp}		1% (Estimated, same value for all elements)
R_{Sp}		
	U	0.1% (Estimated)
	Pu	0.1% (Estimated)
	Am	1% (Estimated)
	Cs	0.1% (Estimated)
	Ce	1% (Estimated)
	Nd	0.5% (Estimated)
	Sm	0.5% (Estimated)
	Eu	0.5% (Estimated)
	Gd	1% (Estimated)
R_S ,R_M, r		Determined according to the method described in the text

Decay corrections

Besides stable isotopes with short-lived mother nuclides, chemical analyses include radioactive nuclides and nuclides with long-lived mother nuclides as well. In these cases, in addition to the analysed value, a value that is decay-corrected back to the end of bombardment (EOB) is reported as well. All applied half-lives are compiled in Table 2-7. All values applied for correcting chemical analysis data are taken from /Magill et al. 2006/. The reference for half-lives applied in gamma scanning is not known. In the case of ^{154}Eu, the different half-lives introduce a potential systematic deviation of less than 4%.

Table 2-7. Half-lives applied for decay corrections.

Nuclide	Half-life	Nuclide	Half-life
^{244}Cm	18.10 a	^{155}Eu	4.761 a
^{144}Ce	284.8 d *284.2 d*	^{134}Cs	2.06 a *2.062 a*
^{241}Pu	14.35 a	^{137}Cs	30.17 a 30.1 a
^{147}Pm	2.62 a	^{106}Ru	*1.02 a*
^{154}Eu	8.8 a *8.5 a*		

Italic: Applied in gamma scanning.

Burnup determination

One of the traditional methods for determining the burnup of irradiated LWR fuel is the ^{148}Nd method according to ASTM E 321 /ASTM 1996/. Probably one of the largest sources for systematic errors in this method is the assumed fission yield, requiring knowledge of the fraction of fissions occurring in ^{238}U (fast neutron fission) and ^{235}U, ^{239}Pu and ^{241}Pu (thermal). Another traditional method for burnup determination is based on the uranium and plutonium isotopic composition (ASTM E 244 /ASTM 1995/); this method is rarely used for LWR fuel due to its rather simplified and rough assumptions regarding the neutron spectrum and fission fractions (the standard has been withdrawn in 2001). However, modern physics codes like CASMO and HELIOS are instead able to calculate the amount of fission products and actinides formed or consumed during reactor operation in a much more sophisticated way, taking changes of irradiating conditions into account in a more detailed way than in the ASTM E 321 and ASTM E 244 methods. The uncertainty of these methods can therefore be eliminated to a certain extent, if the experimentally determined amount of suitable fission products or actinides is compared to the result of, e.g., CASMO calculations. Cross sections applied for CASMO calculations of isotope number densities are in general well known, at least in the case of fission products that are candidates for being used for burnup determination. The accuracy of CASMO results depends primarily on the quality of modelling operating history. In the case of the two analysed rods, operation was well documented, thus allowing a quite detailed modelling. Therefore, the error of CASMO calculations is assumed to be smaller than experimental errors. The method is described in /Zwicky et al. 2005/.

Experimentally determined $^{n}X/^{238}U$ values for ^{146}Nd, ^{148}Nd and ^{150}Nd were compared to values calculated by Studsvik Scandpower, thus allowing a determination of the local pellet burnup. In addition, local pellet burnup was determined by comparing the isotopic abundance of ^{235}U and ^{239}Pu analysed by ICP-MS to CASMO based values.

2.3.4 Nuclide inventory

Release fractions in fuel leaching experiments are calculated on the basis of nuclide inventories given in micrograms of nuclide of concern per gram of uranium initially present in the fuel. Therefore, $^{n}X/^{238}U$ values were transformed accordingly. The remaining amount of ^{238}U at the end of the irradiation was determined on the basis of the CASMO calculations performed by Studsvik Scandpower. The initial nominal enrichment was used for determining the factor that converts $^{n}X/^{238}U$ values into amounts of nuclide per microgram of initial uranium.

2.4 Fuel leaching experiments

The experiments are performed under oxidising conditions in synthetic groundwater (Table 2-8) at ambient temperature (about 20°C with seasonal fluctuations in the order of 1–2°C). In order to make results as comparable as possible to those of the Series 11 experiments, the same procedure and the same leachant as described in /Forsyth 1997/ was used. At least nine consecutive contact periods of one and three weeks and two, three, six and twelve months are planned. The present report covers the first six contact periods up to a cumulative contact time of two years for the samples from rods 3V5-Q13 and AM2-K12, and the first five contact periods up to a cumulative contact time of one year for the samples from rods SUT3-00477 and 4I8-Q12.

Before the experiment, the samples were washed by exposing them to a 10 *mM* NaCl/2 *mM* $NaHCO_3$ solution for about two hours (Figure 2-8). Then they were rinsed with pure water and air-dried.

The samples, kept in position by a platinum wire spiral, are exposed to 200 ml of synthetic groundwater in a Pyrex flask (Figure 2-9). After the contact period, samples are taken for ICP-MS and gamma spectrometric[3] analyses and for pH and carbonate determination. 100 ml are stored as spare sample. The fuel sample is placed in a new flask with fresh synthetic groundwater for the next contact period.

After transfer to the radiochemistry laboratory, the samples are centrifuged. 10 ml of each sample are transferred into a 20 ml vial. Some of the samples are acidified with 0.1 ml of concentrated HNO_3 (Suprapure), before they are analysed. The non-acidified sample is used for iodine analysis, pH and carbonate determination. The used flasks and the centrifuge tubes are stripped by exposing the surface to 2*M* HNO_3 for a few days (200 ml and 10 ml, respectively). The strip solutions are analysed in the same way as the centrifuged samples.

Uranium is analysed by a fluorimetric method (Scintrex) as well as by ICP-MS. ^{137}Cs is determined by gamma spectrometry and by ICP-MS. The majority of nuclides are measured by ICP-MS.

Table 2-8. Composition of synthetic groundwater.

Element	Concentration [mM]	ppm
Ca	0.4477	18
Mg	0.1774	4.3
K	0.1000	3.9
Na	2.836	65
Silicate	0.2056	12
Bicarbonate	2.014	123
Sulfate	0.1000	9.6
Chloride	1.973	70
Fluoride	0.2023	3.8
Phosphate	0.001	0.089

[3] EG&G ORTEC GAMMA-X HPGe (High Purity Germanium) Coaxial PhotonDetector System, CANBERRA Nuclear Data software.

Figure 2-8. *Washing of fuel samples.*

Figure 2-9. *Fuel sample in Pyrex flask.*

2.5 Data evaluation of fuel leaching experiments

2.5.1 ICP-MS analyses

The concentration of fission products and actinides is determined by ICP-MS. All samples contain 1 ppb of ^{115}In as internal standard. Measurements in the mass range 80–254 amu are carried out. Sensitivity factors for the different elements relative to ^{115}In are calculated by a one-point calibration using multielement standards. Nuclide concentrations are calculated by relating the signals to the ^{115}In signal. The detection limit of the instrument is in the ppt range (pg/g) and the quantification limit in the ppb (ng/g) range with an error limit of 20%. The method-specific detection limits are dependent on the sample matrix and are thus specific for each sample. The limits of concern, based on measurements of the corresponding blank and standard solutions, are compiled in Table 2-9. In the case of strontium and caesium, the limits are based on data from the natural isotopes ^{88}Sr and ^{133}Cs. The ICP-MS analyses are performed according to a method for determining trace elements in waters and wastes /EPA 2004/.

Several corrections are applied to the raw ICP-MS data by means of a dedicated Excel template.

- Corrections for natural krypton and xenon contaminations, caused by small amounts of these species contained in the argon carrier gas.
- Potential contaminations of the analysed solutions by natural rubidium, strontium, zirconium, molybdenum, silver and barium.
- Isobaric corrections for fission products and actinides (zirconium, ruthenium, palladium, caesium, barium, neodymium, plutonium and curium). The corrections are based on nuclide abundances determined from the nuclide inventory of the corroded fuel sample. Where radioactive decay is involved, abundances are decay-corrected correspondingly.

Table 2-9. Sample-specific detection limits.

Nuclide	Detection limit [ng/kg]			
	4I8-Q12	3V5-Q13	SUT3-00477	AM2-K12
Rb-85	2.3	2.1	2.3	1.4
Rb-87	1.4	0.9	1.2	1.4
Sr-88	10.8	6.1	10	11.0
Mo-100	0.1	0.5	0.6	1.0
Tc-99	0.2	0.9	0.8	1.4
I-129	1.0	1.0	1.0	1.0
Cs-133	0.4	2.2	2.2	0.2
Ba-138	10	4.4	8.7	4.9
La-139	0.9	0.5	0.9	0.9
Ce-140	0.9	0.9	0.7	1.1
Pr-141	1.0	1.0	1.0	1.0
Nd-144	0.3	0.1	0.2	0.2
Eu-153	1.0	1.0	1.0	1.0
U-238	2.6	6.5	7.3	6.9
Np-237	0.03	0.04	0.03	0.1
Pu-239	0.1	0.2	0.2	0.1

2.5.2 Iodine Analysis

Accurate analysis of low level ^{129}I is difficult because the nuclide emits only low energy beta (maximum energy 0.15 MeV) and gamma (0.035 MeV) rays. Therefore a method was developed for the determination of iodine including isotopic analysis of stable and radioactive iodine by means of ICP-MS. Potential interference by ^{129}Xe is eliminated by using a Dynamic Reaction Cell /Izmer et al. 2003/. Iodine (^{127}I or ^{129}I) can be analysed by this new method down to the lower ng/ml range.

In order to prevent iodine from being lost, the samples were stabilized by adding Tetra Methyl Ammonium Hydroxide (TMAH) to a concentration of 0.5%. The ICP-MS was washed between samples and standards with a solution of 0.1% Trition X-100 /Haldimann et al. 1998/.

2.5.3 Gamma spectrometry

The activity of ^{137}Cs in a 10 ml sample is measured on a correspondingly calibrated Ortec HPGE detector placed in a lead shield with AccuSpec version 03 software from Canberra Nuclear. In order to make them comparable, the data are decay corrected to the same date as the ICP-MS analyses.

2.5.4 Verification of strontium analysis

The analysis of ^{90}Sr in solutions by means of ICP-MS might be questioned due to the isobaric overlap with ^{90}Zr, the most abundant natural zirconium isotope. Even though a corresponding correction is applied to the measured ICP-MS data, it should be verified that the result is correct. An appropriate way is the radiometric analysis of ^{90}Sr in a selection of centrifugate solutions. The radiometric analysis is rather complicated and time consuming. Thus, it would not be very well suited for the analysis of a large number of samples.

In the radiometric ^{90}Sr analysis, strontium is separated from yttrium by means of extraction chromatography, after addition of strontium carrier. After about one week, during which the daughter nuclide ^{90}Y ($t_{1/2}$ = 64.1 h) is growing in, the two elements are separated again, in order to determine the yield of strontium and for determining the activity of ^{90}Y formed after the first separation by means of β measurements in a proportional counter. The ^{90}Y activity at the time of the first separation is determined on the basis of four measurements performed at different decay times. Finally, the ^{90}Sr activity in the original sample can be calculated.

2.5.5 Release fractions

Release fractions are calculated by dividing the total amount of a nuclide of concern in the analysed solution by the total amount in the corroded fuel sample. The reported standard deviation is simply the standard deviation calculated from the individual values of two independent ICP-MS analyses.

Cumulative release fractions are the sum of release fractions up to a certain cumulative contact time. The reported standard deviation is calculated from the standard deviations of the individual release fractions according to the rules of error propagation.

2.5.6 Release rates

Release rates are calculated by dividing release fractions by the length of the contact period of concern.

No attempt was made to calculate release rates normalised to the exposed fuel sample surface.

2.5.7 $^{236}U/^{235}U$ ratio

The $^{236}U/^{235}U$ ratio in irradiated fuel is strongly dependent on burnup, as illustrated in Figure 2-10. The plot shows data calculated for fuel with an initial ^{235}U enrichment of 4% by CASMO for a generic PWR case. As the burnup is significantly higher than the average towards the periphery of a fuel pellet, the $^{236}U/^{235}U$ ratio is higher at the periphery as well. If the fuel matrix would be preferentially dissolved in the high burnup rim structure, the $^{236}U/^{235}U$ ratio in the leachant would be significantly higher than the ratio corresponding to the average pellet burnup.

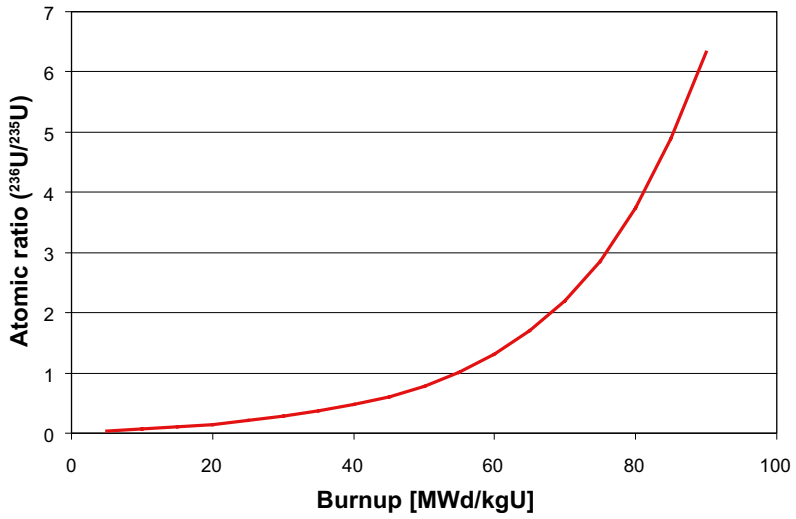

Figure 2-10. *$^{236}U/^{235}U$ ratio as a function of burnup in PWR fuel with an initial ^{235}U enrichment of 4%.*

3 Results and discussion

3.1 Nuclide inventory

3.1.1 Gamma scan evaluation

As an example, Figure 3-1 shows the ^{137}Cs profile from the original scan of fuel rod 4I8-Q12 part 3 performed in February 1995 together with the corresponding data from the scan performed in November 2007 in the framework of this SKB project before and after correction described under 2.3.2. Figure 3-2 shows the profile of the ^{137}Cs activity after transformation into Bq/mm from the part of the rod that was used for the corrosion experiment and for the chemical nuclide analysis. Data from pellet-pellet interfaces were excluded before calculating the average value. $^{n}X/^{238}U$ values and nuclide inventory relative to the initial amount of uranium in the fuel, based on gamma scan evaluation, are compiled in Table 3-1 for all nuclides that could be assessed with confidence. For comparison with results of the chemical analyses and with calculated data, see 3.1.4.

3.1.2 One-point calibration analysis

The results of one-point calibration analyses are compiled in Table 3-2. It should be noted that the values indicated for ^{99}Tc represent the dissolved portion only. Comparison with calculated values indicates that a significant amount remained undissolved (Figure 3-12).

Results for a selection of neodymium, uranium and plutonium isotopes and for ^{133}Cs and ^{243}Am are included as well, allowing a comparison with values determined by IDA.

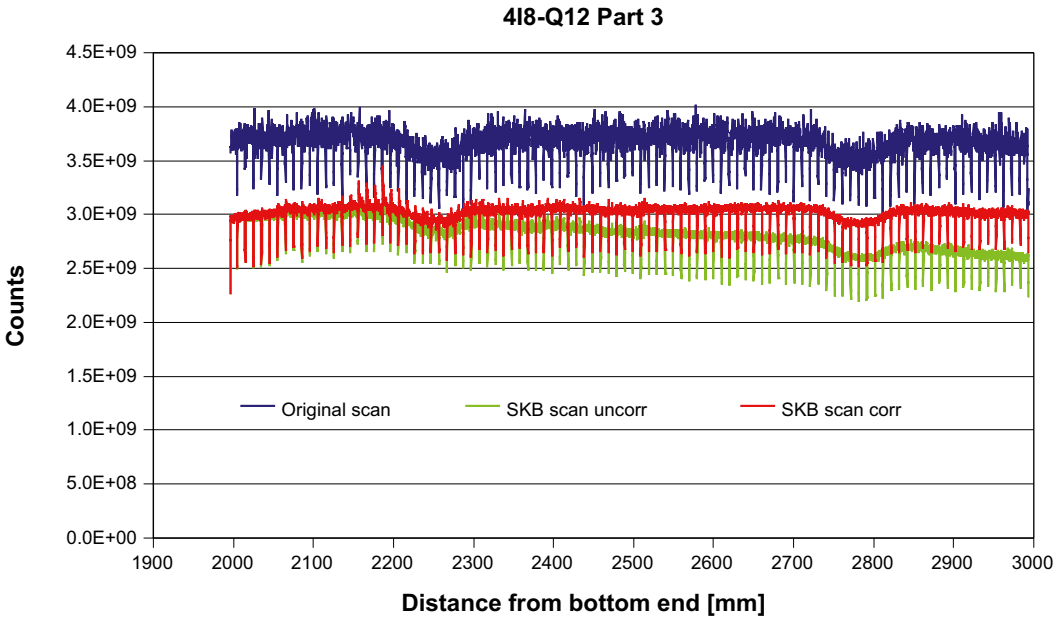

Figure 3-1. *Axial ^{137}Cs profile in part 3 of fuel rod 4I8-Q12, as-measured data (original scan and scan performed within this work) and corrected data from second scan.*

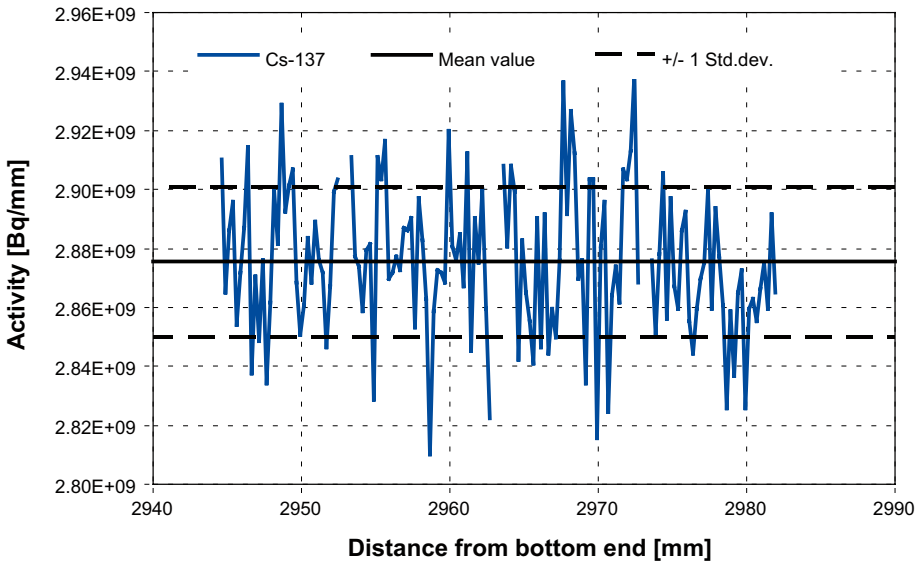

Figure 3-2. *^{137}Cs activity profile in part of fuel rod 4I8-Q12 that was used for corrosion experiment and inventory determination (data from pellet-pellet interfaces excluded).*

Table 3-1. nX/238U values and nuclide inventory relative to initial amount of uranium in the fuel, based on gamma scan evaluation.

Nuclide	$^{n}X/^{238}U$ [wt%]				Inventory [µg/gU$_{init}$]			
	4I8-Q12	3V5-Q13	SUT3-00477	AM2-K12	4I8-Q12	3V5-Q13	SUT3-00477	AM2-K12
^{134}Cs	0.0330	0.0297	0.0345	0.0318	303.2	270.5	315.9	286.6
Uncertainty	0.0024	0.0011	0.0014	0.0012	21.9	10.4	12.5	11.1
^{137}Cs	0.200	0.261	0.250	0.264	1,832.8	2,381.2	2,287.6	2,373.7
Uncertainty	0.006	0.008	0.009	0.009	57.3	73.9	82.3	78.0
^{154}Eu	0.0052		0.0058	0.0067	47.8		52.8	60.1
Uncertainty	0.0005		0.0013	0.0007	5.0		11.5	6.3
^{103}Ru			0.0063				57.5	
Uncertainty			0.0003				2.6	
^{106}Ru			0.0288	0.0206			263.7	185.9
Uncertainty			0.0012	0.0009			11.1	8.2
^{144}Ce			0.0357	n.a.			326.5	
Uncertainty			0.0049				44.8	

Table 3-2. nX/238U values and nuclide inventory relative to initial amount of uranium in the fuel determined by ICP-MS one-point calibration analysis.

Nuclide	$^{n}X/^{238}U$ [wt%]				Inventory [µg/gU_{init}]			
	4I8-Q12	3V5-Q13	SUT3-00477	AM2-K12	4I8-Q12	3V5-Q13	SUT3-00477	AM2-K12
^{99}Tc	0.081	0.072	0.088	0.094	745.5	653.8	810.1	845.6
Uncertainty	0.008	0.007	0.018	0.023	69.9	65.4	160.3	206.7
^{139}La	0.234	0.253	0.239	0.299	2,149.6	2,303.1	2,189.3	2,689.1
Uncertainty	0.004	0.005	0.008	0.012	34.9	47.6	69.1	111.6
^{237}Np	0.084	0.089	0.089	0.111	768.9	811.5	816.7	998.5
Uncertainty	0.002	0.004	0.004	0.004	20.4	37.8	37.9	36.7
^{244}Cm	0.0068	0.0164	0.0134	0.0228	62.7	149.8	122.3	205.6
Uncertainty	0.0006	0.0006	0.0011	0.0013	5.4	5.4	10.4	11.3
At EOB	0.0115	0.0183	0.0159	0.0298	106.1	166.5	145.8	268.5
^{246}Cm	0.000176	0.000372	0.000272	0.000766	1.6	3.4	2.5	6.9
Uncertainty	0.000004	0.000007	0.000006	0.000019	0.1	0.1	0.1	0.2
^{133}Cs	0.185	0.212	0.180	0.242	1,701.4	1,931.1	1,645.4	2,179.6
Uncertainty	0.008	0.002	0.006	0.010	73.5	21.4	56.7	88.0
^{143}Nd	0.093	0.094	0.106	0.129	854.9	851.9	967.3	1,164.5
Uncertainty	0.005	0.013	0.022	0.030	41.8	116.2	201.2	270.3
^{145}Nd	0.090	0.102	0.104	0.142	822.6	925.5	948.3	1,274.7
Uncertainty	0.010	0.014	0.024	0.034	89.4	125.3	222.6	304.0
^{146}Nd	0.109	0.131	0.131	0.197	1,000.7	1,193.1	1,195.3	1,775.3
Uncertainty	0.016	0.019	0.026	0.053	150.7	170.3	235.2	473.0
^{234}U	0.018	0.015	0.016	0.018	167.4	134.4	147.1	164.7
Uncertainty	0.001	0.002	0.002	0.005	8.5	16.5	20.0	45.5
^{235}U	0.423	0.264	0.366	0.209	3,882.6	2,406.3	3,350.2	1,877.9
Uncertainty	0.019	0.028	0.043	0.046	175.4	252.1	389.4	416.4
^{236}U	0.579	0.600	0.589	0.626	5,322.3	5,466.0	5,395.2	5,636.1
Uncertainty	0.027	0.055	0.074	0.134	245.0	503.9	676.5	1,202.9
^{239}Pu	0.572	0.557	0.612	0.648	5,252.7	5,079.1	5,604.2	5,837.6
Uncertainty	0.041	0.066	0.109	0.141	376.4	597.4	994.1	1,271.9
^{240}Pu	0.341	0.335	0.349	0.357	3,128.5	3,051.7	3,195.1	3,217.8
Uncertainty	0.021	0.046	0.058	0.086	191.3	422.3	528.3	775.4
^{243}Am	0.032	0.044	0.041	0.058	291.6	396.5	371.6	526.3
Uncertainty	0.003	0.005	0.006	0.012	30.4	49.2	52.5	107.8

Analysis date: February 29, 2008.

3.1.3 Isotope dilution analysis

Isotopic composition

The isotopic composition of the elements analysed by IDA is compiled in Table 3-3 to Table 3-6. The indicated uncertainty is the standard deviation (1σ) calculated for the five (uranium) and three individual measurements. Only the composition of plutonium has been decay corrected to the end of the irradiation. All other values correspond to the composition at the date of analysis. The small remaining amount of ^{144}Ce that had not yet decayed into ^{144}Nd was neglected.

Analysis of cerium by HPLC-ICP-MS has up till now often caused problems due to unidentified reasons. Even this work seems to have been affected by these troubles. Comparison of the analysed isotopic composition with the modelled composition reveals rather large deviations (see Figure 3-6).

Table 3-3. Isotopic composition of elements analysed by IDA in fuel sample 4I8-Q12.

Uranium	234	235	236	238			
Composition [at%]	0.0177	0.402	0.577	99.003			
Uncertainty	0.0001	0.001	0.001	0.002			
Plutonium	238	239	240	241	242		
Composition [at%]	3.99	47.88	29.02	7.67	11.44		
Uncertainty	0.05	0.06	0.15	0.05	0.12		
At EOB	3.71	44.54	26.61	14.50	10.64		
Americium	241	243					
Composition [at%]	75.84	24.16					
Uncertainty	0.63	0.63					
Cerium	140	142					
Composition [at%]	49.67	50.33					
Uncertainty	0.57	0.57					
Neodymium	142	143	144	145	146	148	150
Composition [at%]	0.80	15.25	36.72	15.01	18.49	9.24	4.50
Uncertainty	0.03	0.34	0.30	0.06	0.18	0.15	0.16
Samarium	147	148	149	150	151	152	154
Composition [at%]	24.91	23.71	0.00	35.38	0.00	11.18	4.82
Uncertainty	0.21	0.19	0.00	0.37	0.00	0.13	0.15
Europium	153	154	155				
Composition [at%]	92.99	7.01	0.00				
Uncertainty	0.52	0.52	0.00				
Gadolinium	154	155	156	157	158		
Composition [at%]	9.70	0.00	79.08	0.00	11.22		
Uncertainty	0.27	0.00	0.41	0.00	0.29		

Date of analyses:
November 2008 (uranium), February 2009 (plutonium, americium), July 2008 (lanthanides).

Table 3-4. Isotopic composition of elements analysed by IDA in fuel sample 3V5-Q13.

Uranium	234	235	236	238			
Composition [at%]	0.0141	0.250	0.590	99.146			
Uncertainty	0.0001	0.001	0.001	0.002			
Plutonium	238	239	240	241	242		
Composition [at%]	4.65	43.76	26.46	12.12	13.01		
Uncertainty	0.13	0.01	0.07	0.05	0.04		
At EOB	4.55	42.79	25.73	14.20	12.73		
Americium	241	243					
Composition [at%]	45.14	54.86					
Uncertainty	1.70	1.70					
Cerium	140	142					
Composition [at%]	50.62	49.38					
Uncertainty	0.14	0.14					
Neodymium	142	143	144	145	146	148	150
Composition [at%]	0.97	13.13	38.46	14.42	19.00	9.42	4.60
Uncertainty	0.03	0.14	0.80	0.28	0.34	0.16	0.16
Samarium	147	148	149	150	151	152	154
Composition [at%]	16.74	27.40	0.00	38.51	0.00	11.62	5.73
Uncertainty	0.05	0.08	0.00	0.44	0.00	0.44	0.13
Europium	153	154	155				
Composition [at%]	86.12	13.88	0.00				
Uncertainty	0.20	0.20	0.00				
Gadolinium	154	155	156	157	158		
Composition [at%]	3.63	0.00	84.56	0.00	11.81		
Uncertainty	0.17	0.00	0.54	0.00	0.42		

Date of analyses:
November 2008 (uranium), February 2009 (plutonium, americium), July 2008 (lanthanides).

Table 3-5. Isotopic composition of elements analysed by IDA in fuel sample SUT3-00477.

Uranium	234	235	236	238			
Composition [at%]	0.0151	0.347	0.584	99.053			
Uncertainty	0.0001	0.001	0.002	0.002			
Plutonium	238	239	240	241	242		
Composition [at%]	4.43	45.64	26.26	11.87	11.79		
Uncertainty	0.09	0.03	0.14	0.03	0.07		
At EOB	4.28	44.12	25.20	15.00	11.40		
Americium	241	243					
Composition [at%]	59.62	40.38					
Uncertainty	3.81	3.81					
Cerium	140	142					
Composition [at%]	50.06	49.94					
Uncertainty	0.46	0.46					
Neodymium	142	143	144	145	146	148	150
Composition [at%]	0.87	14.63	37.37	14.46	19.07	9.14	4.46
Uncertainty	0.01	0.17	0.41	0.12	0.21	0.10	0.19
Samarium	147	148	149	150	151	152	154
Composition [at%]	23.06	25.06	0.00	36.07	0.00	10.63	5.19
Uncertainty	0.23	0.16	0.00	0.75	0.00	0.53	0.15
Europium	153	154	155				
Composition [at%]	86.30	13.70	0.00				
Uncertainty	0.71	0.71	0.00				
Gadolinium	154	155	156	157	158		
Composition [at%]	5.24	0.00	82.84	0.00	11.92		
Uncertainty	0.58	0.00	0.76	0.00	0.25		

Date of analyses:
November 2008 (uranium), February 2009 (plutonium, americium), July 2008 (lanthanides).

Table 3-6. Isotopic composition of elements analysed by IDA in fuel sample AM2-K12.

Uranium	234	235	236	238			
Composition [at%]	0.0188	0.205	0.651	99.125			
Uncertainty	0.0002	0.001	0.004	0.004			
Plutonium	238	239	240	241	242		
Composition [at%]	7.08	44.61	24.82	10.39	13.10		
Uncertainty	0.01	0.14	0.13	0.09	0.07		
At EOB	6.80	42.88	23.39	14.35	12.59		
Americium	241	243					
Composition [at%]	55.30	44.70					
Uncertainty	0.60	0.60					
Cerium	140	142					
Composition [at%]	50.99	49.01					
Uncertainty	0.41	0.41					
Neodymium	142	143	144	145	146	148	150
Composition [at%]	1.09	12.28	39.55	13.62	19.49	9.34	4.64
Uncertainty	0.03	0.24	0.34	0.10	0.48	0.17	0.14
Samarium	147	148	149	150	151	152	154
Composition [at%]	21.81	28.59	0.00	33.42	0.95	9.11	6.12
Uncertainty	0.24	0.24	0.00	0.15	0.06	0.21	0.35
Europium	153	154	155				
Composition [at%]	86.39	13.61	0.00				
Uncertainty	0.41	0.41	0.00				
Gadolinium	154	155	156	157	158		
Composition [at%]	7.92	0.00	79.93	0.00	12.15		
Uncertainty	0.18	0.00	0.30	0.00	0.18		

Date of analyses:
November 2008 (uranium), September 2008 (plutonium, americium), July 2008 (lanthanides).

$^{n}X/^{238}U$ values and nuclide inventories

$^{n}X/^{238}U$ values determined by IDA and nuclide inventories calculated according to the description in Paragraph 2.3.4 are compiled in Table 3-8 to Table 3-11. In the case of nuclides concerned by decay corrections, the value at the date of analysis is reported with the corresponding uncertainty, whereas the uncertainty of the value corrected to the end of the irradiation is not indicated. The uncertainty (1σ) of the *$^{n}X/^{238}U$* values was determined according to the description on page 23. The uncertainty indicated for the inventory corresponds to the same relative value as for *$^{n}X/^{238}U$*. Values used to calculate the factor for converting *$^{n}X/^{238}U$* values into inventory values in $\mu g/gU_{init}$ are compiled in Table 3-7. An error in the conversion of *$^{n}X/^{238}U$* to the inventory value would introduce a systematic deviation, impacting all values by the same factor.

The following corrections for decay between the end of irradiation and the date of the analysis were taken into account:

- Decay of ^{241}Pu into ^{241}Am. Most of the analysed ^{241}Am was formed after the end of the irradiation. Thus, the relative uncertainty of the EOB value is rather large.
- Formation of ^{240}Pu through decay of ^{244}Cm, by subtracting the difference of the ^{244}Cm values at the end of irradiation and at the date of analysis (Table 3-2) from the analysed ^{240}Pu value.
- Formation of ^{144}Nd by decay of ^{144}Ce, starting from the EOB value determined by gamma scanning in the case of sample SUT3-00477 and from the values calculated by CASMO for the other three samples.
- Formation of ^{147}Sm by decay of ^{147}Pm, on the basis of EOB values calculated by CASMO.
- Decay of ^{154}Eu into ^{154}Gd. Most of the analysed ^{154}Gd was formed after the end of the irradiation by this decay.
- Decay of ^{134}Cs and ^{137}Cs. Due to the long decay time, the amount of ^{134}Cs in sample 4I8-Q12 was below the detection limit at the date of analysis.

The analysed amount of ^{140}Ce also includes the amount of ^{140}Ba/La present at the end of irradiation. According to CASMO calculations, this is less than 1%. Therefore, and because the cerium determination by IDA seems to be impacted by unidentified problems, no attempt for a corresponding decay correction was made.

The amount of some nuclides with large cross sections for thermal neutron capture was below the detection limit indicated in the tables. This concerned the following nuclides (thermal neutron capture cross sections in barn or 10^{-24} cm^2 from /Magill 2006/): ^{149}Sm (40100), ^{151}Sm (15200), ^{155}Eu (3900), ^{155}Gd (61000) and ^{157}Gd (254000).

A contamination of the eluent with natural barium in the caesium analysis of sample 3V5-Q13 led to a high background and to a larger uncertainty, in particular for ^{134}Cs.

Table 3-7. Data used for converting nX/238U values into inventory values.

Sample	4I8-Q12	3V5-Q13	SUT3-00477	AM2-K12
Amount of initial ^{238}U left (CASMO) [%]	95.29	94.71	95.07	93.82
Initial ^{235}U enrichment [%]	3.60	3.80	3.70	4.00
Conversion factor *$^{n}X/^{238}U$* to $\mu g/gU_{init}$	918580	911071	915546	900669

Table 3-8. $^{n}X/^{238}U$ values and nuclide inventories determined by IDA in sample 4I8-Q12.

Uranium	234	235	236	238			
$^{n}X/^{238}U$ value [wt%]	0.0175	0.401	0.578				
Uncertainty	0.0004	0.006	0.008				
Inventory [µg/gU$_{init}$]	161	3,682	5,313	918,580			
Uncertainty	4	54	77	9,254			
Plutonium	238	239	240	241	242		
$^{n}X/^{238}U$ value [wt%]	0.045	0.548	0.334	0.089	0.133		
Uncertainty	0.001	0.009	0.006	0.002	0.003		
at EOB			0.329	0.180			
Inventory [µg/gU$_{init}$]	418	5,035	3,065	813	1,219		
Uncertainty	9	80	51	14	23		
at EOB			3,022	1,653			
Americium	241	243					
$^{n}X/^{238}U$ value [wt%]	0.107	0.034					
Uncertainty	0.002	0.001					
at EOB	0.016						
Inventory [µg/gU$_{init}$]	984	316					
Uncertainty	15	12					
at EOB	144						
Cerium	140	142					
$^{n}X/^{238}U$ value [wt%]	0.179	0.184					
Uncertainty	0.017	0.017					
Inventory [µg/gU$_{init}$]	1,647	1,693					
Uncertainty	153	154					
Neodymium	142	143	144	145	146	148	150
$^{n}X/^{238}U$ value [wt%]	0.0055	0.106	0.257	0.106	0.131	0.066	0.033
Uncertainty	0.0002	0.003	0.005	0.002	0.002	0.002	0.001
at EOB			0.227				
Inventory [µg/gU$_{init}$]	51	974	2,361	972	1,206	610	301
Uncertainty	2	28	47	18	18	15	12
at EOB			2,085.3				
Samarium	147	148	149	150	151	152	154
$^{n}X/^{238}U$ value [wt%]	0.0343	0.0329	<0.00008	0.0498	<0.00008	0.0159	0.0070
Uncertainty	0.0013	0.0012		0.0019		0.0005	0.0003
at EOB	0.0166						
Inventory [µg/gU$_{init}$]	315	302	<1	457	<1	146	64
Uncertainty	12	11		17		5	3
at EOB	153						
Europium	153	154	155				
$^{n}X/^{238}U$ value [wt%]	0.0180	0.0014	<0.00007				
Uncertainty	0.0005	0.0001					
at EOB		0.0041					
Inventory [µg/gU$_{init}$]	165	13	<1				
Uncertainty	5	1					
at EOB		38					
Gadolinium	154	155	156	157	158		
$^{n}X/^{238}U$ value [wt%]	0.0031	<0.00008	0.0255	<0.00008	0.0037		
Uncertainty	0.0001		0.0008		0.0001		
at EOB	0.0003						
Inventory [µg/gU$_{init}$]	28	<1	234	<1	34		
Uncertainty	1		7		1		
at EOB	3						
Caesium	133	134	135	137			
$^{n}X/^{238}U$ value [wt%]	0.182	<0.0002	0.068	0.156			
Uncertainty	0.003		0.001	0.002			
at EOB				0.219			
Inventory [µg/gU$_{init}$]	1,675	<2	627	1,431			
Uncertainty	26		10	21			
at EOB				2,010			

Date of analyses:
November 2008 (uranium), February 2009 (plutonium, americium), July 2008 (lanthanides).

Table 3-9. $^{n}X/^{238}U$ values and nuclide inventories determined by IDA in sample 3V5-Q13.

Uranium	234	235	236	238			
$^{n}X/^{238}U$ value [wt%]	0.0140	0.249	0.590				
Uncertainty	0.0003	0.004	0.009				
Inventory [µg/gU$_{init}$]	127	2,265	5,373	911,071			
Uncertainty	3	34	78	9,157			
Plutonium	238	239	240	241	242		
$^{n}X/^{238}U$ value [wt%]	0.057	0.534	0.324	0.149	0.161		
Uncertainty	0.002	0.008	0.005	0.002	0.002		
at EOB			0.322	0.179			
Inventory [µg/gU$_{init}$]	515	4,864	2,954	1,358	1,465		
Uncertainty	16	74	46	21	23		
at EOB			2,937	1,627			
Americium	241	243					
$^{n}X/^{238}U$ value [wt%]	0.041	0.050					
Uncertainty	0.004	0.006					
at EOB	0.011						
Inventory [µg/gU$_{init}$]	369	452					
Uncertainty	35	52					
at EOB	100						
Cerium	140	142					
$^{n}X/^{238}U$ value [wt%]	0.232	0.230					
Uncertainty	0.004	0.004					
Inventory [µg/gU$_{init}$]	2,116	2,093					
Uncertainty	41	40					
Neodymium	142	143	144	145	146	148	150
$^{n}X/^{238}U$ value [wt%]	0.0077	0.105	0.308	0.116	0.154	0.078	0.038
Uncertainty	0.0003	0.003	0.010	0.004	0.002	0.002	0.002
at EOB			0.274				
Inventory [µg/gU$_{init}$]	70	952	2,808	1,060	1,407	707	350
Uncertainty	3	25	89	32	22	21	14
at EOB			2,500				
Samarium	147	148	149	150	151	152	154
$^{n}X/^{238}U$ value [wt%]	0.0253	0.0417	<0.00004	0.0595	<0.00004	0.0182	0.0091
Uncertainty	0.0011	0.0018		0.0027		0.0004	0.0005
at EOB	0.0147						
Inventory [µg/gU$_{init}$]	231	380	<1	542	<1	166	83
Uncertainty	10	17		25		4	4
at EOB	134						
Europium	153	154	155				
$^{n}X/^{238}U$ value [wt%]	0.0210	0.0034	<0.00003				
Uncertainty	0.0003	0.0001					
at EOB		0.0044					
Inventory [µg/gU$_{init}$]	191	31	<1				
Uncertainty	3	1					
at EOB		40					
Gadolinium	154	155	156	157	158		
$^{n}X/^{238}U$ value [wt%]	0.0015	<0.00004	0.0351	<0.00004	0.0050		
Uncertainty	0.0001		0.0007		0.0002		
at EOB	0.0005						
Inventory [µg/gU$_{init}$]	14	<1	320	<1	45		
Uncertainty	1		6		2		
at EOB	5						
Caesium	133	134	135	137			
$^{n}X/^{238}U$ value [wt%]	0.218	0.0159	0.076	0.249			
Uncertainty	0.006	0.0055	0.002	0.004			
at EOB		0.058		0.272			
Uncertainty		0.020					
Inventory [µg/gUinit]	1,989	145	692	2,265			
Uncertainty	58	50	22	40			
at EOB		527		2,474			
Uncertainty		181					

Date of analyses:
November 2008 (uranium), February 2009 (plutonium, americium), July 2008 (lanthanides).

Table 3-10. $^{n}X/^{238}U$ values and nuclide inventories determined by IDA in sample SUT3-00477.

Uranium	234	235	236	238			
$^{n}X/^{238}U$ value [wt%]	0.0150	0.346	0.584				
Uncertainty	0.0004	0.005	0.009				
Inventory [µg/gU$_{init}$]	138	3,171	5,349	915,546			
Uncertainty	4	47	78	9,202			
Plutonium	238	239	240	241	242		
$^{n}X/^{238}U$ value [wt%]	0.056	0.584	0.338	0.153	0.153		
Uncertainty	0.001	0.008	0.005	0.002	0.002		
at EOB			0.335	0.200			
Inventory [µg/gU$_{init}$]	517	5,349	3,091	1,403	1,400		
Uncertainty	13	76	47	20	22		
at EOB			3,068	1,834			
Americium	241	243					
$^{n}X/^{238}U$ value [wt%]	0.058	0.040					
Uncertainty	0.009	0.009					
at EOB	0.011						
Inventory [µg/gU$_{init}$]	533	364					
Uncertainty	83	82					
at EOB	101						
Cerium	140	142					
$^{n}X/^{238}U$ value [wt%]	0.200	0.202					
Uncertainty	0.012	0.012					
Inventory [µg/gU$_{init}$]	1,832	1,854					
Uncertainty	111	110					
Neodymium	142	143	144	145	146	148	150
$^{n}X/^{238}U$ value [wt%]	0.0065	0.110	0.283	0.110	0.146	0.071	0.035
Uncertainty	0.0001	0.002	0.006	0.002	0.002	0.002	0.002
at EOB			0.247				
Inventory [µg/gU$_{init}$]	60	1,006	2,588	1,008	1,339	650	322
Uncertainty	1	22	55	20	19	14	15
at EOB			2,265				
Samarium	147	148	149	150	151	152	154
$^{n}X/^{238}U$ value [wt%]	0.0350	0.0383	<0.00007	0.0559	<0.00007	0.0167	0.0083
Uncertainty	0.0021	0.0022		0.0034		0.0005	0.0005
at EOB	0.0211						
Inventory [µg/gU$_{init}$]	320	351	<1	512	<1	153	76
Uncertainty	19	20		31		4	5
at EOB	193						
Europium	153	154	155				
$^{n}X/^{238}U$ value [wt%]	0.0201	0.0032	<0.00007				
Uncertainty	0.0004	0.0002					
at EOB		0.0047					
Inventory [µg/gU$_{init}$]	184	29	<1				
Uncertainty	4	2					
at EOB		43					
Gadolinium	154	155	156	157	158		
$^{n}X/^{238}U$ value [wt%]	0.0020	<0.00008	0.0318	<0.00008	0.0046		
Uncertainty	0.0002		0.0007		0.0001		
at EOB	0.0005						
Inventory [µg/gU$_{init}$]	18	<1	291	<1	42		
Uncertainty	2		6		1		
at EOB	4						
Caesium	133	134	135	137			
$^{n}X/^{238}U$ value [wt%]	0.193	0.0054	0.070	0.210			
Uncertainty	0.003	0.0003	0.001	0.003			
at EOB		0.036		0.239			
Uncertainty		0.002					
Inventory [µg/gUinit]	1,769	49	641	1,924			
Uncertainty	29	3	10	30			
at EOB		329		2,191			
Uncertainty		21					

Date of analyses:
November 2008 (uranium), February 2009 (plutonium, americium), July 2008 (lanthanides).

Table 3-11. $^{n}X/^{238}U$ values and nuclide inventories determined by IDA in sample AM2-K12.

Uranium	234	235	236	238			
$^{n}X/^{238}U$ value [wt%]	0.0187	0.205	0.651				
Uncertainty	0.0004	0.003	0.010				
Inventory [µg/gU$_{init}$]	168	1,842	5,867	900,669			
Uncertainty	4	28	90	9,090			
Plutonium	238	239	240	241	242		
$^{n}X/^{238}U$ value [wt%]	0.101	0.639	0.357	0.150	0.190		
Uncertainty	0.001	0.009	0.006	0.003	0.003		
at EOB			0.350	0.215			
Inventory [µg/gU$_{init}$]	909	5,751	3,213	1,351	1,709		
Uncertainty	13	82	50	23	26		
at EOB			3,150	1,940			
Americium	241	243					
$^{n}X/^{238}U$ value [wt%]	0.077	0.063					
Uncertainty	0.002	0.002					
at EOB	0.011						
Inventory [µg/gU$_{init}$]	691	563					
Uncertainty	16	19					
at EOB	102						
Cerium	140	142					
$^{n}X/^{238}U$ value [wt%]	0.267	0.261					
Uncertainty	0.009	0.008					
Inventory [µg/gU$_{init}$]	2,408	2,347					
Uncertainty	81	74					
Neodymium	142	143	144	145	146	148	150
$^{n}X/^{238}U$ value [wt%]	0.0102	0.116	0.376	0.130	0.188	0.091	0.046
Uncertainty	0.0004	0.004	0.011	0.004	0.003	0.003	0.002
at EOB			0.355				
Inventory [µg/gU$_{init}$]	92	1,043	3,382	1,172	1,690	821	413
Uncertainty	4	37	102	35	25	28	17
at EOB			3,198				
Samarium	147	148	149	150	151	152	154
$^{n}X/^{238}U$ value [wt%]	0.0417	0.0551	<0.00006	0.0652	0.0019	0.0180	0.0123
Uncertainty	0.0017	0.0021		0.0025	0.0001	0.0005	0.0009
at EOB	0.0304						
Inventory [µg/gU$_{init}$]	376	496	<1	587	17	162	110
Uncertainty	15	19		23	1	5	8
at EOB	274						
Europium	153	154	155				
$^{n}X/^{238}U$ value [wt%]	0.0240	0.0038	<0.00006				
Uncertainty	0.0004	0.0001					
at EOB		0.0068					
Inventory [µg/gU$_{init}$]	216	34	<1				
Uncertainty	3	1					
at EOB		61					
Gadolinium	154	155	156	157	158		
$^{n}X/^{238}U$ value [wt%]	0.0049	<0.00007	0.0501	<0.00007	0.0077		
Uncertainty	0.0001		0.0008		0.0002		
at EOB	0.0019						
Inventory [µg/gU$_{init}$]	44	<1	451	<1	69		
Uncertainty	1		7		2		
at EOB	17						
Caesium	133	134	135	137			
$^{n}X/^{238}U$ value [wt%]	0.248	0.0026	0.096	0.244			
Uncertainty	0.004	0.0001	0.002	0.004			
at EOB		0.040		0.294			
Uncertainty		0.001					
Inventory [µg/gUinit]	2,233	24	868	2,200			
Uncertainty	36	1	14	35			
at EOB		356		2,646			
Uncertainty		11					

Date of analyses:
November 2008 (uranium), September 2008 (plutonium, americium), July 2008 (lanthanides).

Burnup

The results of burnup determination as described on page 25ff are compiled in Table 3-12. Weight factors proportional to the reciprocal absolute error were used for calculating the different weighted average values. Due to the low error compared to other individual values, the weighted average is somewhat dominated by ^{235}U. The indicated uncertainties do not include any uncertainty of CASMO calculations. The overall weighted average values were used in plots and calculations related to this report.

Even if individual values are different in the strict sense in some cases, considering the indicated (1σ) uncertainties, the overall picture is rather consistent. The overall average values from IDA based data agree with values based on gamma scanning given in Table 2-1, which have an uncertainty in the order of 5%.

Table 3-12. Burnup values based on comparison of experimental data with CASMO calculations.

Burnup [MWd/kgU]		4I8-Q12	3V5-Q13	SUT3-00477	AM2-K12
based on	$^{146}Nd/^{238}U$	55.3±0.7	63.3±0.8	60.6±0.7	73.7±0.9
	$^{148}Nd/^{238}U$	54.6±1.3	63.2±1.8	58.1±1.2	73.8±2.4
	$^{150}Nd/^{238}U$	54.4±1.9	63.0±2.2	58.1±2.3	73.2±2.6
Weighted average Nd values		54.9±0.8	63.2±1.0	59.4±0.9	73.6±1.2
based on	^{235}U abundance	57.5±0.3	66.9±0.3	61.1±0.3	76.0±0.3
	^{239}Pu abundance	62.2±0.6	67.8±0.8	63.7±0.7	73.9±1.6
Overall weighted average		58.2±0.3	66.5±0.4	61.4±0.4	75.4±0.7

3.1.4 Comparison of experimental data to CASMO calculations

Experimentally determined $^{n}X/^{238}U$ values, decay corrected to the end of irradiation, if necessary, are compared to CASMO based data in Figure 3-3 to Figure 3-13. Experimental data from Table 3-1, Table 3-2 and Table 3-8 to Table 3-11 are represented by symbols, whereas CASMO data, individually calculated for each sample, are shown by solid lines in the corresponding colour. The burnup for plotting the experimental values is the weighted overall average value from Table 3-12.

The comparison of experimental ^{234}U and ^{236}U values with CASMO results (Figure 3-3) indicates that these nuclides might have been slightly overestimated in IDA. The measurement of the isotopic composition of uranium with the Studsvik instrument is rather demanding, because the dominating ^{238}U is measured in a different mode than all other isotopes. A small deficiency in the intercalibration of the two modes leads to a systematic error, which not only impacts ^{234}U and ^{236}U, but ^{235}U as well. Because the isotopic ^{235}U content was one of the parameters used for determining the sample burnup, the systematic error would have caused a slight underestimation of the burnup value the data in Figure 3-3 are plotted against.

The experimental americium values shown in Figure 3-5 agree astonishingly well with calculated data. Even if the relative differences in the ^{241}Am values are quite large, they are smaller than the uncertainty in the experimental data. It should be kept in mind that the amount of ^{241}Am at the end of the irradiation is only a small portion of the amount present at the date of analysis.

The experimentally determined contents of cerium are systematically lower than the calculated values (Figure 3-6). Moreover, the isotopic ratios of ^{140}Ce and ^{142}Ce deviate significantly from the calculation. This is most probably due to experimental difficulties in IDA of cerium that had occurred in the past already from time to time. So far, the reason for these difficulties has not been identified.

The neodymium data (Figure 3-7) exhibit a consistent overall picture. Only in the case of ^{145}Nd and, to a certain extent, ^{143}Nd, a systematic difference between experiment and calculation is observed.

Considering the large thermal neutron capture cross sections involved in formation and consumption of many samarium nuclides, the experimental and calculated data agree well (Figure 3-8). When assessing the ^{147}Sm data, it should be kept in mind that a large portion of the analysed amount was formed through decay of ^{147}Pm and that the corresponding correction was based on calculated ^{147}Pm data.

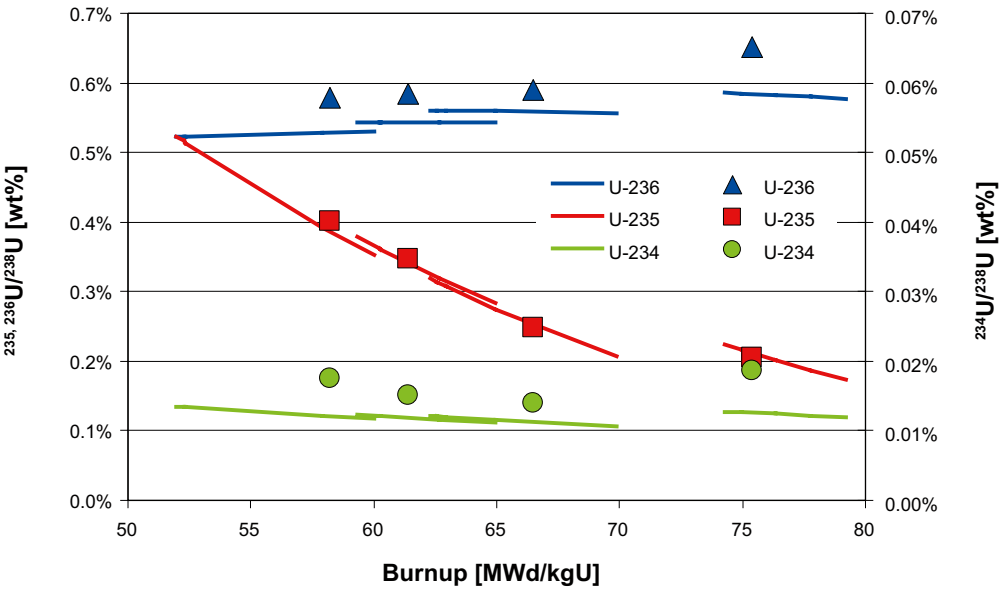

Figure 3-3. *Comparison of experimental and calculated $^{n}X/^{238}U$ values; uranium isotopes.*

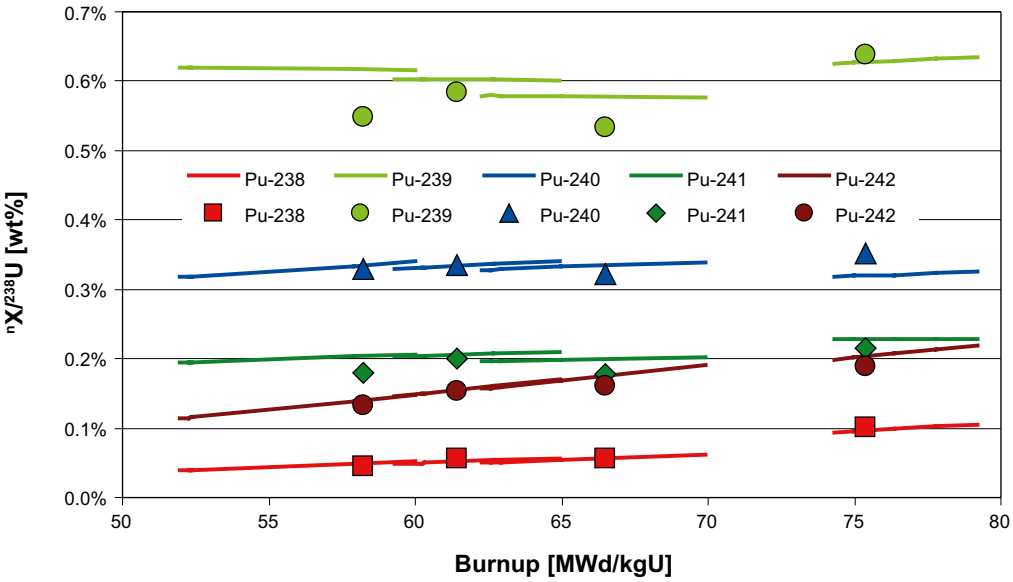

Figure 3-4. *Comparison of experimental and calculated $^{n}X/^{238}U$ values; plutonium isotopes.*

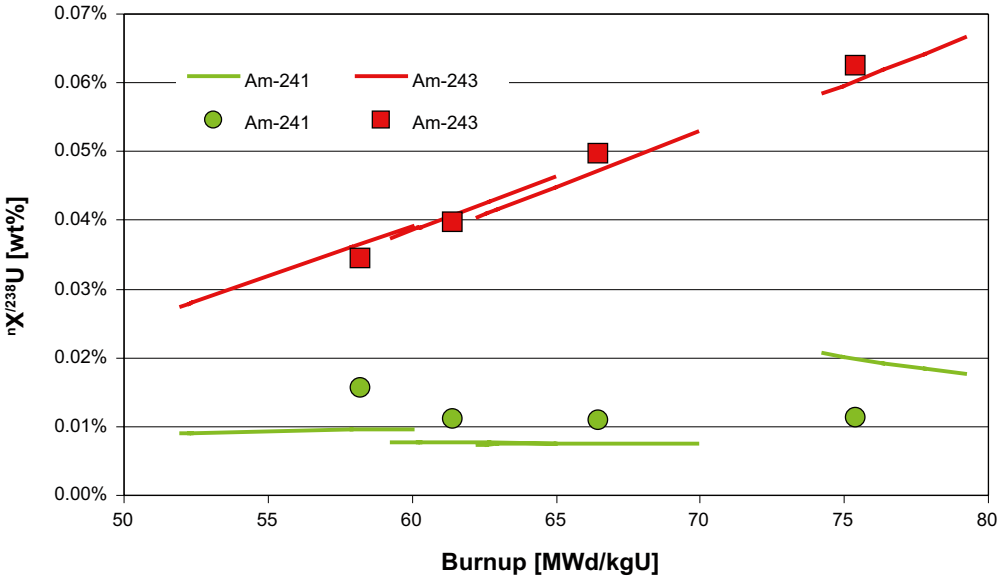

Figure 3-5. *Comparison of experimental and calculated $^{n}X/^{238}U$ values; ^{241}Am and ^{243}Am.*

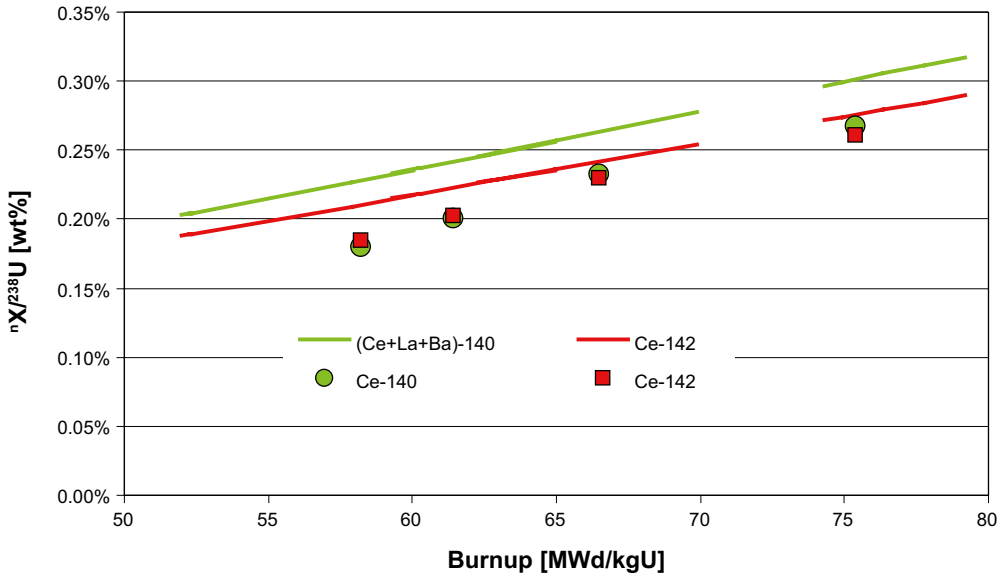

Figure 3-6. *Comparison of experimental and calculated $^{n}X/^{238}U$ values; cerium isotopes.*

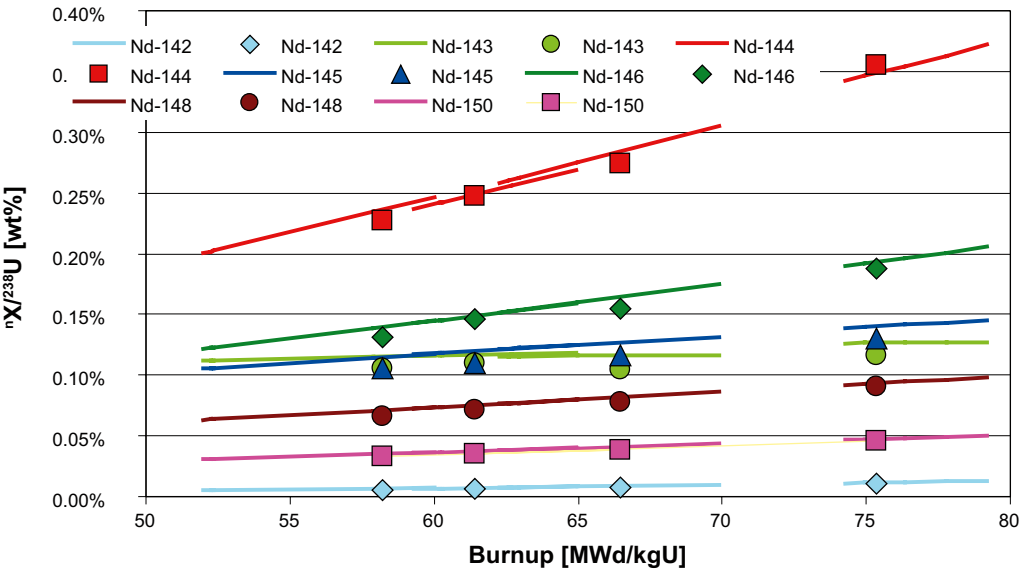

Figure 3-7. *Comparison of experimental and calculated $^{n}X/^{238}U$ values; neodymium isotopes.*

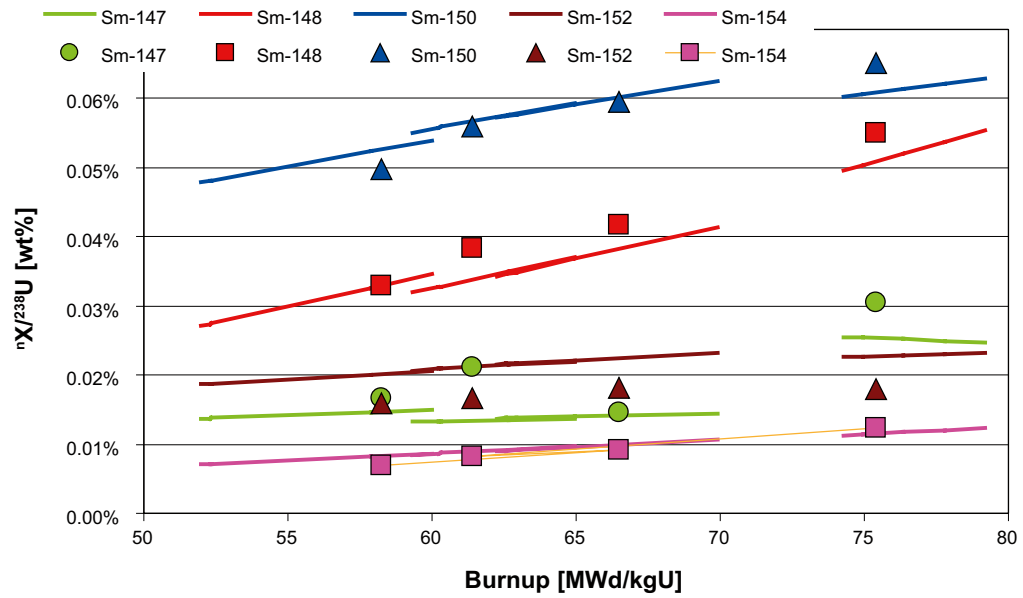

Figure 3-8. *Comparison of experimental and calculated $^{n}X/^{238}U$ values; samarium isotopes.*

^{154}Eu contents based on IDA and on gamma scan agree quite well, despite the low inventory (Figure 3-9). This indicates that IDA results should be reliable. In addition to ^{154}Eu, even experimental ^{156}Gd data agree well with calculations, in contrast to ^{153}Eu, ^{154}Gd and ^{158}Gd, which indicates that modelling of these isotopes might be challenging.

With a few exceptions, IDA, one-point analysis and gamma scanning caesium results are consistent with each other and with calculated data (Figure 3-10). The uncertainty of the ^{134}Cs IDA value of sample 3V5-Q13 (burnup 66.5 MWd/kgU) is 0.02% (Table 3-9), which corresponds to the deviation from the calculated value. The gamma scan ^{134}Cs data agree quite well with the CASMO predictions. No reason could be identified for the high ^{137}Cs IDA value in sample AM2-K12 (burnup 75.4 MWd/kgU). The high ^{133}Cs values in the same sample could be a consequence of a contamination of the sample with natural caesium.

^{244}Cm and ^{246}Cm experimental data are consistent with each other, but they are systematically lower than the calculations. Analysed ^{244}Cm values are about 60% of the predicted ones, ^{246}Cm values are 65–80% lower.

The experimental ^{99}Tc data are of no practical value. Comparison with calculations confirms that technetium was only partly dissolved, with a significant portion remaining in the undissolved alloy particles. Excellent agreement is observed between calculated and experimental ^{139}La and ^{237}Np data (Figure 3-12).

Figure 3-13 compares some experimental $^{n}X/^{238}U$ values of nuclides determined by gamma scan with calculated data. The agreement is quite good.

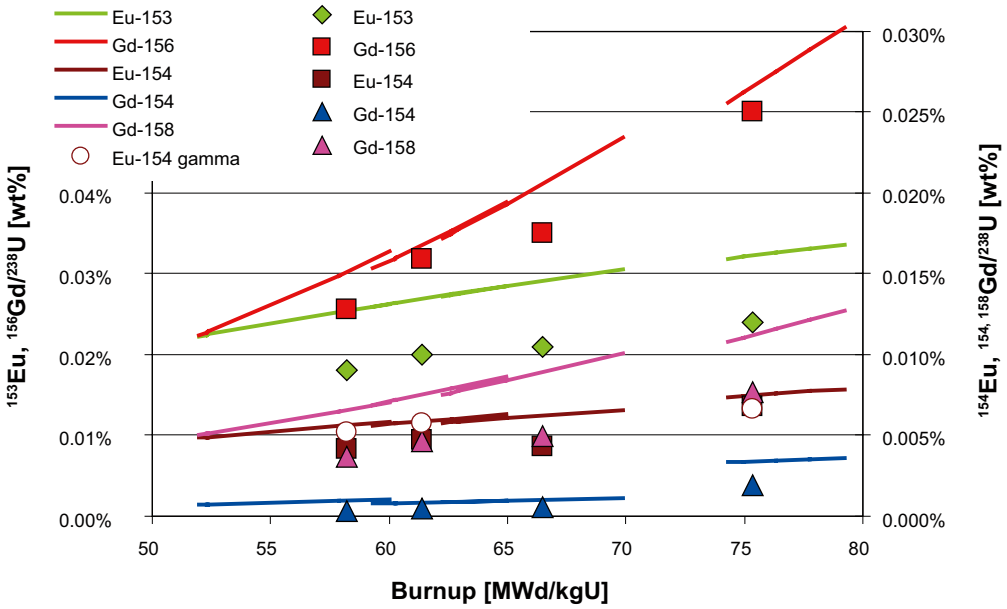

Figure 3-9. *Comparison of experimental and calculated $^{n}X/^{238}U$ values; europium and gadolinium isotopes.*

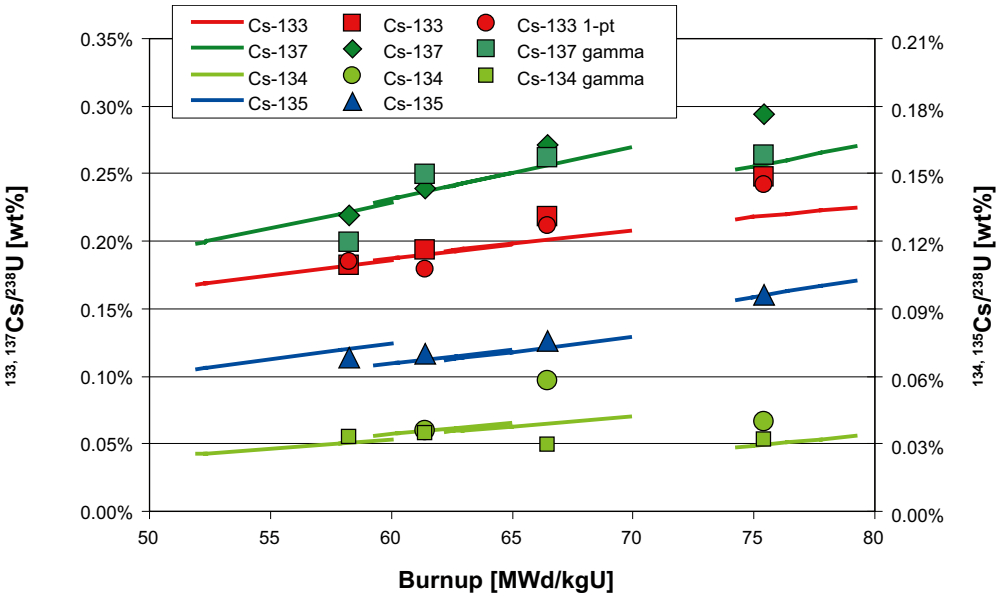

Figure 3-10. *Comparison of experimental and calculated $^{n}X/^{238}U$ values; caesium isotopes.*

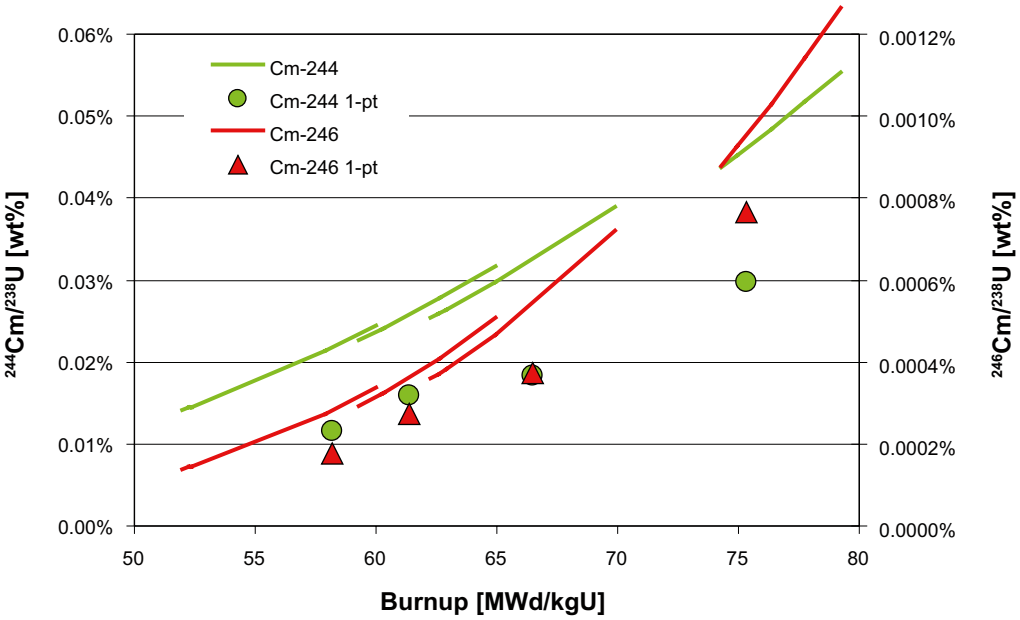

Figure 3-11. *Comparison of experimental and calculated $^{n}X/^{238}U$ values; ^{244}Cm and ^{246}Cm determined by one-point calibration analysis.*

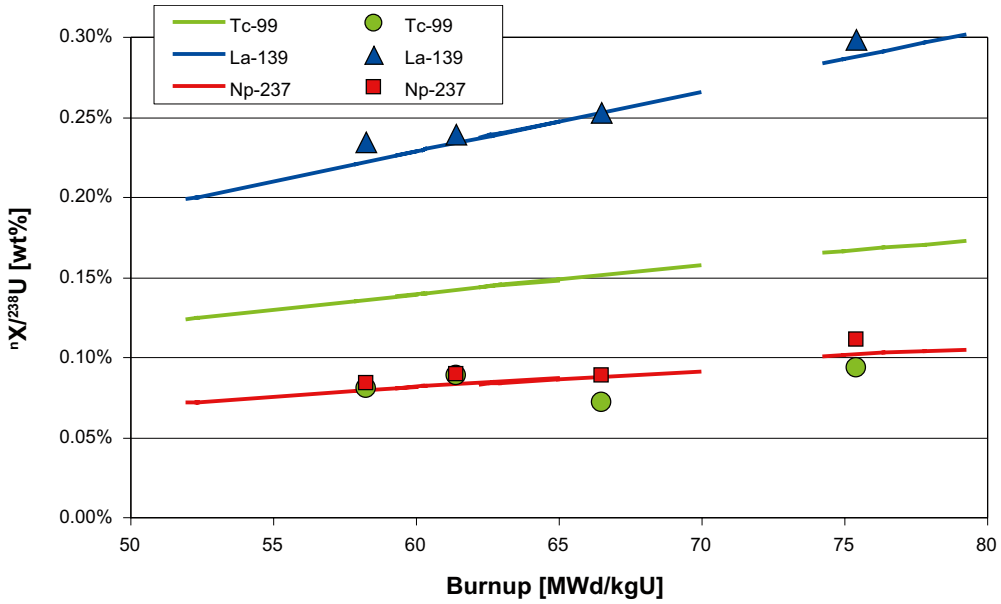

Figure 3-12. *Comparison of experimental and calculated $^{n}X/^{238}U$ values; some isotopes determined by one-point calibration analysis.*

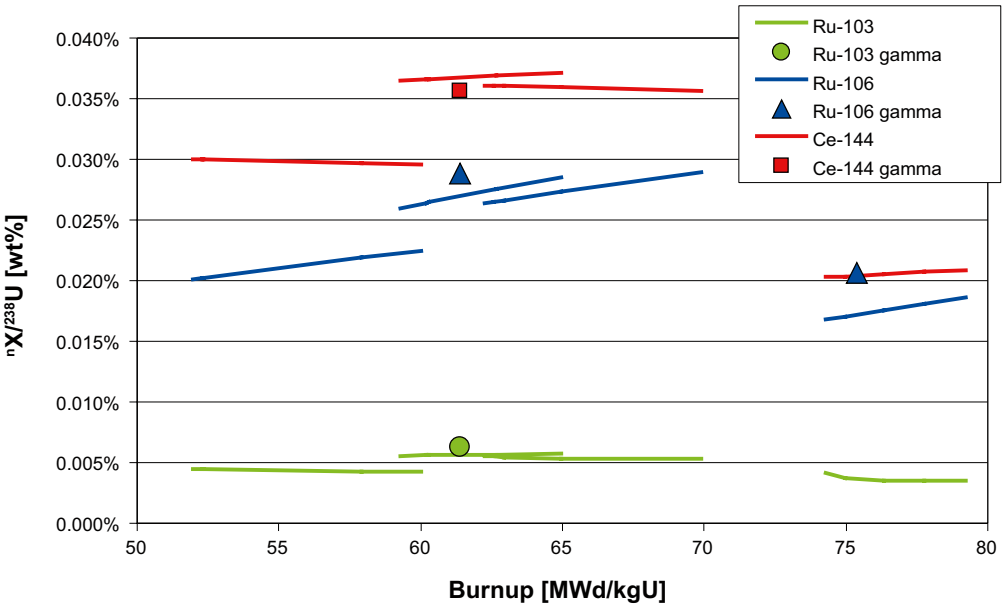

Figure 3-13. *Comparison of experimental and calculated $^{n}X/^{238}U$ values; some nuclides determined by gamma scan.*

3.1.5 Nuclide inventory used for determining release fractions

Nuclide inventories used for determining release fractions in the fuel leaching experiments are compiled in Table 3-13. Experimentally determined values were directly extracted from the tables above. Calculated values are based on CASMO calculated $^{n}X/^{238}U$ values, interpolated for the experimentally determined burnup. Calculated ^{99}Tc values were used, because the experimentally determined values do not include the portion that remained undissolved in the alloy particles. As stated above, analysed cerium values do not seem to be reliable. Therefore, even in the case of ^{140}Ce, release fractions were based on calculated values.

Table 3-13. Nuclide inventories used for determining release fractions.

		Nuclide inventory (end of irradiation) [µg/gU_{init}]			
		4I8-Q12	**3V5-Q13**	**SUT3-00477**	**AM2-K12**
Experimentally determined	^{133}Cs	1,675	1,989	1,769	2,233
	^{135}Cs	627	692	641	868
	^{137}Cs	2,010	2,474	2,191	2,647
	^{139}La	2,150	2,303	2,189	2,689
	^{144}Nd	2,085	2,500	2,265	3,198
	^{153}Eu	165	191	184	216
	^{237}Np	769	812	818	999
	^{239}Pu	5,035	4,868	5,349	5,751
	^{244}Cm	106	167	146	269
Calculated by CASMO	^{85}Rb	161	180	168	214
	^{87}Rb	372	417	390	460
	^{90}Sr	791	889	837	839
	^{99}Tc	1,247	1,383	1,302	1,504
	^{100}Mo	1,638	1,870	1,727	2,118
	^{129}I	268	305	283	347
	^{138}Ba	2,237	2,552	2,359	2,886
	^{140}Ce	2,095	2,397	2,211	2,713
	^{141}Pr	1,847	2,084	1,930	2,366
	^{238}U	918,580	911,071	915,546	900,669

3.2 pH, carbonate concentration

The length of the contact periods, the pH measured in the centrifugate and the carbonate concentration are compiled in Table 3-14. All values are well within corresponding results obtained in the Series 11 experiments.

Table 3-14. Contact period length, pH and carbonate concentration in centrifugate.

		Contact Period #					
		1	**2**	**3**	**4**	**5**	**6**
Contact Period Length [d]		7	22	63	92	182	370
pH	3V5-Q13	8.30	8.17	8.50	8.15	8.13	8.38
	AM2-K12	8.08	8.18	8.26	8.18	8.10	8.46
	SUT3-00477	8.06	8.10	8.22	8.47	8.01	
	4I8-Q12	8.00	8.02	8.18	8.41	8.15	
Carbonate [ppm]	3V5-Q13	126	98	118	117	125	121
	AM2-K12	118	130	119	122	123	129
	SUT3-00477	120	119	132	124	119	
	4I8-Q12	124	121	127	123	123	

3.3 Comparison of ICP-MS and gamma spectrometry (^{137}Cs)

All centrifugates and vessel strip solutions were analysed by ICP-MS and by gamma spectrometry. Comparison of ^{137}Cs concentrations determined by both methods revealed that ICP-MS results are often larger than gamma spectrometry data, as illustrated in Figure 3-14. Only in two cases, in the strip solutions of sample AM2-K12 contact periods 1 and 6, gamma spectrometry resulted in a significantly higher ^{137}Cs concentration than determined by ICP-MS. Although the scatter is significant, ratios (and absolute values) from sibling samples are always close to each other. The ratio of fractional release rates based on ^{137}Cs and ^{133}Cs concentrations, respectively, determined by ICP-MS, follows the same trend as the ratio of ^{137}Cs concentrations determined by ICP-MS and gamma spectrometry. This is illustrated in Figure 3-15. The data shown in Figure 3-14 are sorted by sample identity and plotted separately, together with the ratio of fractional release rates based on ^{137}Cs and ^{133}Cs ICP-MS concentrations. The only obvious exceptions are the two cases from sample AM2-K12 mentioned above. The correlation is somewhat less pronounced, but still very clear, for strip solutions, which can be explained by lower concentrations and larger uncertainties. From these data, it can be concluded that analysis of ^{137}Cs by ICP-MS in solutions from fuel corrosion experiments can be disturbed due to still unidentified reasons. The error exclusively impacts mass 137. The fact that results from sibling solutions form pairs indicates that the reason is not random. Consequently, the cause is in some way related to sample properties and not to the instrument. Fractional release of ^{137}Cs was therefore based on solution concentrations determined by gamma spectrometry.

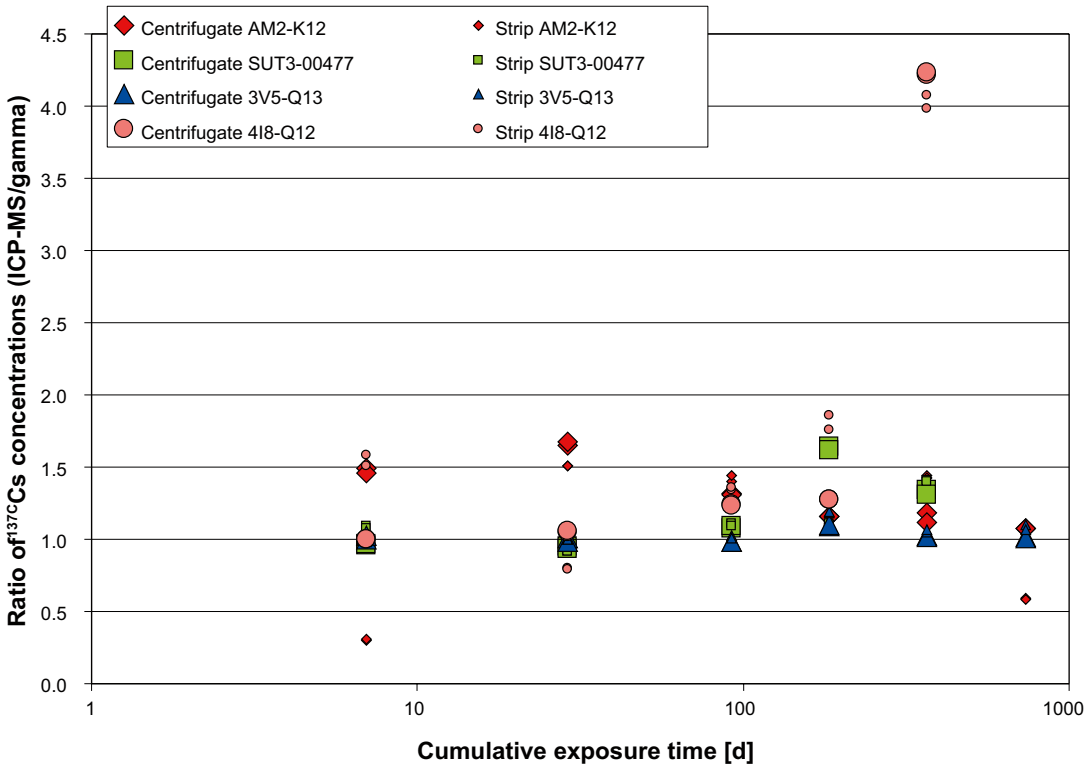

Figure 3-14. *Ratios of ^{137}Cs concentration determined by ICP-MS and gamma spectrometry in centrifugates and in strip solutions, plotted as a function of cumulative exposure.*

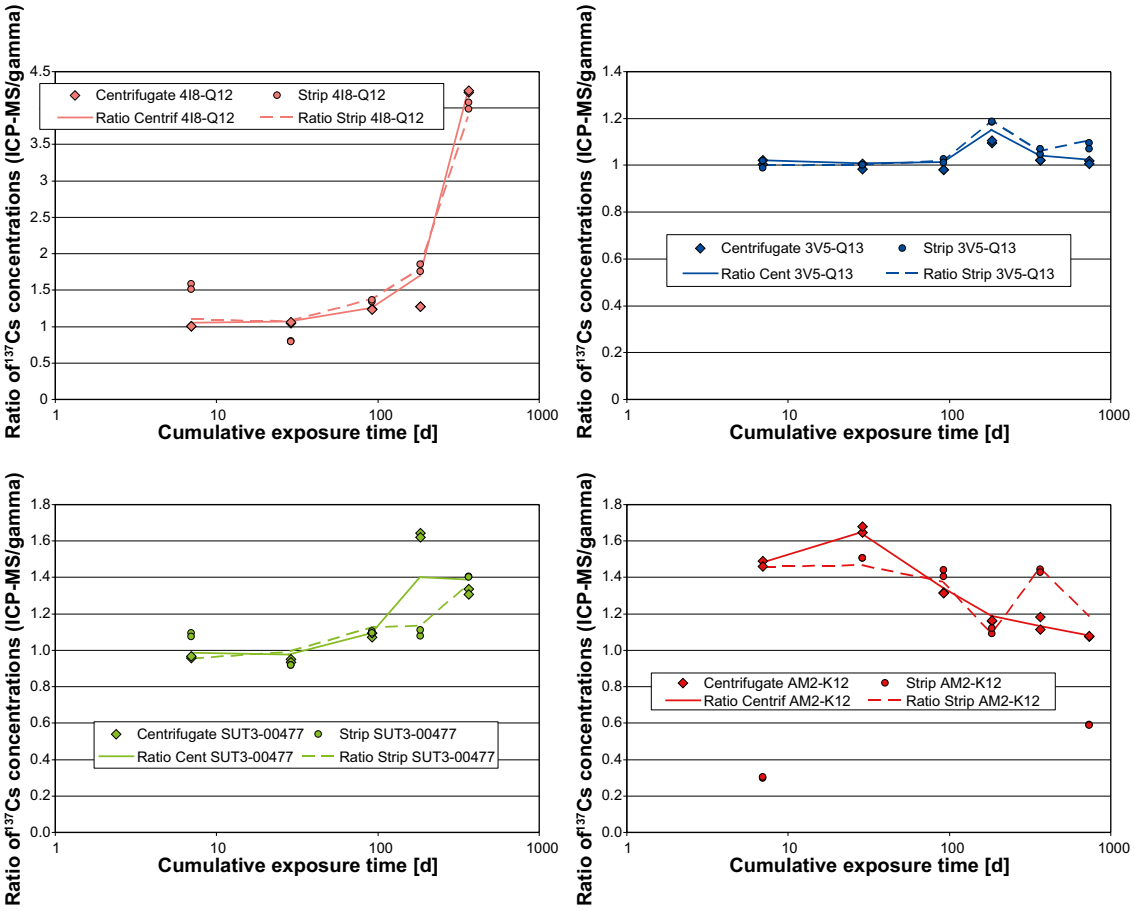

Figure 3-15. *Ratio of ^{137}Cs concentrations analysed by ICP-MS and gamma spectrometry in centrifugates and strip solutions (symbols) and of $^{137}Cs/^{133}Cs$ ratio of fractional release rates based on ICP-MS data for centrifugates (solid lines) and strip solutions (dotted lines).*

3.4 Verification of strontium analysis

Concentrations of ^{90}Sr determined in four centrifugates by ICP-MS as well as by radiometry are compiled in Table 3-15. In Figure 3-16 the same data are plotted against each other, together with a linear regression line passing through the origin.

The data and the plot demonstrate that ICP-MS analysis of ^{90}Sr in solutions from fuel corrosion experiments is reliable and correct, with an uncertainty in the order of 5–10%.

Table 3-15. Comparison of ^{90}Sr concentrations determined in a selection of centrifugates by ICP-MS and by radiometry.

	Concentration determined by radiometry		
Sample identity	**Activity [Bq/ml]**	**Amount [ng/ml]**	**ICP-MS [ng/ml]**
21.1.2	2,436	0.477	0.357
21.1.5	29,435	5.762	5.866
22.1.2	8,729	1.709	1.746
22.1.4	11,165	2.186	2.673

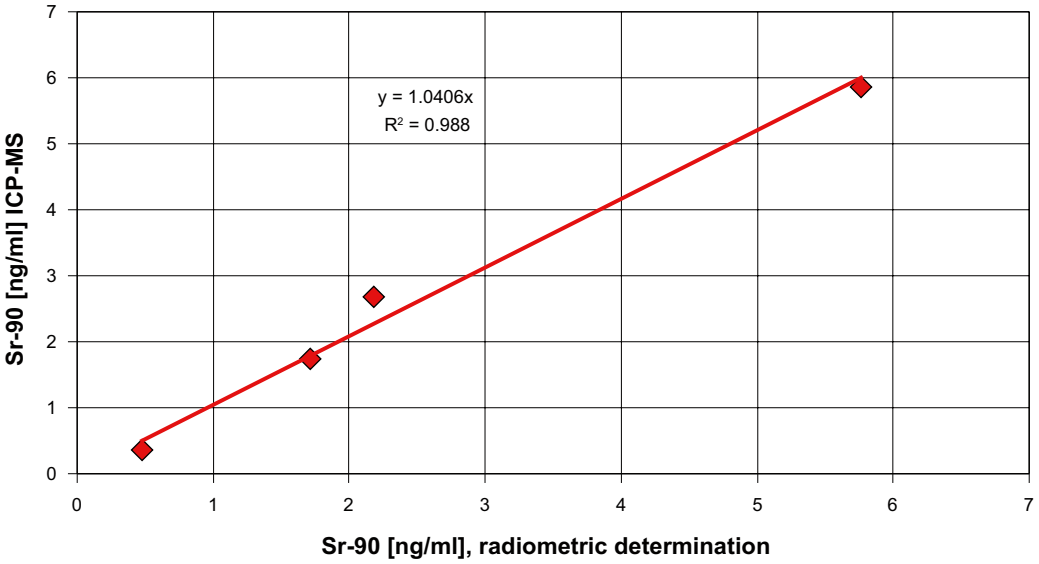

Figure 3-16. *Comparison of ^{90}Sr concentrations determined in a selection of centrifugates by ICP-MS and by radiometry.*

3.5 Concentrations

In order to get the basis for assessing whether the concentration of a nuclide in the leachant was solubility limited, nuclide concentrations determined by ICP-MS were transformed in a first step into nuclide molarity values. Elemental molarities were then calculated for a selection of elements by dividing the nuclide molarity by the corresponding isotopic abundance. The abundance values were taken from the inventory analysis or, if not analysed, from CASMO calculations. Centrifugate molarities are compiled for all contact periods in Table 3-16 to Table 3-19 and plotted in Figure 3-17 to Figure 3-20.

The concentrations of uranium for all contact periods are relatively low (less than $4 \cdot 10^{-6}$ *M*) and quite similar for the four fuel samples investigated. They are much lower than the solubility of the kinetically favoured phase shoepite under such conditions and in good agreement with the concentrations measured with a similar groundwater by /Jégou et al. 2001, 2004/ up to 313 days. Another observation is that they are several (2–10) times lower than the uranium concentrations measured for the 10 fuel samples of series 11 (Figure 3-20) /Forsyth 1997/. These observations indicate that very probably no secondary uranium minerals affect uranium releases in our data.

The lanthanides are most probably not precipitated, but absorbed on glass surfaces, as discussed further in Paragraph 3.7.

Table 3-16. Sample 4I8-Q12, molarity in centrifugate.

Element	Based on	Isotopic Abundance	Molarity in Centrifugate of Contact Period #				
			1	2	3	4	5
Sr	Sr-90	52%	2.91E-08	4.18E-08	7.25E-08	7.20E-08	7.16E-08
Tc	Tc-99	100%	7.99E-08	1.19E-08	1.88E-08	8.54E-09	2.05E-08
Mo	Mo-100	28%	1.41E-07	9.04E-08	1.38E-07	6.49E-08	1.47E-07
Cs	Cs-133	45%	9.33E-06	2.52E-06	2.43E-06	7.25E-07	6.52E-07
Ba	Ba-138	69%	3.74E-08	3.03E-08	1.19E-07	2.66E-07	4.46E-07
La	La-139	100%	3.12E-10	1.87E-10	9.43E-11	7.58E-10	1.38E-09
Ce	Ce-140	50%	1.47E-10	7.92E-11	1.47E-10	2.11E-10	2.04E-10
Pr	Pr-141	100%	2.27E-10	1.58E-10	6.15E-11	5.08E-10	9.94E-10
Nd	Nd-144	37%	7.42E-10	4.92E-10	2.26E-10	2.42E-09	4.24E-09
Eu	Eu-153	93%	2.31E-10	8.26E-11	1.98E-10	2.42E-10	7.66E-10
U	U-238	99%	1.81E-06	1.30E-06	1.90E-06	1.81E-06	3.01E-06
Np	Np-237	100%	1.32E-09	1.22E-09	9.03E-10	1.09E-09	1.30E-09
Pu	Pu-239	48%	2.79E-09	1.73E-09	1.38E-09	1.97E-09	1.19E-09

Table 3-17. Sample 3V5-Q13, molarity in centrifugate.

Element	Based on	Isotopic Abundance	Molarity in Centrifugate of Contact Period #					
			1	2	3	4	5	6
Sr	Sr-90	58%	1.00E-08	6.52E-09	6.97E-08	3.11E-07	1.14E-07	1.82E-07
Tc	Tc-99	100%	3.72E-08	1.03E-08	9.30E-09	4.80E-09	2.93E-09	4.08E-09
Mo	Mo-100	28%	1.64E-07	1.02E-07	8.34E-08	4.53E-08	3.08E-08	3.15E-08
Cs	Cs-133	40%	1.64E-06	5.81E-06	1.24E-05	5.68E-06	4.11E-06	9.27E-06
Ba	Ba-138	80%	1.26E-08	1.45E-08	3.84E-08	8.36E-07	1.54E-07	3.59E-07
La	La-139	100%	1.77E-10	1.48E-10	1.42E-10	1.42E-09	1.28E-09	2.24E-09
Ce	Ce-140	51%	3.46E-10	4.94E-10	5.17E-10	9.98E-10	5.61E-10	2.73E-09
Pr	Pr-141	100%	1.22E-10	8.41E-11	8.58E-11	1.12E-09	9.85E-10	1.81E-09
Nd	Nd-144	37%	3.94E-10	2.90E-10	2.33E-10	4.06E-09	3.91E-09	6.42E-09
Eu	Eu-153	86%	3.04E-11	6.52E-11	1.17E-10	4.82E-10	2.30E-10	3.93E-10
U	U-238	99%	1.24E-06	8.02E-07	1.05E-06	9.55E-07	1.23E-06	1.64E-06
Np	Np-237	100%	7.35E-10	4.28E-10	5.37E-10	9.23E-10	7.13E-10	2.42E-10
Pu	Pu-239	44%	2.46E-09	1.80E-09	1.65E-09	2.59E-09	2.62E-09	1.45E-09

Table 3-18. Sample SUT3-00477, molarity in centrifugate.

Element	Based on	Isotopic Abundance	Molarity in Centrifugate of Contact Period #				
			1	2	3	4	5
Sr	Sr-90	57%	2.99E-08	5.20E-08	3.38E-07	1.10E-07	4.47E-08
Tc	Tc-99	100%	3.41E-08	1.51E-08	1.19E-08	1.96E-08	1.14E-08
Mo	Mo-100	28%	2.34E-07	1.29E-07	9.68E-08	1.33E-07	8.06E-08
Cs	Cs-133	41%	3.34E-06	5.06E-06	5.04E-06	1.51E-06	4.46E-07
Ba	Ba-138	79%	2.03E-08	2.97E-08	3.27E-07	2.17E-07	1.42E-07
La	La-139	100%	3.44E-10	2.22E-10	9.01E-10	2.36E-10	9.36E-10
Ce	Ce-140	50%	2.02E-10	1.60E-10	1.52E-10	1.72E-10	1.18E-10
Pr	Pr-141	100%	3.20E-10	1.57E-10	6.27E-10	1.69E-10	6.37E-10
Nd	Nd-144	37%	1.04E-09	6.21E-10	2.54E-09	7.03E-10	2.99E-09
Eu	Eu-153	86%	5.15E-11	5.09E-11	3.60E-10	4.26E-10	2.47E-10
U	U-238	99%	3.35E-06	2.09E-06	2.77E-06	2.18E-06	1.93E-06
Np	Np-237	100%	3.70E-09	1.87E-09	2.87E-09	1.15E-09	1.26E-09
Pu	Pu-239	46%	6.45E-09	4.82E-09	2.81E-09	1.16E-09	2.03E-09

Table 3-19. Sample AM2-K12, molarity in centrifugate.

Element	Based on	Isotopic Abundance	Molarity in Centrifugate of Contact Period #					
			1	2	3	4	5	6
Sr	Sr-90	52%	1.72E-07	3.88E-08	6.87E-08	5.83E-08	6.51E-08	2.06E-07
Tc	Tc-99	100%	9.31E-09	4.23E-09	4.72E-09	2.70E-09	3.76E-09	6.86E-09
Mo	Mo-100	28%	5.35E-08	2.74E-08	3.78E-08	2.76E-08	4.70E-08	9.05E-08
Cs	Cs-133	43%	3.83E-06	4.00E-07	8.06E-07	1.03E-06	1.60E-06	4.60E-05
Ba	Ba-138	64%	6.86E-07	1.20E-07	1.58E-07	1.31E-07	1.51E-07	1.79E-06
La	La-139	100%	9.23E-09	7.18E-09	8.48E-09	4.48E-09	4.15E-09	4.55E-09
Ce	Ce-140	51%	2.85E-09	8.40E-10	7.81E-10	3.41E-10	3.47E-10	2.83E-10
Pr	Pr-141	100%	8.05E-09	6.59E-09	8.07E-09	4.31E-09	3.92E-09	3.89E-09
Nd	Nd-144	40%	2.37E-08	2.05E-08	2.52E-08	1.42E-08	1.33E-08	1.45E-08
Eu	Eu-153	86%	1.54E-09	9.80E-10	1.19E-09	7.31E-10	7.36E-10	2.33E-09
U	U-238	99%	1.85E-06	1.91E-06	2.86E-06	1.19E-06	1.58E-06	3.24E-06
Np	Np-237	100%	5.21E-10	2.97E-10	3.97E-10	4.49E-10	9.33E-10	1.98E-09
Pu	Pu-239	45%	1.39E-08	1.09E-08	1.28E-08	1.06E-08	1.37E-08	1.55E-08

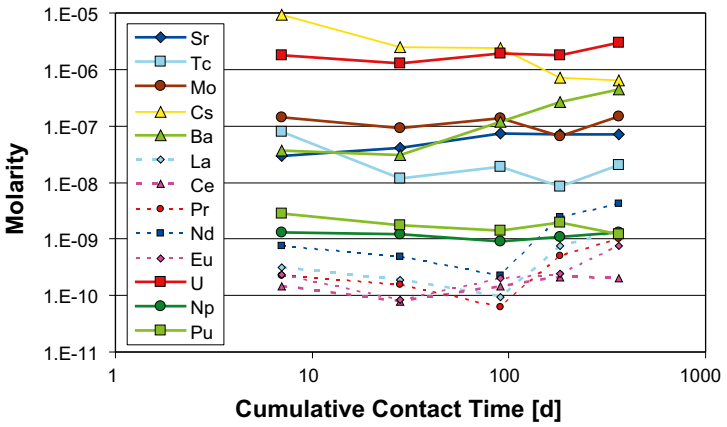

Figure 3-17. *Sample 4I8-Q13, molarity as a function of cumulative contact time.*

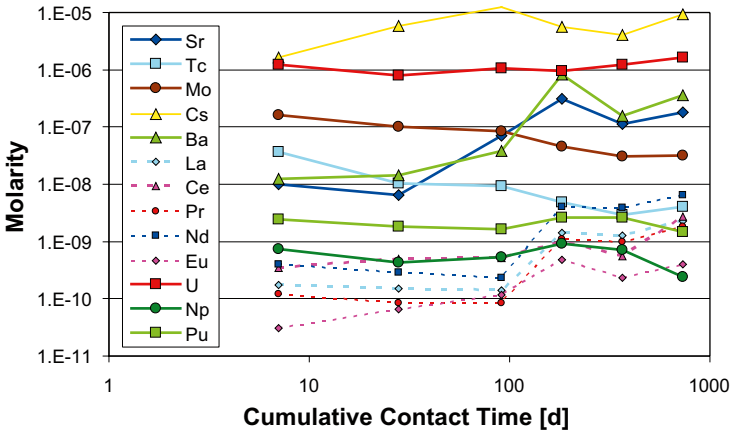

Figure 3-18. *Sample 3V5-Q12, molarity as a function of cumulative contact time.*

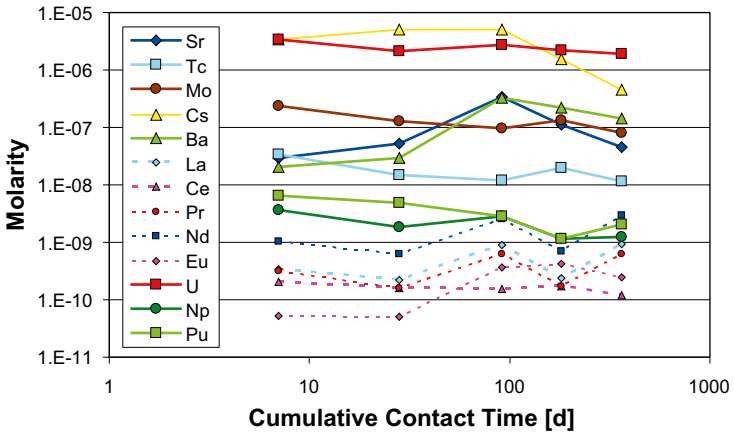

Figure 3-19. *Sample SUT3-00477, molarity as a function of cumulative contact time.*

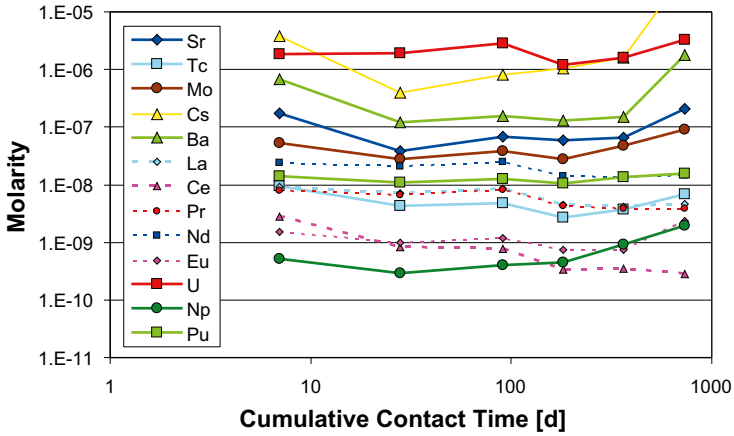

Figure 3-20. *Sample AM2-K12, molarity as a function of cumulative contact time.*

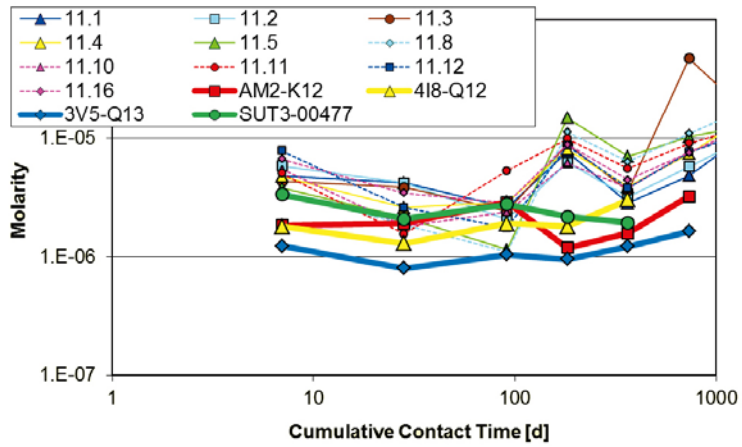

Figure 3-21. *Molarity of uranium as a function of cumulative contact time; comparison of present data with Series 11.*

3.6 Correction of rubidium data

The correction of the ^{85}Rb and ^{87}Rb ICP-MS data for the contribution of natural rubidium was based on the assumption that both nuclides are released from the fuel in the same way and that the isotopic ratio in the leachant is the same as in the fuel inventory. Critical review of the data revealed that this assumption does not seem to be correct. As in the Series 11 experiments, it was found that the corrections were unreasonably large, but in contrast to Series 11, where a standardised rubidium background could be established on the basis of later contact periods, no clear trends were found in the present data. This is illustrated in Figure 3-22, which demonstrates that the applied corrections are significant and shifting over a wide range. In contrast to Series 11 experiments, establishing of standardised rubidium backgrounds was thus not possible. Therefore, release fractions based on uncorrected ^{85}Rb data were included in the tables together with the corrected ones. For ^{87}Rb, release fractions were based on fully corrected data and on concentrations that were corrected for the contribution of natural ^{87}Sr only.

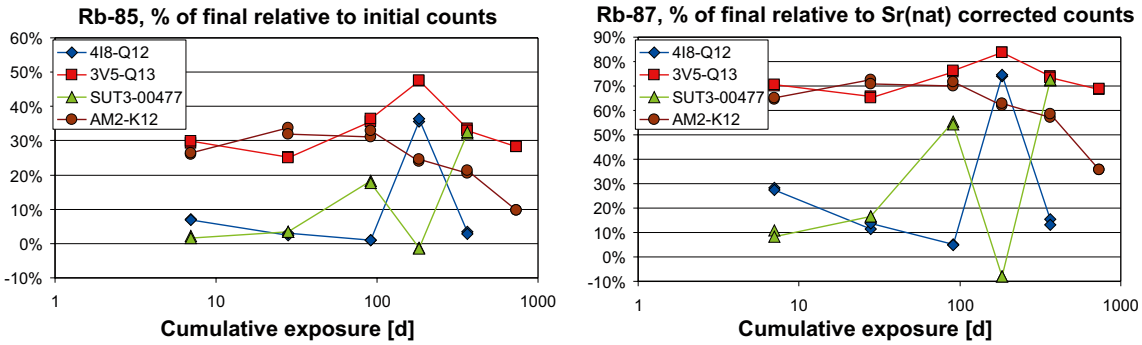

Figure 3-22. *Correction of ICP-MS data for natural rubidium background; percentage of corrected number of counts, relative to number of counts before correction, assuming isotopic composition in released rubidium is similar to composition of rubidium produced by fission.*

3.7 Vessel strip solutions

Nuclides found in the strip solutions stem from several sources:

- They might have been absorbed on the glass surfaces of the flask after having been released from the fuel matrix.
- They stem from fuel fines and grains fallen out from the fuel sample, which were then dissolved in the strip solution.
- A small portion might stem from leaching solution that remained in the flask, before the stripping acid was added.

It is not possible to quantitatively distinguish the different sources, but at least a qualitative assessment is possible, based on a comparison of apparent release fractions of different nuclides with the release fraction of uranium. Even the percentage found in the strip solutions, relative to the sum of centrifugate and strip solution, might be illustrative.

Figure 3-23 shows release fractions for all analysed nuclides, based on vessel strip solutions from all evaluated leaching experiments, plotted as a function of the strip based uranium release fraction. Data from a dissolved fuel particle with a composition corresponding to the nuclide inventory would fall on the 1:1 line. As the burnup and thus the nuclide concentration in the fuel varies significantly over the fuel pellet cross section, data points from a dissolved fuel fragment might deviate from the line up to about a factor of two. In Figure 3-24, selections from the same data are grouped and plotted together. When comparing the neptunium, plutonium and curium data with a similar plot for Series 11 data in /Forsyth 1997/, it becomes obvious that only the neptunium data points follow the 1:1 line in the present work, whereas curium and plutonium data are clearly above the line. This means that curium and neptunium probably are preferentially absorbed on the glass surface of the vessel. The same behaviour is found for lanthanides as well. Rubidium, caesium, strontium and barium found in the strip solutions probably stem from leaching solutions that remained in the flask. Although they seem to dominate the strip solution, the portion found in the strip solution is only small, compared to the total released amount. This is illustrated in Table 3-20 to Table 3-23. Only in the most obvious cases of dissolved fuel fragments, SUT3-00477, contact period 4 (Table 3-22) and AM2-K12, contact period 5 (Table 3-23), a significant portion of these elements was found in the strip solution.

In all cases, a significant portion of the lanthanides (La, Ce, Pr, Nd, Eu) was found in the strip solutions, indicating that a major part of these elements was absorbed on the glass surfaces. Curium and plutonium exhibit roughly the same behaviour as the lanthanides.

Rubidium data in Table 3-20 to Table 3-23 should be interpreted with care, because the portion was calculated on the basis of corrected data. As discussed in Section 3.6, the corrected data do not represent reality.

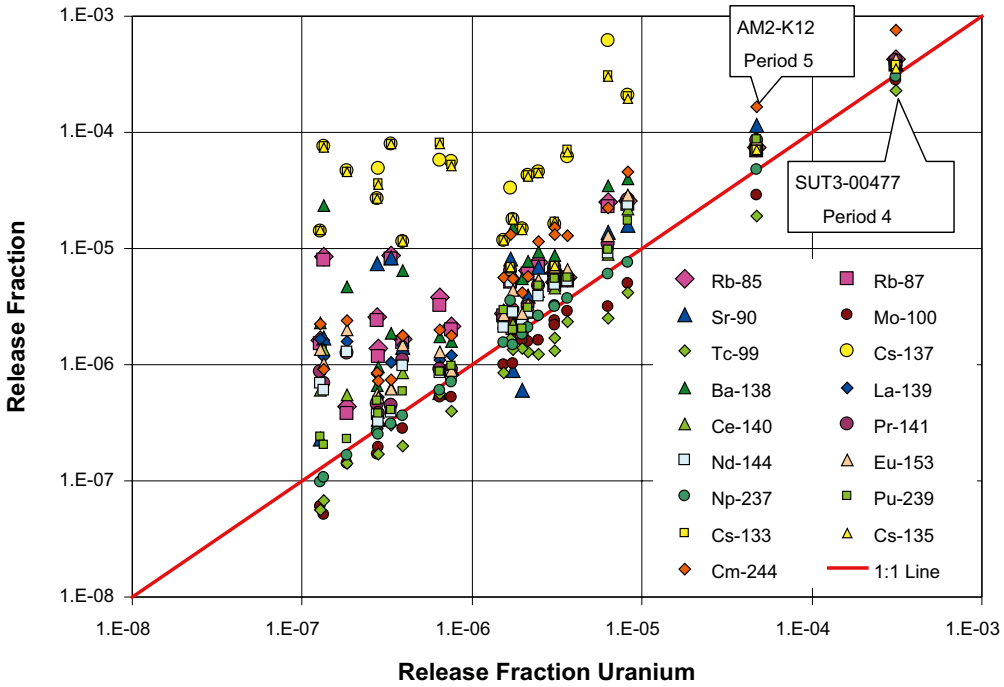

Figure 3-23. *Release fractions for all analysed nuclides, calculated from vessel strip solution concentrations of all evaluated leaching experiments, plotted as a function of the corresponding uranium release fraction.*

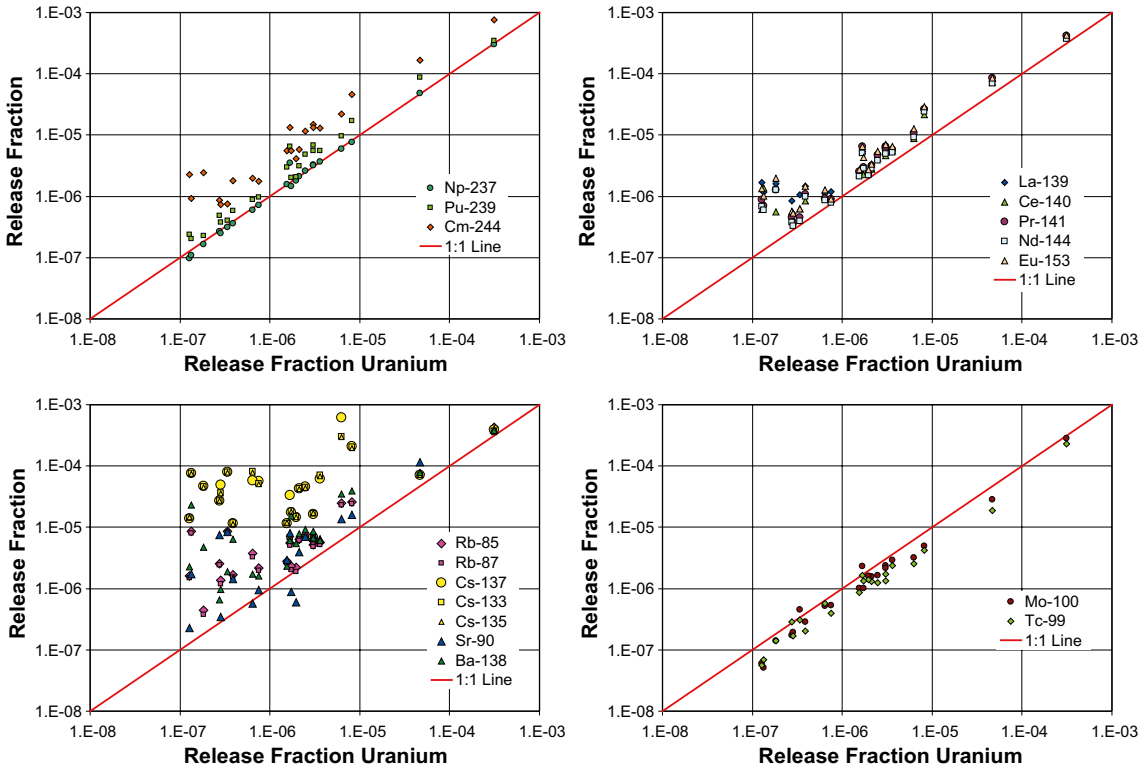

Figure 3-24. *Release fractions for selected groups of nuclides, calculated from vessel strip solution concentrations of all evaluated leaching experiments, plotted as a function of the corresponding uranium release fraction.*

Technetium and molybdenum are not absorbed. Their apparent release fractions in the strip solutions are in general slightly below the 1:1 line.

In addition to the most obvious cases, SUT3-00477, contact period 4 and AM2-K12, contact period 5, many other strip solutions contained probably some dissolved fuel fines, in particular those containing more than 10% of the total uranium. With increasing strip based uranium release fraction, the scatter decreases. The data points get closer to the 1:1 line, onto which they would fall, if a fuel fragment would be dissolved.

Table 3-20. Sample 4I8-Q12, percentage of total amount in glass flask strip solution.

	Contact Period				
Nuclide	**1**	**2**	**3**	**4**	**5**
Rb-85	0.80%	1.66%	1.78%	1.21%	9.44%
Rb-87	0.80%	1.66%	1.78%	1.21%	9.44%
Sr-90	1.07%	0.56%	<0.30%	1.17%	1.40%
Mo-100	0.98%	0.57%	0.27%	6.26%	1.82%
Tc-99	0.41%	0.81%	0.43%	8.55%	3.65%
Cs-133	1.10%	1.82%	2.37%	2.56%	3.49%
Cs-135	1.07%	1.80%	2.36%	2.70%	3.50%
Cs-137	0.74%	2.28%	1.92%	1.51%	0.81%
Ba-138	4.72%	3.29%	4.08%	2.16%	3.52%
La-139	71.42%	66.39%	92.27%	67.49%	61.17%
Ce-140	90.11%	86.98%	83.85%	93.94%	93.80%
Pr-141	70.80%	59.04%	92.54%	73.46%	64.14%
Nd-144	70.13%	57.40%	92.02%	64.98%	57.49%
Eu-153	22.80%	25.37%	34.78%	37.67%	23.20%
U-238	5.96%	3.73%	1.70%	16.20%	9.30%
Np-237	6.35%	2.94%	2.66%	19.81%	14.39%
Pu-239	38.69%	30.45%	24.92%	67.63%	77.23%
Cm-244	82.05%	70.71%	91.25%	60.27%	61.84%

Table 3-21. Sample 3V5-Q13, percentage of total amount in glass flask strip solution.

	Contact Period					
Nuclide	**1**	**2**	**3**	**4**	**5**	**6**
Rb-85	2.16%	0.57%	0.76%	1.29%	1.89%	3.28%
Rb-87	2.16%	0.57%	0.76%	1.29%	1.89%	3.28%
Sr-90	16.97%	44.73%	7.78%	0.39%	2.39%	5.71%
Mo-100	1.79%	0.50%	1.61%	0.33%	13.26%	31.99%
Tc-99	1.41%	1.68%	1.99%	0.88%	21.69%	38.91%
Cs-133	1.18%	0.77%	1.06%	2.19%	1.70%	3.54%
Cs-135	1.19%	0.77%	1.06%	2.19%	1.67%	3.56%
Cs-137	1.15%	0.76%	1.04%	1.92%	1.63%	3.54%
Ba-138	16.04%	4.49%	4.79%	2.78%	4.97%	10.22%
La-139	91.45%	80.70%	84.56%	37.85%	65.84%	90.22%
Ce-140	90.94%	61.54%	64.48%	67.13%	88.27%	92.24%
Pr-141	93.21%	78.07%	77.55%	29.19%	67.92%	90.55%
Nd-144	92.51%	74.88%	79.54%	25.48%	62.82%	89.68%
Eu-153	85.23%	36.06%	25.54%	12.00%	48.41%	82.58%
U-238	17.65%	5.57%	5.23%	2.35%	22.99%	46.45%
Np-237	24.40%	8.65%	8.13%	1.76%	31.02%	82.78%
Pu-239	71.34%	35.98%	33.63%	13.90%	70.95%	96.07%
Cm-244	95.02%	87.00%	86.63%	27.86%	70.77%	89.46%

Table 3-22. Sample SUT3-00477, percentage of total amount in glass flask strip solution.

	Contact Period				
Nuclide	**1**	**2**	**3**	**4**	**5**
Rb-85	11.46%	1.70%	1.41%	104.05%	1.86%
Rb-87	11.41%	1.70%	1.41%	104.05%	1.86%
Sr-90	12.32%	1.18%	1.33%	69.73%	2.00%
Mo-100	3.37%	1.13%	4.51%	85.52%	0.98%
Tc-99	3.94%	1.53%	5.84%	87.48%	1.04%
Cs-133	3.03%	1.49%	1.30%	26.78%	3.77%
Cs-135	2.95%	1.48%	1.33%	25.83%	3.81%
Cs-137	2.71%	1.65%	1.21%	21.26%	2.67%
Ba-138	22.88%	5.00%	2.71%	63.45%	4.23%
La-139	91.93%	79.37%	79.70%	99.91%	52.90%
Ce-140	97.51%	88.77%	97.57%	99.97%	91.16%
Pr-141	91.85%	78.29%	82.55%	99.93%	51.44%
Nd-144	91.70%	73.60%	77.03%	99.92%	42.07%
Eu-153	88.98%	52.73%	48.67%	98.46%	27.31%
U-238	16.07%	5.96%	13.62%	96.18%	3.43%
Np-237	13.50%	5.62%	12.46%	97.61%	4.26%
Pu-239	65.72%	30.80%	79.16%	99.85%	38.97%
Cm-244	94.64%	74.47%	87.04%	99.96%	49.34%

Table 3-23. Sample AM2-K12, percentage of total amount in glass flask strip solution.

	Contact Period					
Nuclide	**1**	**2**	**3**	**4**	**5**	**6**
Rb-85	1.82%	8.56%	4.63%	1.25%	32.07%	1.31%
Rb-87	1.82%	8.56%	4.63%	1.25%	32.07%	1.31%
Sr-90	3.10%	11.54%	6.18%	0.27%	54.72%	4.25%
Mo-100	12.98%	22.92%	16.38%	0.74%	67.62%	10.75%
Tc-99	10.85%	17.77%	19.81%	1.42%	77.58%	20.08%
Cs-133	0.32%	3.03%	3.56%	2.39%	7.23%	1.16%
Cs-135	0.32%	3.05%	3.59%	2.44%	7.30%	1.15%
Cs-137	1.03%	1.81%	2.59%	1.99%	6.51%	2.13%
Ba-138	1.29%	7.57%	7.47%	2.52%	43.48%	2.78%
La-139	33.84%	41.67%	36.90%	24.64%	93.96%	65.79%
Ce-140	77.11%	91.55%	90.97%	75.33%	99.73%	98.17%
Pr-141	38.05%	42.90%	36.40%	13.37%	94.29%	67.84%
Nd-144	36.27%	39.68%	34.12%	11.32%	93.28%	62.61%
Eu-153	24.05%	34.48%	30.21%	11.91%	89.69%	28.84%
U-238	13.56%	21.64%	15.55%	1.80%	83.71%	25.07%
Np-237	56.28%	67.68%	60.28%	3.95%	90.79%	36.44%
Pu-239	53.13%	60.55%	50.94%	5.17%	93.85%	60.13%
Cm-244	36.44%	43.61%	35.51%	15.19%	93.58%	66.94%

3.8 Release fractions

Results for the following nuclides are reported: $^{85, 87}$Rb, ^{90}Sr, ^{100}Mo, ^{99}Tc, $^{133, 135, 137}$Cs, ^{138}Ba, ^{139}La, ^{140}Ce, ^{141}Pr, ^{144}Nd, ^{153}Eu, ^{238}U, ^{237}Np, ^{239}Pu and ^{244}Cm. This selection allows a comparison to Series 11 results. In addition, ^{129}I is included.

All single values had been compared to the corresponding detection limit. In those cases, where both individual values were below the limit, a corresponding (rounded) limit is included in the tables. In cases, where only one of the two values was below the detection limit, the corresponding value is disregarded and the release fraction based on the single value that was larger than the limit. In these cases, no standard deviation is shown.

In general, the standard deviations indicate that discrepancies between twin analyses are small, at least as long as concentrations are not very close to the detection limit.

For each sample, the following data are compiled in Appendix A:

- Release fractions, for each contact period and cumulative, based on nuclide concentrations in the centrifugate.
- Release fractions, for each contact period and cumulative, based on nuclide concentrations in the strip solution.

Release fractions of groups of nuclides are discussed below on the basis of plots depicting cumulative release fractions as a function of cumulative exposure time. The release fractions are based on the centrifugate solution concentrations. In the case of most nuclides, plots based on the sum of centrifugate and strip data would lead to the same findings, but in the case of the lanthanides and of some actinides, the amount found in the strip solutions represents a significant portion of the total. Rubidium release fractions are based on uncorrected ^{85}Rb data and on ^{87}Rb concentrations corrected for natural ^{87}Sr only.

When discussing nuclide release from irradiated fuel, it should be kept in mind that we deal with a complex system. During irradiation, quite homogeneous UO_2 is transformed into an inhomogeneous conglomerate. Burnup varies in the order of a factor of two or more over the fuel pellet cross section. The original UO_2 grain structure is partly restructured in different ways, depending, amongst others from the fuel temperature. Fission and activation products are formed. Some of them are incorporated in the fuel matrix, others form inclusions or migrate to grain boundaries, pores or the free volume of the fuel rod. When exposed to the leachant, this complex system does not remain stable. Preferential corrosion along grain boundaries may increase the surface accessible to the leachant and preferentially release species located at grain boundaries. On the other hand, precipitation of secondary phases may hinder leachant access in other cases. Therefore, simple burnup effects might be masked by effects that are, in the best case, only partly reproducible and hardly identifiable.

All data are plotted in Figure 3-25 with a logarithmic scale on the y axis. The cumulative release fractions after one to two years exposure spread over roughly four orders of magnitude, with the highest values observed for caesium, rubidium and iodine, allocated to the instant release fraction, and the lowest values for the lanthanides. With a few exceptions discussed below, the sequence of nuclides is similar in all samples. The burnup of samples 4I8-Q12, 3V5-Q13 and SUT3-00477 lies between 58 and 67 MWd/kgU, whereas the burnup of sample AM2-K12 is significantly higher (75.4 MWd/kgU). At a first glance, no dramatic high burnup effect on nuclide release can be observed.

Cumulative release fractions for rubidium and caesium isotopes and for ^{129}I are plotted in Figure 3-26 with a linear scale. Similar behaviour is observed in the two samples with the lowest burnup (4I8-Q12, SUT3-00477). ^{85}Rb, with the long-lived mother nuclide ^{85}Kr, is released to the same extent as caesium isotopes. In the two samples with higher burnup, release of caesium is higher than rubidium release. As discussed in Paragraph 3.6, no satisfying correction procedure for mass 85 and 87 data could be established. Therefore, rubidium data should be interpreted with care. An interesting shape of the caesium and rubidium release curves is observed in high burnup sample AM2-K12, where release was comparatively low up to one year, but increased by more than a factor of five during the second year of exposure. The behaviour might be impacted by a closer cold gap, compared to samples with lower burnup. Overall, the released fraction after two years is still below the fission gas release of 5%.

^{129}I release does not exhibit any clear trends. In the low burnup samples 4I8-Q12 and SUT3-00477, less than half a percent of the total iodine inventory is released up to one year. In sample 3V5-Q13, the released amount stays below one percent up to one year as well, before another three percent are released during the second year of exposure, which is atypical and unexpected, because it is more than the portion of released fission gases (2.7%). In the high burnup sample AM2-K12, over two percent were released after three months already, but roughly nothing more afterwards.

A contributing factor to the initial part of the complex rubidium, caesium and iodine release curves could be the washing step at the beginning of the experiments. This washing might have removed differing portions of elements allocated to the instant release fraction. This is illustrated by unpublished results of experiments going on at Studsvik that aim at determining the instant release from sibling samples of those used in the present experiments. The experiments were conducted slightly different from the present fuel corrosion experiments. The samples had the same size, but instead of the washing step, they were exposed to simulated groundwater for an initial 2 hour contact period. Afterwards, the cladding was axially cut up on opposite sides and the fuel fragments were shaked out. Framgents and cladding halves were placed in a basket and exposed to simulated groundwater for increasingly longer contact periods in the same way as in the series described in this report. After a cumulative contact time of four weeks, more than 4% of the ^{129}I inventory and about 2% of the caesium inventory was released from sample AM2-K12. From the other three samples, about 2% of the iodine and 1–1.5% caesium had been released during the same period. This pattern corresponds reasonably well to the measured fission gas release of about 5% in rod AM2-K12 and 0.9–2.7% in the other three rods (Table 2-3).

Figure 3-27 shows release fractions of barium and strontium, compared to uranium. The two elements are preferentially released, maybe due to the fact that they partly accumulate in the so called grey phase, a multicomponent perovskite oxide phase of general comopistion $(Ba_{1-x-y}\,Sr_xCs_y)(U,Pu,Zr,Mo,REE)O_3$ /Kleykamp 1985/.

Release of technetium and molybdenum, illustrated in Figure 3-28, exhibit a burnup effect. At low burnup, these elements are preferentially released. Once metallic alloy particles start growing with increasing burnup and temperature, release fractions get smaller, reaching values close to or even slightly below uranium release fractions in high burnup sample AM2-K12. This effect seems to start slightly earlier for technetium than for molybdenum, as illustrated in Figure 3-29.

Figure 3-30 shows release fractions for lanthanides and actinides. Release of uranium is comparable in all four samples. No pronounced burnup effect can be observed. If there is any at all, the data so far indicate that it goes towards lower release with increasing burnup.

In most cases, the cumulative release fractions of lanthanides and actinides based on centrifugate concentrations are significantly lower than the released uranium fraction. This might be attributed to two effects. As discussed in Paragraph 3.7, a significant part is found in the vessel strip solutions, partly because some fuel particles have been dissolved, but also because the nuclides of concern had been absorbed by the vessel walls. In addition, preferential oxidation to the better soluble U^{VI}, as it is discussed in /Hanson 2008/, might lead to a higher uranium release, compared to other actinides and to lanthanides. Nevertheless, it is hard in some cases to find any consistencies or trends between the different samples. This is particularly true for ^{244}Cm and ^{153}Eu, but also for ^{237}Np. Curium release is very low in all samples but AM2-K12, where it is released more than uranium. In this sample, europium is released even more than curium and about five times more than in all other samples. In contrast, the lowest release of neptunium was observed in high burnup sample AM2-K12, whereas neptunium was released from the other three samples to an extent comparable to uranium.

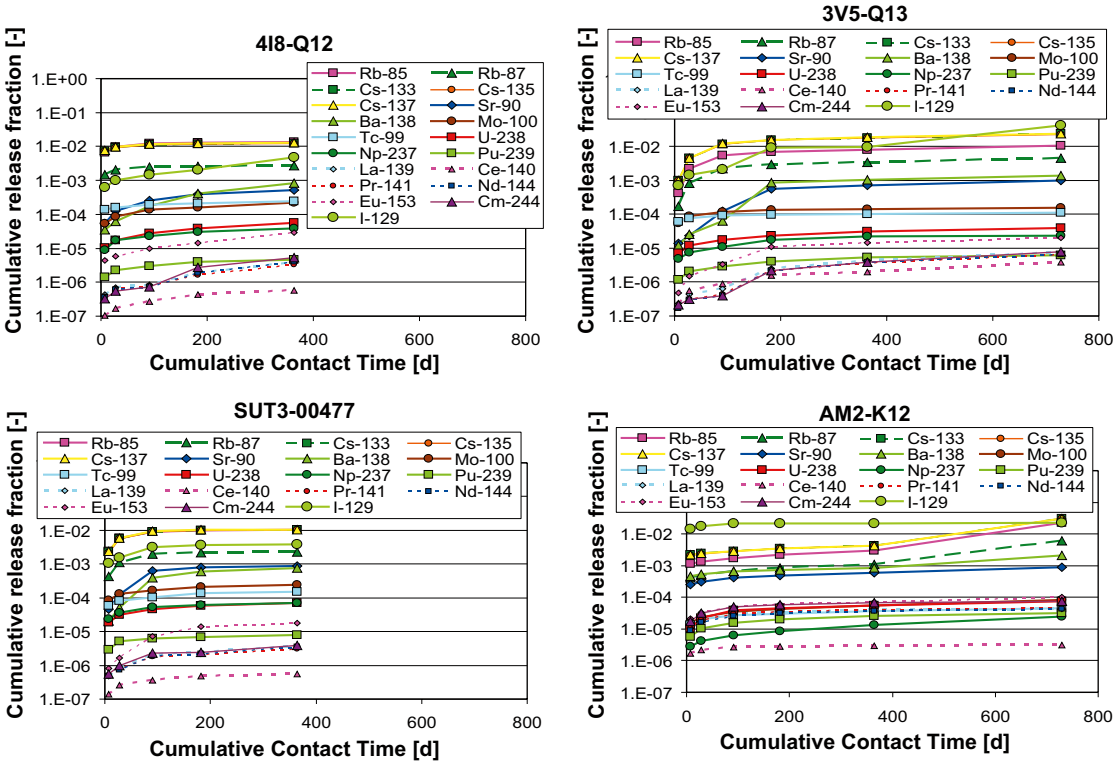

Figure 3-25. *Cumulative release fractions based on centrifugate concentrations as a function of cumulative exposure time; all nuclides plotted with logarithmic scale on y axis.*

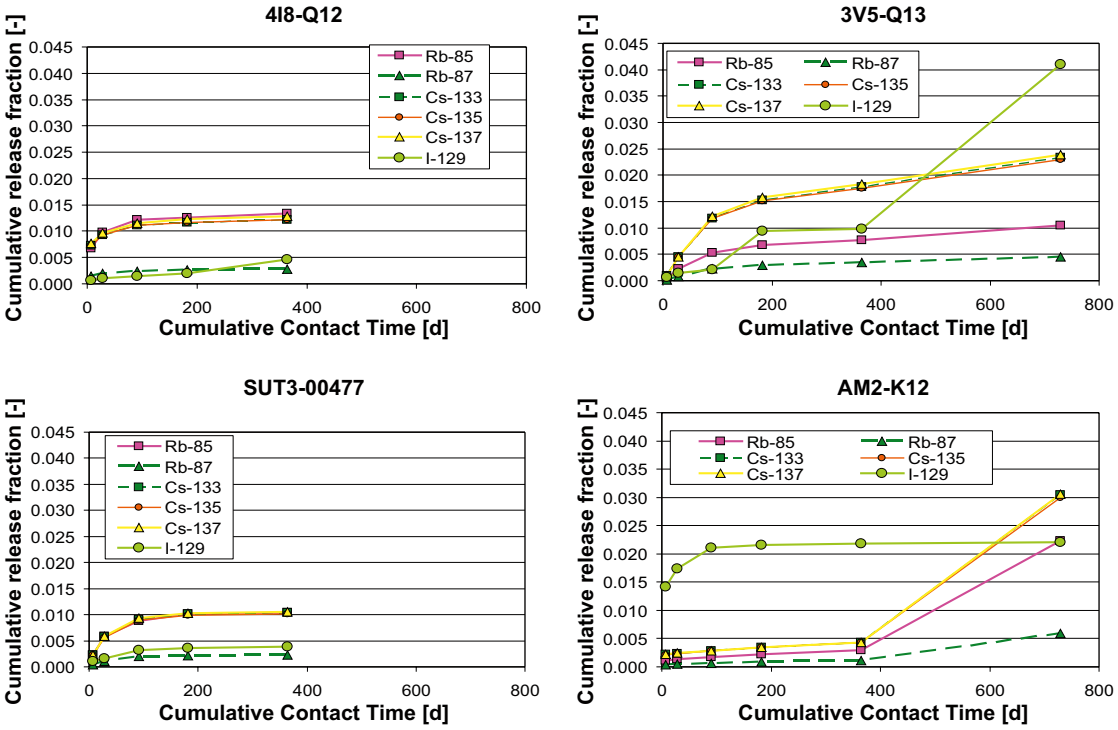

Figure 3-26. *Cumulative release fractions based on centrifugate concentrations as a function of cumulative exposure time; rubidium, caesium and iodine.*

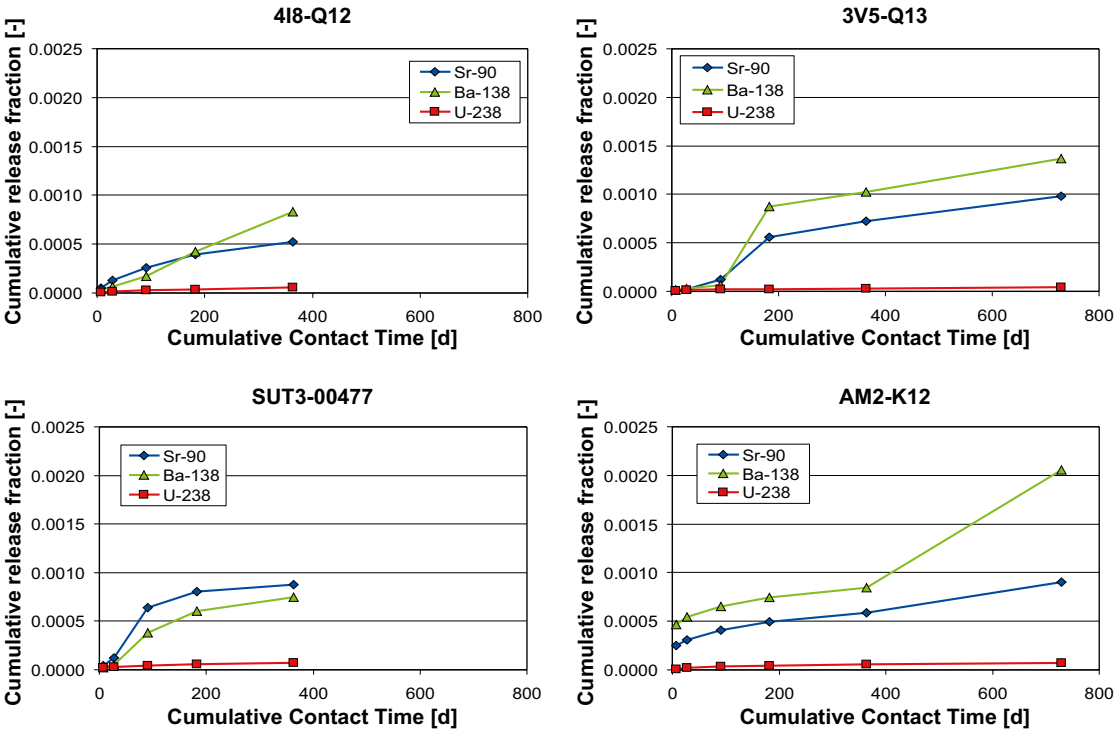

Figure 3-27. *Cumulative release fractions based on centrifugate concentrations as a function of cumulative exposure time; strontium and barium compared to uranium.*

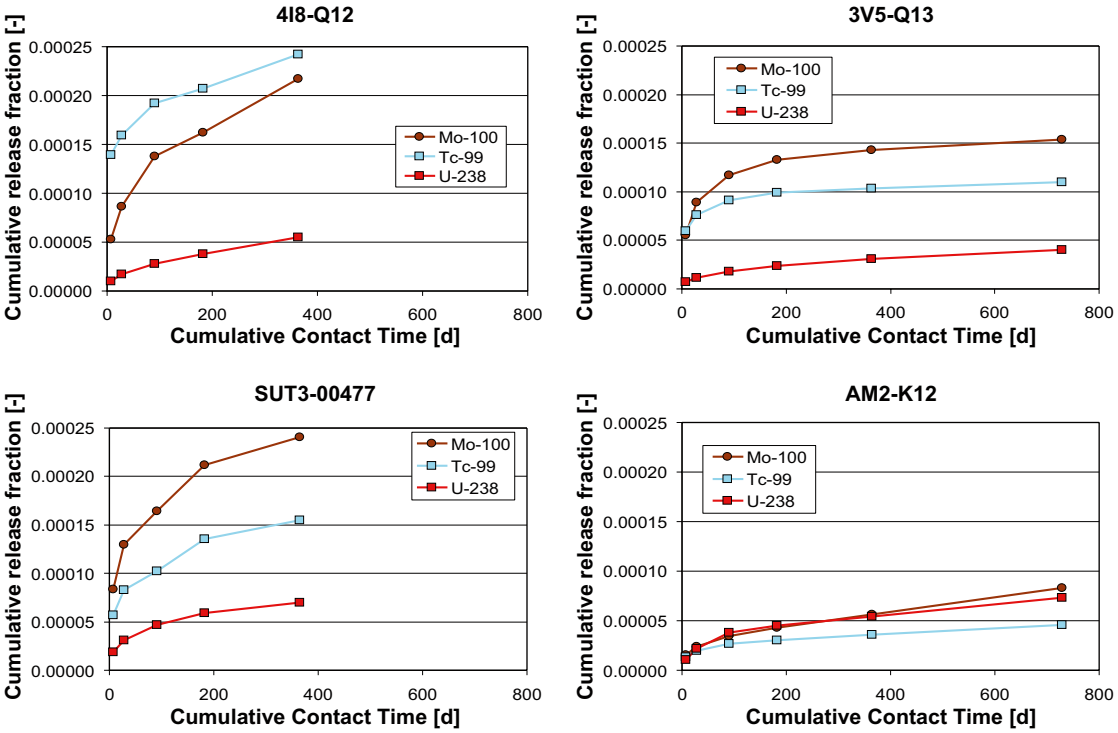

Figure 3-28. *Cumulative release fractions based on centrifugate concentrations as a function of cumulative exposure time; technetium and molybdenum compared to uranium.*

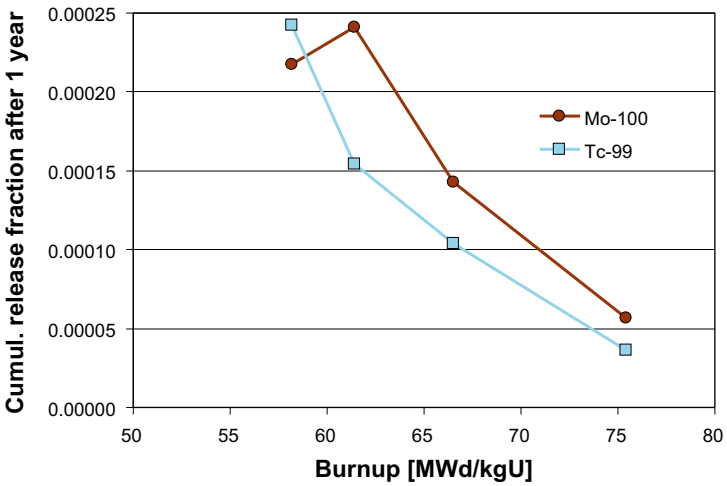

Figure 3-29. *Cumulative release fractions of ^{99}Tc and ^{100}Mo based on centrifugate concentrations after one year of exposure as a function of burnup.*

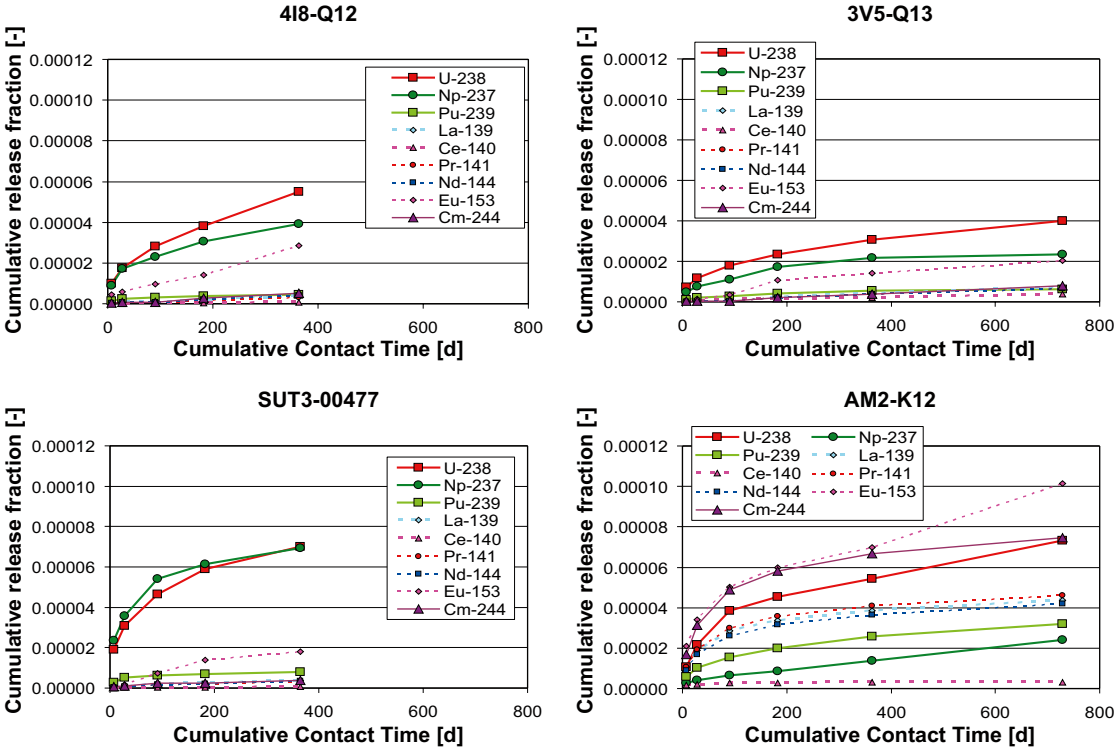

Figure 3-30. *Cumulative release fractions based on centrifugate concentrations as a function of cumulative exposure time; lanthanides and actinides.*

3.9 Fractional release rates

Fractional release rates are calculated by dividing release fractions compiled in Appendix A by the length of the contact period. Fractional release rates for some selected elements are plotted below together with corresponding data from Series 11 experiments /Forsyth 1997/.

Caesium (Figure 3-31) and rubidium (Figure 3-32) release rates exhibit the same pattern. During the first period of exposure the values are comparable to those determined in the Series 11 experiments, although with significantly larger scatter. The release rate from sample AM2-K12 with the highest burnup dropped markedly during the second period. Afterwards, it dropped slowly only, before even increased markedly, by a factor of 3.5, during period 6. For the other three samples, the release rates drop less than in Series 11. Even in the case of 3V5-Q13, a slight increase was observed during period 6. A potential reason for the observed differences might be the accessibility for the leachant through the cold gap, which is probably significantly narrower in a high burnup PWR sample, compared to a BWR sample with a burnup below 50 MWd/kgU.

Some similarities in the fractional release rate patterns can be seen for strontium (Figure 3-33) and barium (Figure 3-34) as well, although the ratio between barium and strontium varies between about 0.5 and 2.5 for different samples and contact periods. The general trend is similar to the one observed in Series 11 experiments.

The behaviour of molybdenum (Figure 3-35) and technetium (Figure 3-36) in the Series 11 experiments was rather complex, with a minimum in the release rates during contact periods 2 and 3. No such effect can be seen in the present data. Release rates decrease monotonously with exposure time for all four samples.

Apparent uranium release rates in the present experiments are rather close to those of Series 11, as illustrated in Figure 3-37. In contrast to the Series 11 data, the curves decrease monotonously, with a trend that corresponds to the early general trend of Series 11. No clear influence of the burnup is visible. As stated in Paragraph 3.5, it is assumed that the leachants had not been saturated with respect to uranium, thus the release rates should reflect dissolution rates of the fuel matrix.

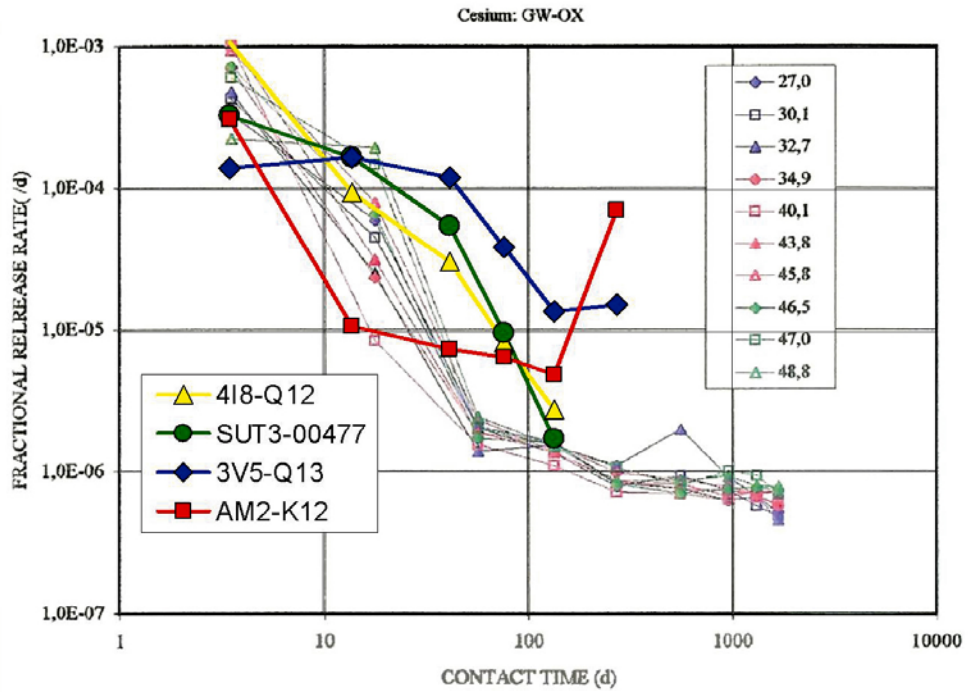

Figure 3-31. *Caesium fractional release rates based on centrifugate concentrations as a function of cumulative contact time; comparison to Series 11 data /Forsyth 1997/.*

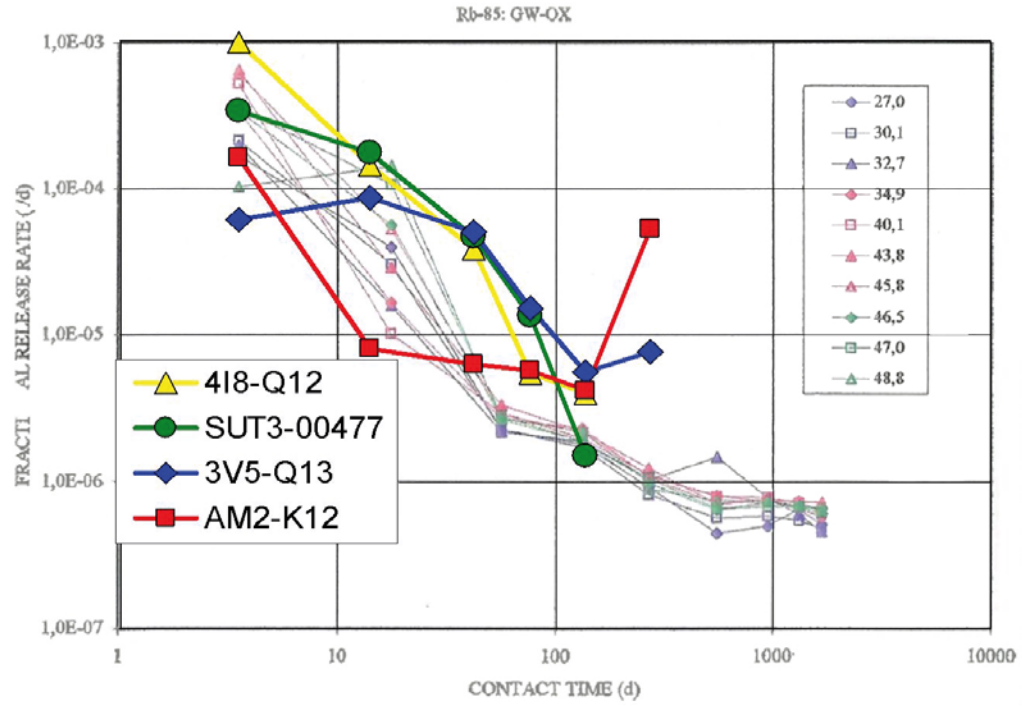

Figure 3-32. *^{85}Rb fractional release rates based on centrifugate concentrations as a function of cumulative contact time; comparison to Series 11 data /Forsyth 1997/.*

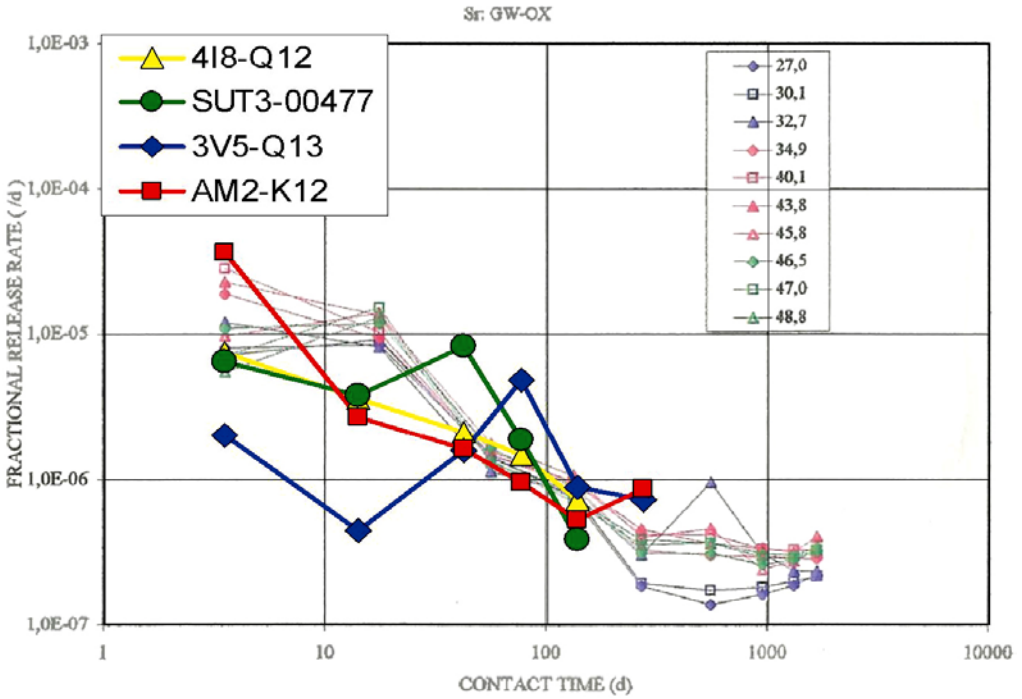

Figure 3-33. *Strontium fractional release rates based on centrifugate concentrations as a function of cumulative contact time; comparison to Series 11 data /Forsyth 1997/.*

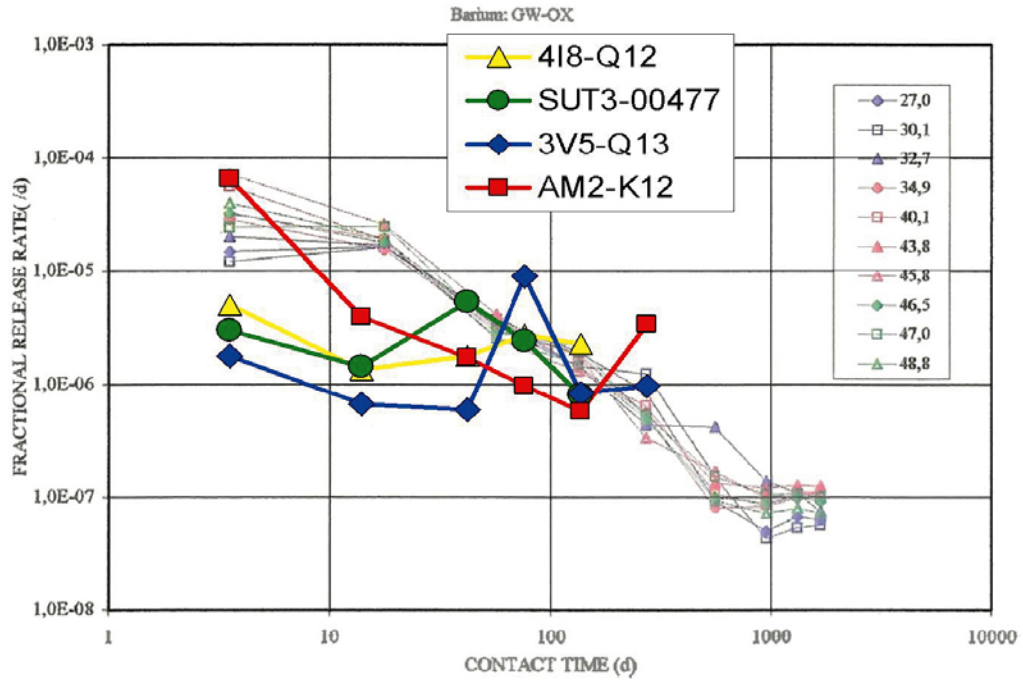

Figure 3-34. *Barium fractional release rates based on centrifugate concentrations as a function of cumulative contact time; comparison to Series 11 data /Forsyth 1997/.*

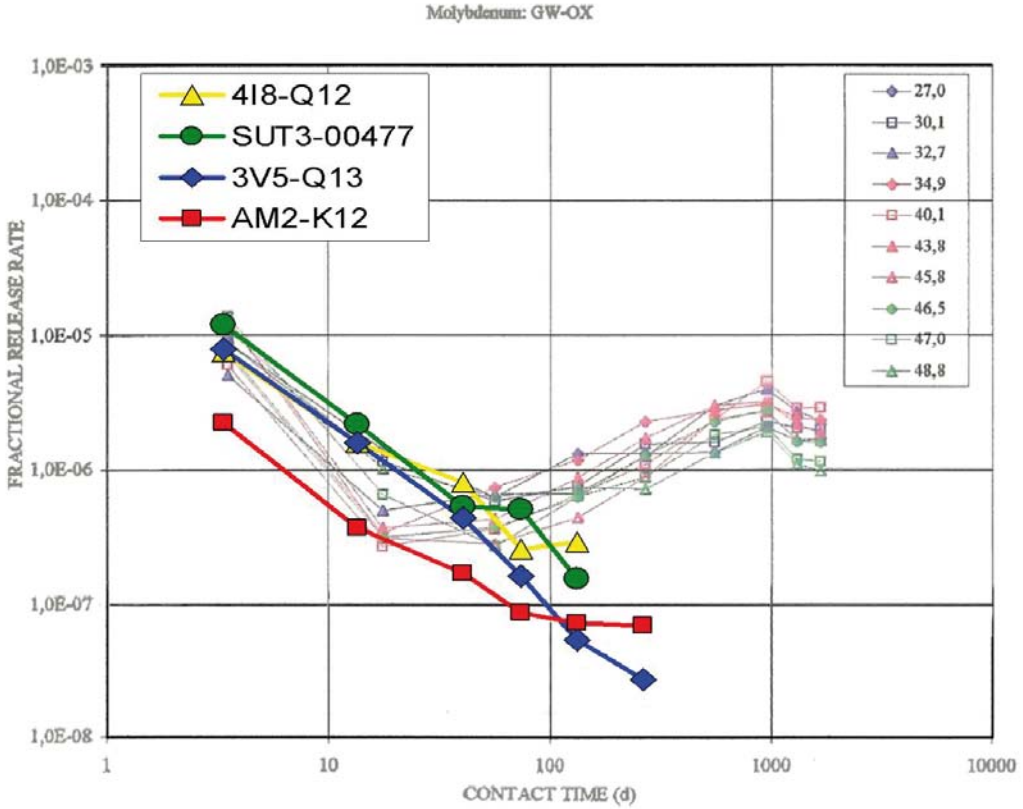

Figure 3-35. *Molybdenum fractional release rates based on centrifugate concentrations as a function of cumulative contact time; comparison to Series 11 data /Forsyth 1997/.*

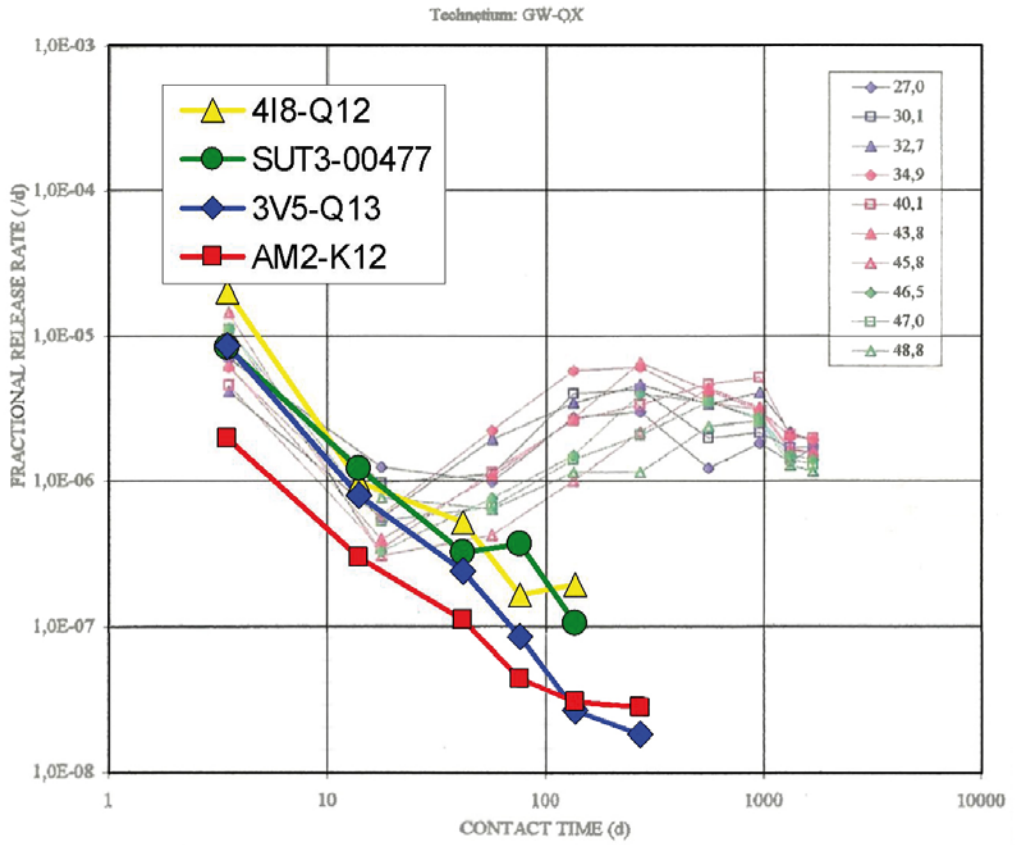

Figure 3-36. *Technetium fractional release rates based on centrifugate concentrations as a function of cumulative contact time; comparison to Series 11 data /Forsyth 1997/.*

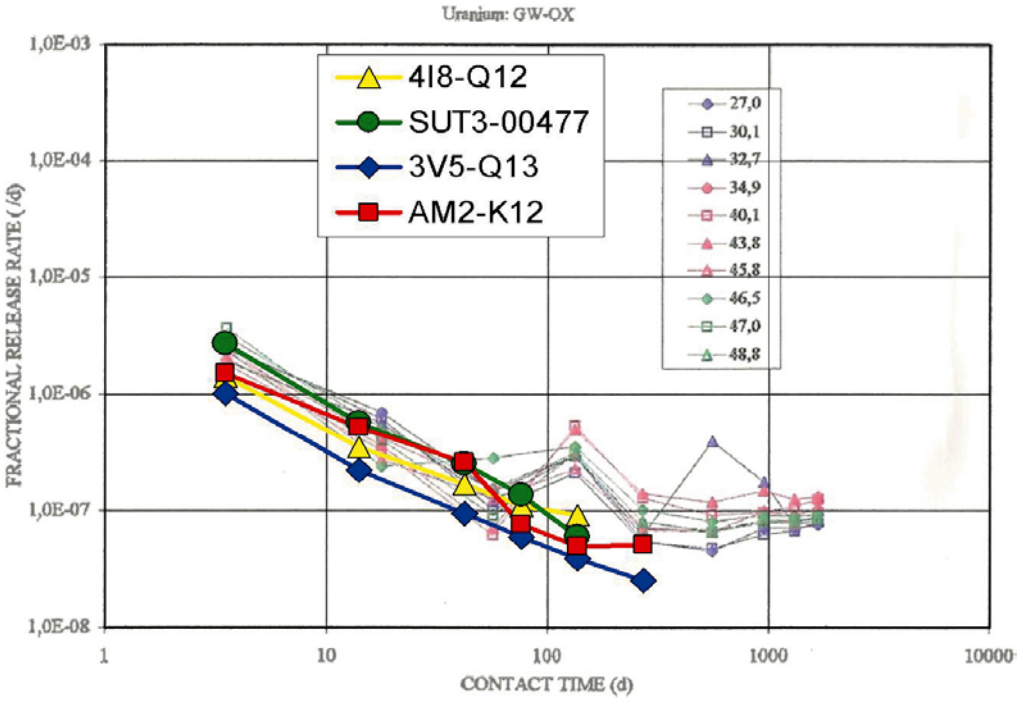

Figure 3-37. *Uranium fractional release rates based on centrifugate concentrations as a function of cumulative contact time; comparison to Series 11 data /Forsyth 1997/.*

3.10 Cumulative release as a function of burnup

In the discussion of high burnup fuel dissolution, the influence of the smaller grain size and increased porosity in the rim region are mentioned as factors which cause an increase of the surface area. The increased actinide content in spent fuel at higher burnup leads to a higher α-dose rate in the surrounding water and the higher content of fission products also contributes to a higher β- and γ-dose rate initially. Both factors should contribute to higher cumulative release fractions for uranium and for other "matrix bound nuclides" with increasing burnup. Only in recent work, the influence of a third factor, namely the increased content of dopant nuclides, i.e. non uranium fission product and actinide atoms in the UO_2 matrix of the spent fuel with fuel burnup, has been discussed in connection with fuel dissolution studies /He et al. 2007, Hanson and Stout 2004, Hanson et al. 2004, Hanson 2005/. Unirradiated UO_2 has a fluorite structure. In order to be dissolved in simulated ground water under oxidative conditions, U^{IV} is oxidized to U^{VI}, which is dissolved by forming carbonate complexes. During irradiation, U^{IV} positions are gradually occupied by fission products and minor actinides, in general with a lower oxidation state than four. The maximum possible amount of oxygen in the fluorite structure corresponds to $UO_{2.4}$, with the next step requiring a transformation of the structure. This becomes increasingly difficult with the rising amount of dopant nuclides. Thus, burnup leads to a more stable fuel matrix that might well compensate opposite effects like radiolysis, smaller grains and increased porosity. The same effect was observed with unirradiated UO_2 doped with gadolinium /Casella et al. 2008/. Calorimetric measurements of /Mazeina et al. 2008/ show increased stability of UO_2 doped with yttrium and calcium towards oxidation and oxidative leaching.

A comparison of the present data with selected Series 11 results on the basis of cumulated releases for a total contact time of one year (five contact periods) is compiled in Table 3-24, corresponding data for two years (samples 3V5-Q13 and AM2-K12 only) are included in Table 3-25. Figure 3-38, Figure 3-39, Figure 3-40 and Figure 3-41 show the same data plotted as a function of sample burnup. The data are based on centrifugate concentrations.

When comparing the present data with Series 11 results, it should be kept in mind that the Series 11 samples formed a quite homogeneous set. They all stemmed from the same fuel rod. The fuel was fabricated by the same method and it was irradiated roughly under the same operating conditions. Burnup differences were a consequence of different axial positions only. On the other hand, the samples of the present study stem from fuel rods fabricated by different fuel suppliers. They were irradiated in different reactors with significantly different power histories. They experienced certainly higher fuel temperatures than the Series 11 samples, because they were irradiated in a PWR and not in a BWR.

Figure 3-39 illustrates that rubidium and caesium fractional release is higher than for Series 11. The decreasing trend as a function of burnup found after a cumulative exposure time after one year disappeared, as rubidium and caesium release were very high during the second year of exposure. A contributing factor may be our short washing time to eliminate the instant release fraction, which usually increases at higher burnups /Johnson et al. 2005/. Another important factor is the difference in power history. Under PWR conditions, these easily movable elements migrate to a larger extent to colder locations like cladding inner surface, pellet-cladding gap, pellet-pellet interfaces, cracks and grain boundaries. From there, they are easier released to the leachant than from the fuel matrix.

The cumulative release fractions for strontium and barium are quite similar to the corresponding releases from the lower burnup Series 11 samples, with no clear dependency on burnup (Figure 3-40). Molybdenum and technetium cumulative release fractions on the other hand are lower than those for Series 11 and decrease with increasing burnup. As stated in Section 3.8, this might be due to the fact that a significant part of their inventory is in the form of metallic alloy particles, which grow larger with increasing burnup and temperature. A rough idea on the portion of the inventory bound in alloy particles gives Figure 3-12. Only 50–60% of the calculated total amount of ^{99}Tc was found in solution from the samples dissolved for the inventory determination. On the other hand, as seen in Figure 3-12, both the total inventory Tc and the part found in metallic particles increase with burnup. It is well known also that molybdenum buffers the oxygen potential of the fuel (together with Zr) through its oxidation from metallic to oxide form dissolved in the matrix /Matzke 1995/. Mo and Tc are thus released both from the fuel matrix and the metallic particles /Cui et al. 2001/. It is difficult to sort out which factor is dominating in the decreasing release of Mo and Tc with burnup.

The uranium releases (Figure 3-41) are similar or lower than the Series 11 results. Data after one year indicate a trend towards lower release with increasing burnup. After two years of exposure, the difference between Series 11 and the two data points already available from this study is even more pronounced.

When assessing the release of activation and fission products in fuel corrosion experiments, it should be kept in mind that irradiated fuel represents by no means a homogeneous material, as it was mentioned earlier already. A large portion of the fuel still has maintained the original grain structure, whereas at the pellet periphery, it is restructured at higher burnup, forming the high burnup structure mentioned in the introduction. Fission products might migrate and form new phases. Corrosion attack is not at all a uniform process; it rather takes place along grain boundaries, as illustrated by Figure 3-42. Note that this example is not from a fuel sample used in the present studies. As discussed above already, this preferential attack might open "deposits" of fission products after a while, leading to a marked increase of fractional release of certain nuclides. Such a mechanism could explain the marked increase of caesium and rubidium release during the sixth contact period of sample AM2-K12.

The absence of any marked impact of increased burnup on fuel dissolution rates has been observed in other work carried out under quite similar conditions /Jégou et al. 2001, 2004/. The same trend is observed in flow-through fuel leaching tests with fuel powder in carbonate solutions /Hanson 2008/, where the cumulative uranium releases are highest from a fuel in the intermediate burnup interval (44 MWd/kgU) even as compared to high burnup fuels (up to 70 MWd/kgU). Finally, tests carried out at the Institute for Transuranium Elements in Karlsruhe during the EU-Project NF-PRO /Clarens et al. 2008/ with fuel samples taken from the drilled central part of a high burnup pellet and the outer part which contains also the rim, showed slightly lower releases from the outer part (i.e. higher burnup) for almost all radionuclides. Thus, the most plausible explanation to our results seems to be that the increased amount of dopants at higher burnup causes an increased resistance to oxidative dissolution of the UO_2 matrix, which counteracts effectively the increased surface area and radiation dose.

Table 3-24. Cumulative release fractions under oxidising conditions in synthetic groundwater for a cumulative contact time of one year. Present results in comparison with a selection of data from Series 11 experiments.

Specimen	11-01	11-02	11-04	11-05	11-10	11-16	4I8-Q12	SUT3-00477	3V5-Q13	AM2-K12
Burnup [MWd/kgU]	27	30.1	34.9	40.1	45.8	48.8	58.2	61.4	66.5	75.4
Rb-85	2.49E-03	2.60E-03	3.32E-03	4.45E-03	6.03E-03	4.39E-03	1.33E-02	1.04E-02	7.68E-03	2.98E-03
Rb-87	1.58E-03	1.59E-03	2.00E-03	2.37E-03	2.62E-03	1.91E-03	2.78E-03	2.30E-03	3.35E-03	1.11E-03
Cs	4.02E-03	4.30E-03	5.81E-03	7.73E-03	8.71E-03	6.24E-03	1.28E-02	1.05E-02	1.83E-02	4.36E-03
Sr	4.29E-04	4.42E-04	5.66E-04	6.79E-04	6.51E-04	5.37E-04	5.23E-04	8.77E-04	7.21E-04	5.91E-04
Ba	1.03E-03	1.03E-03	9.92E-04	1.20E-03	1.08E-03	1.11E-03	8.34E-04	7.50E-04	1.02E-03	8.45E-04
Mo	4.94E-04	4.79E-04	1.11E-03	3.32E-04	3.22E-04	3.41E-04	2.17E-04	2.41E-04	1.43E-04	5.65E-05
Tc	9.30E-04	1.28E-03	1.82E-03	9.61E-04	6.20E-04	4.32E-04	2.42E-04	1.55E-04	1.04E-04	3.60E-05
U	7.83E-05	6.72E-05	7.51E-05	9.71E-05	6.57E-05	8.63E-05	5.51E-05	6.99E-05	3.06E-05	5.44E-05
Np	2.20E-05	2.15E-05	1.84E-05	1.31E-05	1.89E-05	1.34E-05	3.92E-05	6.94E-05	2.18E-05	1.37E-05
Pu	1.09E-05	9.78E-06	7.98E-06	8.69E-06	8.47E-06	9.07E-06	4.51E-06	7.82E-06	5.39E-06	2.56E-05
La	2.37E-06	2.85E-06	6.57E-06	1.09E-05	1.01E-05	7.41E-06	3.85E-06	3.69E-06	4.27E-06	3.84E-05
Ce	3.36E-06	3.30E-06	3.14E-06	2.34E-06	2.93E-06	3.12E-06	5.75E-07	5.62E-07	1.95E-06	3.01E-06
Pr	4.17E-07	1.72E-06	5.28E-06	5.86E-06	8.57E-06	5.66E-06	3.25E-06	3.08E-06	3.63E-06	4.08E-05
Nd	1.47E-06	2.89E-06	7.49E-06	9.44E-06	1.09E-05	6.94E-06	4.00E-06	3.58E-06	3.83E-06	3.66E-05
Eu	7.03E-06	5.44E-06	1.00E-05	1.74E-05	2.62E-05	1.37E-05	2.85E-05	1.79E-05	2.04E-05	6.99E-05

Table 3-25. Cumulative release fractions under oxidising conditions in synthetic groundwater for a cumulative contact time of two years. Present results in comparison with a selection of data from Series 11 experiments.

Specimen	11-01	11-02	11-04	11-05	11-10	11-16	3V5-Q13	AM2-K12
Burnup [MWd/kgU]	27	30.1	34.9	40.1	45.8	48.8	66.5	75.4
Rb-85	2.66E-03	2.81E-03	3.58E-03	4.74E-03	6.33E-03	4.66E-03	1.05E-02	2.23E-02
Rb-87	1.76E-03	1.79E-03	2.25E-03	2.65E-03	2.90E-03	2.14E-03	4.45E-03	5.97E-03
Cs	4.30E-03	4.64E-03	6.14E-03	7.99E-03	9.01E-03	6.56E-03	2.39E-02	3.06E-02
Sr	4.80E-04	5.07E-04	6.78E-04	8.36E-04	8.23E-04	6.75E-04	9.83E-04	9.00E-04
Ba	1.37E-03	1.60E-03	1.02E-03	1.24E-03	1.14E-03	1.14E-03	1.37E-03	2.06E-03
Mo	9.95E-04	1.08E-03	2.14E-03	1.21E-03	1.21E-03	8.37E-04	1.54E-04	8.30E-05
Tc	1.39E-03	2.01E-03	3.11E-03	2.67E-03	2.23E-03	1.32E-03	1.10E-04	4.61E-05
U	9.54E-05	8.51E-05	1.00E-04	1.31E-04	9.14E-05	1.11E-04	4.01E-05	7.32E-05
Np	2.35E-05	2.25E-05	2.06E-05	1.90E-05	2.93E-05	1.76E-05	2.34E-05	2.41E-05
Pu	1.12E-05	1.00E-05	8.22E-06	9.03E-06	8.87E-06	9.74E-06	6.09E-06	3.21E-05
La	2.37E-06	3.57E-06	6.69E-06	1.17E-05	1.17E-05	7.91E-06	7.31E-06	4.36E-05
Ce	4.08E-06	4.06E-06	3.88E-06	2.69E-06	3.40E-06	3.45E-06	3.77E-06	3.17E-06
Pr	4.17E-07	2.47E-06	5.72E-06	6.42E-06	9.75E-06	6.06E-06	6.38E-06	4.60E-05
Nd	1.72E-06	3.50E-06	8.65E-06	1.03E-05	1.27E-05	7.58E-06	6.60E-06	4.21E-05
Eu	7.78E-06	7.57E-06	1.11E-05	1.81E-05	2.81E-05	1.48E-05	2.04E-05	1.01E-04

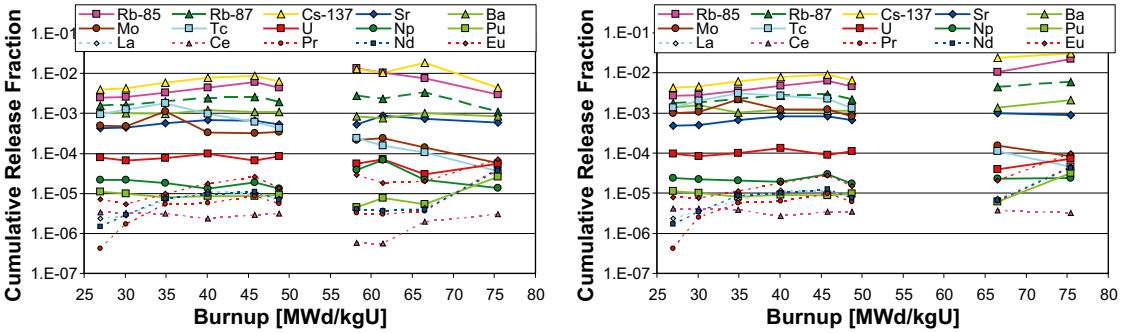

Figure 3-38. *Cumulative release fractions based on centrifugate concentrations for a cumulative contact time of one (left) and two years in comparison with a selection of data from Series 11 experiments, logarithmic scale.*

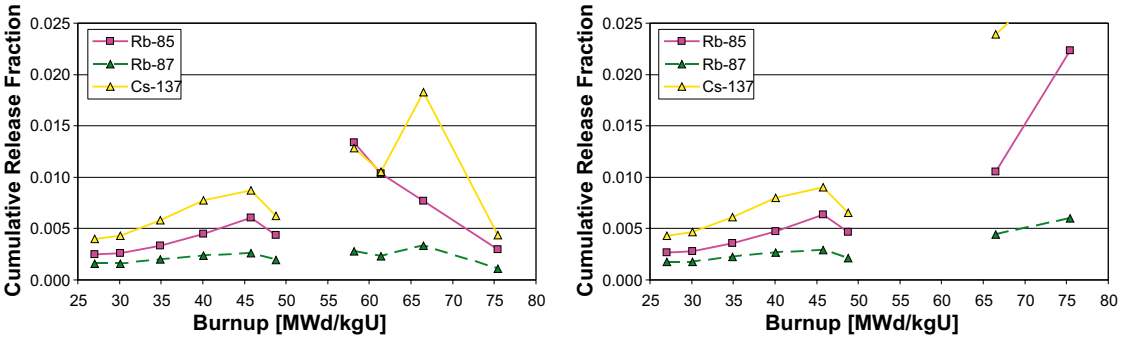

Figure 3-39. *Cumulative release fractions for rubidium and caesium based on centrifugate concentrations for a cumulative contact time of one (left) and two years in comparison with a selection of data from Series 11 experiments, linear scale.*

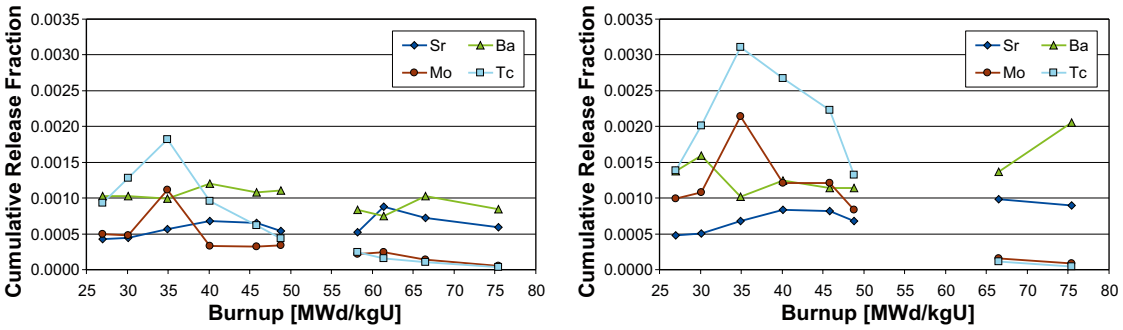

Figure 3-40. *Cumulative release fractions of strontium, barium, technetium and molybdenum based on centrifugate concentrations for a cumulative contact time of one (left) and two years in comparison with a selection of data from Series 11 experiments, some selected isotopes, linear scale.*

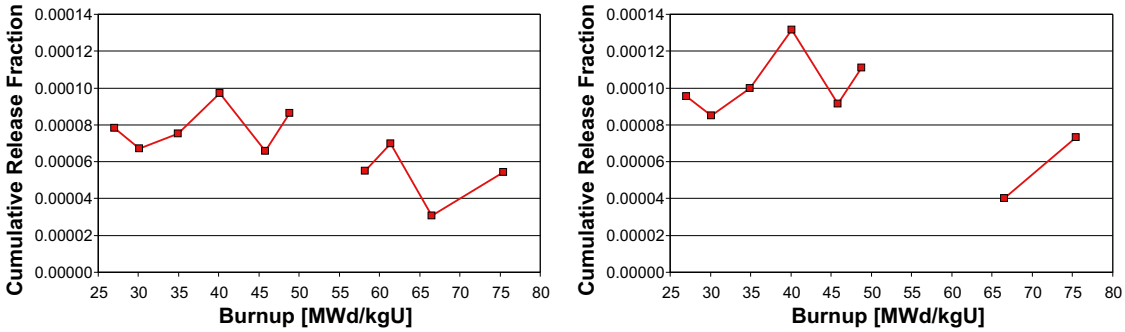

Figure 3-41. *Cumulative release fractions of uranium based on centrifugate concentrations for a cumulative contact time of one (left) and two years in comparison with a selection of data from Series 11 experiments, some selected isotopes, linear scale.*

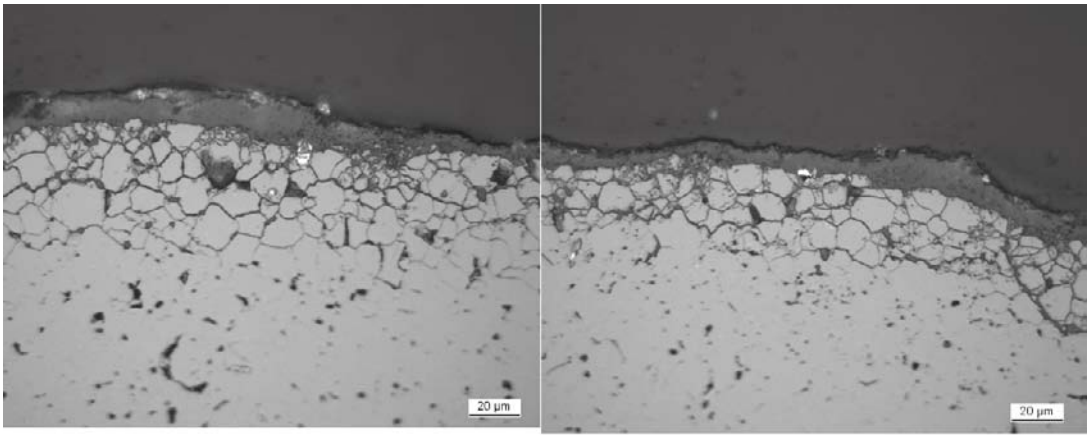

Figure 3-42. *Cross section through irradiated fuel fragment exposed to simulated ground water under oxidising conditions.*

3.11 $^{236}U/^{235}U$ ratio

$^{236}U/^{235}U$ ratios analysed in the centrifugates are plotted in Figure 3-43 as a function of sample burnup. A selection of Series 11 data was included as well. The data are compared to the experimentally determined sample inventory values represented by open circles and to the sample specific values calculated by CASMO, represented by lines. Figure 3-44 shows the same data plotted as a function of cumulative contact time. Data from the present study are shown as large symbols, connected with fat solid lines. Some Series 11 data are shown with small symbols connected with smaller dotted lines. The level of the inventory values for the four samples is indicated by a fat dotted line in the left part of the plot, the two determined Series 11 inventory values by fine dotted lines. In three cases, 4I8-Q12, 3V5-Q13 and AM2-K12, the initial values were below the inventory value and increased with time, approaching the pellet average. In the case of sample SUT3-00477, all values but the one from contact period 4 were around the inventory value. Overall, the data indicate that fuel was not preferentially dissolved from the high burnup region.

It is interesting to note that the increase of the $^{236}U/^{235}U$ ratio in progressive contact periods was observed also in Series 11. However, data for centrifugates in Series 11 seem to be below the pellet average $^{236}U/^{235}U$ ratio during the first contact periods, indicating that the corrosion occurs to a lesser extent in the rim zone despite a higher surface area and dose rate in this region.

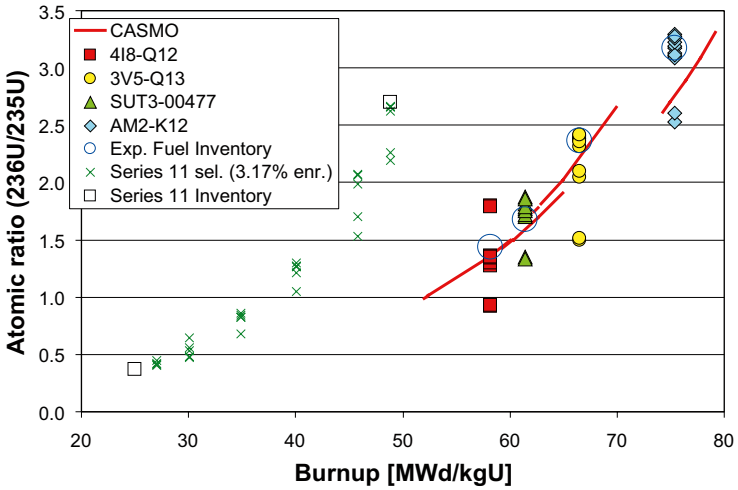

Figure 3-43. *$^{236}U/^{235}U$ ratios analysed in centrifugate, compared to values calculated by CASMO and with ratios from the inventory analysis.*

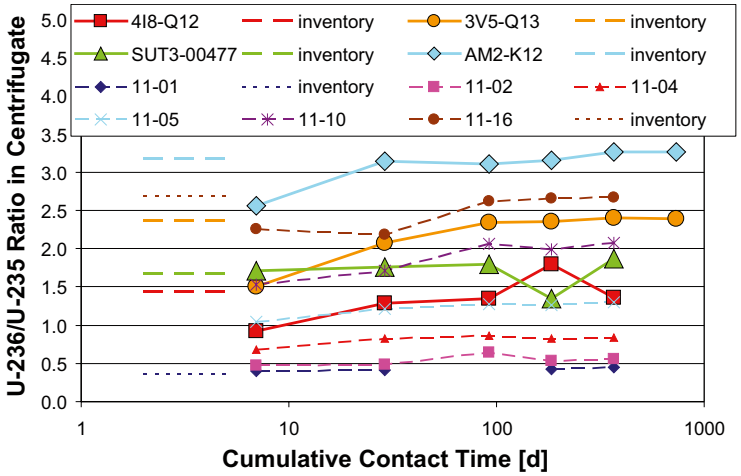

Figure 3-44. *$^{236}U/^{235}U$ ratios analysed in centrifugate as a function of cumulative contact time, compared to inventory values.*

4 Conclusions

A selection of data acquired in corrosion tests with high burnup PWR fuel under oxidising conditions in simulated groundwater during a cumulative contact time of up to two yeas has been evaluated and compared to corresponding results from experiments performed under similar conditions with BWR fuel samples with a burnup between 27 and 49 MWd/kgU (Series 11).

Release of individual nuclides was related to nuclide inventories that were experimentally determined by means of state-of-the-art methods, complemented by modelling calculations with modern codes.

Caesium and rubidium were released to a significantly larger extent in the high burnup samples, compared to the Series 11 experiments. This is probably more a consequence of different operating conditions than of burnup. Under PWR conditions, the temperature of the fuel is higher, which causes a higher portion of mobile fission products to diffuse to grain boundaries, to pellet-pellet interfaces and to the pellet cladding gap, from where they are more readily released than nuclides retained in the fuel matrix. In all cases, the cumulative caesium and rubidium release was lower than the fission gas release determined in the respective rods.

A marked opposite effect is observed for molybdenum and technetium. These elements are part of the group of elements that form alloy particles or the so called ε-phase. Formation of these particles is influenced by the inventory that increases with burnup and by the temperature of the fuel. Lower releases of these elements are observed in high burnup PWR fuel samples, compared to Series 11 results.

Based on apparent uranium release, it can be concluded that the stabilising effect of the increased content of dopant nuclides, i.e. fission product and actinide atoms in the UO_2 matrix of the spent fuel, more than compensates the potentially adverse effects of radiolysis and of smaller grains and higher porosity. The $^{236}U/^{235}U$ ratio in the leachant indicates that uranium is not preferentially released from the peripheral part of the pellets.

Some potential differences in corrosion performance of the different fuel types might not just be a function of burnup, but caused by differences in fuel fabrication and, even more important, in fuel operation. Nevertheless, it can be concluded that corrosion performance of high burnup PWR fuel under oxidising conditions is well comparable to the performance of BWR fuel with lower burnup.

5 Acknowledgements

The fuel samples and all necessary information on fabrication and irradiation were made available by Vattenfall Nuclear Fuel, by Westinghouse and by AREVA. Many thanks go to these organisations and in particular to David Schrire, Lars Hallstadius and Peter Dewes for their valuable support.

Many members of the Studsvik Nuclear staff contributed to the successful completion of this work. Anders Thanger cut the fuel rod samples; Vanja Liljedahl and Lotta Molin performed all work in the hotcell and transferred the analytical samples to the radiochemistry laboratory, assisted by radiation protection officer Rose-Marie Carlsson. Michael Granfors helped out with ICP-MS analyses, Cecilia Janzon Sjöstedt and Rikard Källström helped to choose suitable fuel rod samples and Per Ekberg performed all hotcell gamma spectrometry. Gustav Pettersson determined ^{90}Sr in centrifugates by radiometry, thus confirming that ICP-MS analysis is reliable and correct. The authors are grateful for all this support and wish to thank them all very much for their contribution.

Last but not least, the support by SKB, in particular through Kastriot Spahiu, is very much appreciated.

6 References

SKB's (Svensk Kärnbränslehantering AB) publications can be found at www.skb.se/publications.

ASTM, 1995. Standard test method for atom percent fission in uranium and plutonium fuel (mass spectrometric method) (Withdrawn 2001). ASTM Standard E 244-80(1995), ASTM International.

ASTM, 1996. Standard test method for atom percent fission in uranium and plutonium fuel (neodymium-148 method). ASTM Standard E321-96(1996), ASTM International.

Børresen S, 2008. Calculation of isotopic inventories in 3 high burnup fuel samples from Ringhals-3 and Ringhals-4 fuel rods. Report SSP-08/203, Studsvik Scandpower AB.

Børresen S, 2009. Calculation of isotopic inventories in a high burnup North Anna fuel rod. Report SSP-09/201, Studsvik Scandpower AB.

Casella A, Hanson B, Miller W, 2008. Factors affecting UO_2 dissolution under geological disposal conditions. Proceedings of the 2008 International High-Level Radioactive Waste Management Conference, Las Vegas, Nevada, 7–11 September 2008. La Grange, IL: American Nuclear Society, pp 388–394.

Clarens F, Serrano-Purroy D, Martínez-Esparza A, Wegan D, Gonzalez-Robles E, de Pablo J, Casas I, Giménez J, Christiansen B, Glatz J P, 2008. RN fractional release of High Burn-Up fuel: effect of HBS and estimation of accessible Grain Boundary. In: Lee W E (ed). Scientific basis for nuclear waste management XXXI : symposium held in Sheffield, United Kingdom, 16–21 September 2007. Warrendale, PA: Materials Research Society. (Materials Research Society Symposium Proceedings 1107), pp 439–446.

Cobos J, Papaioannou D, Spino J, Coquerelle M, 1998. Phase characteriation of simulated high burn-up UO_2 fuel. Journal of Alloys and Compounds, 271–273, pp 610–615.

Cui D, Eriksen T, Eklund U-B, 2001. On metal aggregates in spent fuel, synthesis and leaching of Mo-Ru-Pd-Rh alloy. In : Hart K P, Lumpkin G R (eds). Scientific basis for nuclear waste management XXIV: symposium held in Sydney, Australia, 27–31 August 2000. Warrendale, PA: Materials Research Society. (Materials Research Society Symposium Proceedings 663), pp 427–434.

Einziger R E, Thomas L E, Buchanan H C, Stout R B, 1992. Oxidation of spent fuel in air at 175 to 195°C. Journal of Nuclear Materials, 190, pp 53–60.

Ekeroth E, Roth O, Jonsson M, 2006. The relative impact of radiolysis products in radiation induced oxidative dissolution of UO2. Journal of Nuclear Materials, 355, pp 38–46.

Ekeroth E, Low J, Zwicky H U, Spahiu K, 2009. Corrosion studies with high burnup LWR fuel in simulated groundwater. In : Hyatt N C, Pickett D A, Rebak R B (eds). Scientific basis for nuclear waste management XXXII. Warrendale, PA: Materials Research Society. (Materials Research Society Symposium Proceedings 1124), pp Q02–07.

Forsyth R, 1997. The SKB Spent Fuel Corrosion Programme. An evaluation of results from the experimental programme performed in the Studsvik Hot Cell Laboratory. SKB TR 97-25, Svensk Kärnbränslehantering AB.

Haldimann M, Zimmerli B, Als C, Gerber H, 1998. Direct determinations of urinary iodine by inductively coupled plasma mass spectrometry using isotope dilution with iodine-129. Clinical Chemistry, 44, pp 817–824.

Hanson B D, 1998. The burnup dependence of light water reactor spent fuel oxidation. Report PNNL-11929, Pacific Northwest National Laboratory.

Hanson B D, 2008. Examining the conservatisms in dissolution rates of commercial spent nuclear fuel. Proceedings of the 2008 International High-Level Radioactive Waste Management Conference, Las Vegas, Nevada, 7–11 September 2008. La Grange, IL: American Nuclear Society, pp 404–411.

Hanson B D, Stout R B, 2004. Reexamining the dissolution of spent fuel: a comparison of different methods for calculating rates. In: Hanchar J M, Stroes-Gascoyne S, Browning L (eds). Scientific Basis for Nuclear Waste Management XXVIII: symposium held in San Francisco, California, USA, 13–16 April 2004. Warrendale, PA: Materials Research Society. (Materials Research Society Symposium Proceedings 824), CC2.4.1–2.4.6.

Hanson B D, Friese J I, Soderquist C Z, 2004. Initial results from dissolution testing of spent fuel under acidic conditions. In: Hanchar J M, Stroes-Gascoyne S, Browning L (eds). Scientific Basis for Nuclear Waste Management XXVIII: symposium held in San Francisco, California, USA, 13–16 April 2004. Warrendale, PA: Materials Research Society. (Materials Research Society Symposium Proceedings 824), CC8.6.1–8.6.6.

He H, Keech P G, Broczkowski M E, Noël J J, Shoesmith D W, 2007. Characterization of the influence of fission product doping on the anodic reactivity of uranium dioxide. Canadian Journal of Chemistry, 85, pp 702–713.

Izmer A V, Boulyga S F, Becker J S, 2003. Determination of $^{129}I/^{127}I$ isotope ratios in liquid solutions and environmental soil samples by ICP-MS with hexapole collision cell. Journal of Analytical Atomic Spectrometry, 18, pp 1339–1345.

Janzon Sjöstedt C, 2006. PIE of a HTP rod with duplex cladding irradiated in Ringhals 3. Technical Note N-06/220, Studsvik AB.

Jégou C, Peuget S, Lucchini J F, Corbel C, Broudic V, Bart J M, 2001. Effect of spent fuel burnup and composition on alteration of the $U(Pu)O_2$ Matrix. In : Hart K P, Lumpkin G R (eds). Scientific basis for nuclear waste management XXIV: symposium held in Sydney, Australia, 27–31 August 2000. Warrendale, PA: Materials Research Society. (Materials Research Society Symposium Proceedings 663), pp 399–407.

Jégou C, Peuget S, Broudic V, Roudil D, Deschanels X, Bart J M, 2004. Identification of the mechanism limiting the alteration of clad spent fuel segments in aerated carbonated groundwater. Journal of Nuclear Materials, 326, pp 144–155.

Johnson L H, Shoesmith D W, 1988. Spent fuel. In: Lutze W, Ewing R C (eds). Radioactive waste forms for the future. Amsterdam: North-Holland, pp 635–698.

Johnson L, Ferry C, Poinssot C, Lovera P, 2005. Spent fuel radionuclide source-term model for assessing spent fuel performance in geographical disposal. Part I: Assessment of the instant release fraction. Journal of Nuclear Materials, 346, pp 56–65.

Jonsson T, Källström R, 1995. Examination of three 4I8 fuel rods irradiated in Ringhals 3 1989–1994 – non-destructive examinations. Report N(H)-95/24, Studsvik AB.

Kleykamp H, 1985. The chemical state of the fission products in oxide fuels. Journal of Nuclear Materials, 131, pp 221–246.

Kleykamp H, 1988. The chemical state of fission products in oxide fuels at different stages of the nuclear fuel cycle. Nuclear Technology, 80, pp 412–421.

Källström R, 2002. PIE of North Anna rods. Results from length measurement, puncturing and gas analysis. Technical Note N(H)-02/078, Studsvik AB.

Magill J, Pfennig G, Galy J, 2006. Karlsruher Nuklidkarte (Chart of the nuclides). 7th ed. Karlsruhe: Haberbeck. /i texten förekommer Magill 2006 (utan “et al.”)/

Manzel R, Walker C T, 2000. High burnup fuel microstructure and its effect on fuel rod performance. Proceedings of ANS International Topical Meeting on Light Water Reactor Fuel Performance, Park City, Utah, 10– 13 April 2000.

Matzke H, 1995. Oxygen potential measurements in high burnup LWR UO2 fuel. Journal of Nuclear Materials, 223, pp 1–5.

Mazeina L, Navrotsky A, Greenblatt M, 2008. Calorimetric determination of energetics of solid solutions of UO_{2+x} with CaO and Y_2O_3. Journal of Nuclear Materials, 373, pp 39–43.

EPA, 1994. Determination of trace elements in waters and wastes by inductively coupled plasma-mass spectrom etry. EPA Method 200.8, Revision 5.4, U.S. Environmental Protection Agency, Washington, D.C.

Thomas L E, Einziger R E, Buchanan H C, 1993. Effect of fission products on air-oxidation of LWR spent fuel. Journal of Nuclear Materials, 201, pp 310–319.

Zwicky H-U, 2004. Post-irradiation examination of a Framatome ANP fuel rod from Ringhals 4 with M5™ cladding. Report N-04/132 Rev. 1, Studsvik AB.

Zwicky H-U, Low J, Lidén A, Lysell G, Schrire D, 2005. Burnup determination in irradiated fuel by means of isotopic analysis compared to CASMO calculations. 2005 Water Reactor Fuel Performance Meeting, Kyoto, Japan, 2–6 October 2005.

Appendix A

Release fractions

Table A-1. Release fractions, sample 4I8-Q12, centrifugate.

Nuclide	Contact Period 1	2	3	4	5	Cumulative
Rb-85	4.71E-04	8.07E-05	2.43E-05	1.79E-04	2.25E-05	**7.77E-04**
	2.74%	*15.54%*	*0.54%*	*3.16%*	*11.56%*	***2.45%***
uncorrected	6.77E-03	2.98E-03	2.39E-03	4.98E-04	7.20E-04	**1.33E-02**
Rb-87	4.07E-04	6.98E-05	2.10E-05	1.55E-04	1.94E-05	**6.72E-04**
	2.74%	*15.54%*	*0.54%*	*3.16%*	*11.56%*	***2.45%***
Sr corr. only	1.46E-03	5.55E-04	4.17E-04	2.08E-04	1.36E-04	**2.78E-03**
Sr-90	5.26E-05	7.54E-05	1.32E-04	1.32E-04	1.32E-04	**5.23E-04**
	3.71%	*1.95%*	*0.86%*	*0.26%*	*0.10%*	***0.52%***
Mo-100	5.27E-05	3.38E-05	5.17E-05	2.42E-05	5.49E-05	**2.17E-04**
	0.30%	*2.55%*	*0.12%*	*1.94%*	*0.66%*	***0.49%***
Tc-99	1.39E-04	2.06E-05	3.26E-05	1.48E-05	3.55E-05	**2.42E-04**
	0.29%	*1.96%*	*1.20%*	*0.85%*	*1.10%*	***0.33%***
Cs-133	7.28E-03	1.96E-03	1.89E-03	5.66E-04	5.09E-04	**1.22E-02**
	0.27%	*1.26%*	*0.13%*	*1.04%*	*0.91%*	***0.27%***
Cs-135	7.31E-03	1.95E-03	1.88E-03	5.21E-04	4.91E-04	**1.22E-02**
	0.22%	*1.99%*	*1.42%*	*1.17%*	*1.04%*	***0.42%***
Cs-137	7.64E-03	1.99E-03	1.93E-03	7.52E-04	5.13E-04	**1.28E-02**
	0.00%	*1.27%*	*0.12%*	*0.40%*	*0.07%*	***0.20%***
Ba-138	3.47E-05	2.82E-05	1.10E-04	2.47E-04	4.14E-04	**8.34E-04**
	1.28%	*0.95%*	*0.57%*	*0.23%*	*1.22%*	***0.62%***
La-139	4.40E-07	2.64E-07	1.33E-07	1.07E-06	1.95E-06	**3.85E-06**
	5.56%	*9.40%*	*17.82%*	*2.64%*	*3.88%*	***2.36%***
Ce-140	1.07E-07	5.78E-08	1.07E-07	1.54E-07	1.49E-07	**5.75E-07**
	12.42%	*21.63%*	*8.85%*	*3.48%*	*2.74%*	***3.77%***
Pr-141	3.79E-07	2.64E-07	1.03E-07	8.46E-07	1.66E-06	**3.25E-06**
	1.09%	*3.51%*	*14.60%*	*0.80%*	*0.96%*	***0.77%***
Nd-144	3.66E-07	2.43E-07	1.11E-07	1.19E-06	2.09E-06	**4.00E-06**
	6.50%	*2.51%*	*24.06%*	*1.61%*	*4.48%*	***2.55%***
Eu-153	4.34E-06	1.55E-06	3.72E-06	4.55E-06	1.44E-05	**2.85E-05**
	2.20%	*1.76%*	*2.03%*	*8.10%*	*0.70%*	***1.41%***
U-238	1.01E-05	7.31E-06	1.07E-05	1.01E-05	1.69E-05	**5.51E-05**
	0.35%	*2.39%*	*0.01%*	*0.76%*	*0.76%*	***0.42%***
Np-237	8.88E-06	8.23E-06	6.08E-06	7.31E-06	8.74E-06	**3.92E-05**
	3.43%	*1.66%*	*4.84%*	*0.21%*	*1.78%*	***1.20%***
Pu-239	1.39E-06	8.59E-07	6.89E-07	9.78E-07	5.94E-07	**4.51E-06**
	0.24%	*3.73%*	*0.87%*	*0.42%*	*2.16%*	***0.79%***
Cm-244	3.22E-07	2.24E-07	1.70E-07	2.02E-06	2.53E-06	**5.27E-06**
	24.58%	*1.76%*	*28.79%*	*4.14%*	*0.30%*	***2.38%***
I-129	6.26E-04	4.00E-04	4.15E-04	5.73E-04	2.68E-03	**4.70E-03**
	1.46%	*2.05%*	*1.22%*	*0.89%*	*6.50%*	***3.73%***

Italic: relative standard deviation.

Table A-2. Release fractions, sample 4I8-Q12, strip solution.

Nuclide	Contact Period 1	2	3	4	5	Cumulative
Rb-85	3.79E-06	1.36E-06	4.38E-07	2.20E-06	2.34E-06	**1.01E-05**
	3.65%	*14.78%*	*87.14%*	*10.14%*	*0.64%*	***4.99%***
uncorrected	4.54E-05	3.12E-05	2.78E-05	1.02E-05	1.08E-05	**1.25E-04**
Rb-87	3.27E-06	1.18E-06	3.79E-07	1.90E-06	2.02E-06	**8.75E-06**
	3.65%	*14.78%*	*87.14%*	*10.14%*	*0.64%*	***5.00%***
Sr corr. only	1.02E-05	6.17E-06	5.08E-06	3.25E-06	3.43E-06	**2.82E-05**
Sr-90	5.70E-07	4.27E-07	<4E-7	1.56E-6	1.88E-6	**4.43E-06**
	3.30%					
Mo-100	5.20E-07	1.93E-07	1.41E-07	1.62E-06	1.02E-06	**3.49E-06**
	5.27%	*8.54%*	*7.49%*	*2.66%*	*7.11%*	***2.60%***
Tc-99	5.68E-07	1.68E-07	1.40E-07	1.38E-06	1.35E-06	**3.61E-06**
	3.94%	*6.92%*	*0.29%*	*4.29%*	*35.41%*	***13.33%***
Cs-133	8.08E-05	3.64E-05	4.61E-05	1.49E-05	1.84E-05	**1.97E-04**
	0.91%	*0.52%*	*1.26%*	*3.21%*	*0.24%*	***0.54%***
Cs-135	7.88E-05	3.57E-05	4.53E-05	1.45E-05	1.78E-05	**1.92E-04**
	1.38%	*0.37%*	*1.96%*	*4.06%*	*0.36%*	***0.80%***
Cs-137	5.73E-05	4.90E-05	4.66E-05	1.47E-05	1.77E-05	**1.85E-04**
	0.45%	*0.47%*	*0.00%*	*0.72%*	*0.02%*	***0.20%***
Ba-138	1.72E-06	9.58E-07	4.69E-06	5.45E-06	1.51E-05	**2.79E-05**
	1.13%	*8.53%*	*3.46%*	*4.80%*	*0.69%*	***1.20%***
La-139	1.10E-06	5.21E-07	1.59E-06	2.22E-06	3.06E-06	**8.50E-06**
	3.16%	*1.11%*	*1.93%*	*4.40%*	*0.14%*	***1.28%***
Ce-140	9.76E-07	3.86E-07	5.56E-07	2.39E-06	2.25E-06	**6.55E-06**
	3.35%	*0.22%*	*2.21%*	*3.42%*	*1.42%*	***1.44%***
Pr-141	9.18E-07	3.80E-07	1.27E-06	2.34E-06	2.96E-06	**7.88E-06**
	0.09%	*2.85%*	*3.43%*	*4.08%*	*1.46%*	***1.45%***
Nd-144	8.58E-07	3.27E-07	1.28E-06	2.21E-06	2.83E-06	**7.51E-06**
	2.97%	*4.17%*	*2.80%*	*3.07%*	*1.32%*	***1.20%***
Eu-153	1.28E-06	5.27E-07	1.99E-06	2.75E-06	4.35E-06	**1.09E-05**
	4.46%	*7.04%*	*6.74%*	*4.32%*	*0.21%*	***1.76%***
U-238	6.41E-07	2.83E-07	1.84E-07	1.96E-06	1.73E-06	**4.80E-06**
	1.92%	*0.35%*	*0.15%*	*3.38%*	*0.41%*	***1.41%***
Np-237	6.02E-07	2.49E-07	1.66E-07	1.80E-06	1.47E-06	**4.29E-06**
	1.37%	*3.03%*	*1.89%*	*4.32%*	*2.08%*	***1.97%***
Pu-239	8.76E-07	3.76E-07	2.29E-07	2.04E-06	2.01E-06	**5.54E-06**
	3.71%	*1.57%*	*1.11%*	*3.47%*	*0.94%*	***1.45%***
Cm-244	1.99E-06	7.32E-07	2.40E-06	4.15E-06	5.56E-06	**1.48E-05**
	10.21%	*9.35%*	*8.05%*	*1.24%*	*0.11%*	***1.98%***

Italic: relative standard deviation.

Table A-3. Release fractions, sample 3V5-Q13, centrifugate.

Nuclide	Contact Period 1	2	3	4	5	6	Cumulative
Rb-85	1.25E-04	4.42E-04	1.12E-03	6.49E-04	3.32E-04	7.59E-04	**3.43E-03**
	2.86%	*1.14%*	*1.74%*	*1.02%*	*0.23%*	*2.21%*	***0.80%***
uncorrected	4.30E-04	1.77E-03	3.15E-03	1.39E-03	1.02E-03	2.76E-03	**1.05E-02**
Rb-87	1.18E-04	4.16E-04	1.06E-03	6.11E-04	3.13E-04	7.07E-04	**3.22E-03**
	2.86%	*1.14%*	*1.74%*	*1.02%*	*0.23%*	*2.21%*	***0.80%***
Sr corr. only	1.71E-04	6.40E-04	1.40E-03	7.41E-04	4.32E-04	1.06E-03	**4.45E-03**
Sr-90	1.42E-05	9.20E-06	9.83E-05	4.38E-04	1.61E-04	2.62E-04	**9.83E-04**
	4.53%	*6.93%*	*0.48%*	*1.61%*	*1.83%*	*1.99%*	***0.95%***
Mo-100	5.52E-05	3.42E-05	2.80E-05	1.52E-05	1.03E-05	1.06E-05	**1.54E-04**
	2.70%	*0.36%*	*0.47%*	*1.78%*	*3.76%*	*1.59%*	***1.03%***
Tc-99	5.97E-05	1.66E-05	1.49E-05	7.71E-06	4.70E-06	6.54E-06	**1.10E-04**
	0.88%	*0.26%*	*0.32%*	*2.16%*	*0.69%*	*1.13%*	***0.51%***
Cs-133	9.81E-04	3.48E-03	7.41E-03	3.40E-03	2.47E-03	5.56E-03	**2.33E-02**
	1.08%	*0.02%*	*1.39%*	*1.27%*	*1.16%*	*1.94%*	***0.68%***
Cs-135	9.78E-04	3.48E-03	7.35E-03	3.33E-03	2.44E-03	5.33E-03	**2.29E-02**
	1.61%	*0.20%*	*1.04%*	*0.96%*	*0.58%*	*2.29%*	***0.65%***
Cs-137	9.90E-04	3.54E-03	7.67E-03	3.56E-03	2.52E-03	5.62E-03	**2.39E-02**
	0.50%	*1.13%*	*0.39%*	*0.17%*	*0.54%*	*0.35%*	***0.23%***
Ba-138	1.22E-05	1.40E-05	3.72E-05	8.10E-04	1.50E-04	3.48E-04	**1.37E-03**
	5.84%	*0.83%*	*1.64%*	*0.45%*	*1.46%*	*6.44%*	***1.66%***
La-139	2.39E-07	2.00E-07	1.93E-07	1.92E-06	1.73E-06	3.03E-06	**7.31E-06**
	2.82%	*8.43%*	*11.99%*	*0.95%*	*5.31%*	*18.19%*	***7.67%***
Ce-140	2.31E-07	3.30E-07	3.45E-07	6.66E-07	3.74E-07	1.82E-06	**3.77E-06**
	9.31%	*1.53%*	*13.13%*	*22.83%*	*0.05%*	*14.32%*	***8.12%***
Pr-141	1.85E-07	1.27E-07	1.30E-07	1.70E-06	1.49E-06	2.75E-06	**6.38E-06**
	8.02%	*0.79%*	*21.17%*	*3.83%*	*0.45%*	*17.71%*	***7.71%***
Nd-144	1.70E-07	1.25E-07	1.01E-07	1.75E-06	1.69E-06	2.76E-06	**6.60E-06**
	4.47%	*15.00%*	*4.62%*	*0.42%*	*3.09%*	*18.91%*	***7.97%***
Eu-153	4.69E-07	1.01E-06	1.81E-06	7.44E-06	3.56E-06	6.07E-06	**2.04E-05**
	9.57%	*8.82%*	*0.26%*	*0.52%*	*8.74%*	*10.34%*	***3.48%***
U-238	7.18E-06	4.65E-06	6.08E-06	5.53E-06	7.12E-06	9.49E-06	**4.01E-05**
	1.82%	*1.35%*	*0.51%*	*0.51%*	*0.34%*	*3.75%*	***0.97%***
Np-237	4.81E-06	2.80E-06	3.51E-06	6.04E-06	4.66E-06	1.58E-06	**2.34E-05**
	1.76%	*2.04%*	*2.14%*	*1.46%*	*1.28%*	*7.98%*	***0.89%***
Pu-239	1.19E-06	8.74E-07	8.00E-07	1.25E-06	1.27E-06	7.03E-07	**6.09E-06**
	2.24%	*2.34%*	*2.11%*	*2.73%*	*0.87%*	*18.32%*	***2.28%***
Cm-244	2.17E-07	9.50E-08	8.52E-08	1.76E-06	1.77E-06	3.98E-06	**7.91E-06**
	19.43%	*2.25%*	*40.79%*	*11.62%*	*2.08%*	*26.89%*	***13.81%***
I-129	7.10E-04	7.24E-04	6.58E-04	7.28E-03	4.11E-04	3.12E-02	**4.10E-02**
	0.92%	*2.73%*	*1.68%*	*5.60%*	*3.12%*	*0.75%*	***1.15%***

Italic: relative standard deviation.

Table A-4. Release fractions, sample 3V5-Q13, strip solution.

Nuclide	Contact Period 1	2	3	4	5	6	Cumulative
Rb-85	2.77E-06	2.55E-06	8.62E-06	8.50E-06	6.41E-06	2.58E-05	**5.46E-05**
	5.44%	*5.94%*	*7.40%*	*0.05%*	*0.64%*	*1.36%*	***1.39%***
uncorrected	6.31E-06	1.24E-05	2.58E-05	2.27E-05	1.62E-05	7.03E-05	**1.54E-04**
Rb-87	2.61E-06	2.40E-06	8.12E-06	8.00E-06	6.04E-06	2.40E-05	**5.12E-05**
	5.44%	*5.94%*	*7.40%*	*0.05%*	*0.64%*	*1.36%*	***1.39%***
Sr corr. only	3.20E-06	4.05E-06	1.10E-05	1.04E-05	7.67E-06	3.14E-05	**6.77E-05**
Sr-90	2.89E-06	7.45E-06	8.40E-06	1.71E-06	3.93E-06	1.59E-05	**4.03E-05**
	10.16%			*2.19%*	*12.87%*	*15.25%*	***6.19%***
Mo-100	1.01E-06	1.71E-07	4.58E-07	5.07E-08	1.58E-06	4.98E-06	**8.25E-06**
	0.11%	*32.54%*	*44.21%*	*102.74%*	*1.54%*	*6.33%*	***4.65%***
Tc-99	8.57E-07	2.84E-07	3.03E-07	6.82E-08	1.30E-06	4.17E-06	**6.98E-06**
	1.49%	*61.18%*	*33.30%*	*2.07%*	*1.77%*	*3.03%*	***3.42%***
Cs-133	1.17E-05	2.69E-05	7.92E-05	7.62E-05	4.27E-05	2.04E-04	**4.41E-04**
	0.17%	*0.45%*	*0.62%*	*0.58%*	*1.49%*	*0.73%*	***0.40%***
Cs-135	1.18E-05	2.71E-05	7.89E-05	7.46E-05	4.16E-05	1.97E-04	**4.31E-04**
	0.72%	*1.69%*	*0.62%*	*0.68%*	*1.31%*	*1.02%*	***0.52%***
Cs-137	1.17E-05	2.69E-05	7.92E-05	7.65E-05	4.27E-05	2.08E-04	**4.45E-04**
	1.11%	*0.29%*	*0.20%*	*0.68%*	*0.42%*	*0.87%*	***0.43%***
Ba-138	2.33E-06	6.59E-07	1.87E-06	2.32E-05	7.83E-06	3.96E-05	**7.55E-05**
	2.91%	*0.40%*	*7.87%*	*2.15%*	*3.23%*	*1.17%*	***0.99%***
La-139	2.56E-06	8.37E-07	1.06E-06	1.17E-06	3.33E-06	2.80E-05	**3.69E-05**
	0.29%	*1.20%*	*2.91%*	*0.49%*	*1.76%*	*1.14%*	***0.88%***
Ce-140	2.31E-06	5.28E-07	6.27E-07	1.36E-06	2.82E-06	2.16E-05	**2.93E-05**
	0.09%	*6.40%*	*4.96%*	*2.01%*	*1.39%*	*0.71%*	***0.57%***
Pr-141	2.53E-06	4.54E-07	4.50E-07	7.00E-07	3.16E-06	2.63E-05	**3.36E-05**
	0.28%	*2.76%*	*2.85%*	*2.08%*	*1.17%*	*0.95%*	***0.75%***
Nd-144	2.10E-06	3.73E-07	3.91E-07	5.99E-07	2.85E-06	2.40E-05	**3.03E-05**
	0.07%	*3.68%*	*1.02%*	*3.07%*	*0.28%*	*1.12%*	***0.89%***
Eu-153	2.71E-06	5.67E-07	6.20E-07	1.02E-06	3.34E-06	2.88E-05	**3.70E-05**
	0.27%	*0.16%*	*3.07%*	*0.28%*	*0.32%*	*0.03%*	***0.07%***
U-238	1.54E-06	2.74E-07	3.36E-07	1.33E-07	2.13E-06	8.23E-06	**1.26E-05**
	0.77%	*0.55%*	*0.11%*	*0.10%*	*0.37%*	*0.45%*	***0.31%***
Np-237	1.55E-06	2.65E-07	3.11E-07	1.08E-07	2.10E-06	7.61E-06	**1.19E-05**
	1.65%	*3.15%*	*1.17%*	*3.25%*	*0.46%*	*0.75%*	***0.53%***
Pu-239	2.96E-06	4.91E-07	4.05E-07	2.03E-07	3.10E-06	1.72E-05	**2.44E-05**
	0.13%	*0.49%*	*1.02%*	*2.48%*	*0.65%*	*0.25%*	***0.20%***
Cm-244	5.61E-06	8.60E-07	7.47E-07	9.19E-07	5.81E-06	4.58E-05	**5.97E-05**
	3.95%	*9.69%*	*2.47%*	*0.42%*	*0.69%*	*1.68%*	***1.35%***

Italic: relative standard deviation.

Table A-5. Release fractions, sample SUT3-00477, centrifugate.

Nuclide	Contact Period 1	2	3	4	5	Cumulative
Rb-85	4.38E-05	1.24E-04	5.30E-04	<3E-7	8.83E-05	**7.86E-04**
	21.02%	*1.17%*	*0.08%*		*2.82%*	***1.23%***
uncorrected	2.33E-03	3.61E-03	2.93E-03	1.22E-03	2.74E-04	**1.04E-02**
Rb-87	4.04E-05	1.14E-04	4.88E-04	<7E-8	8.07E-05	**7.23E-04**
	21.02%	*1.17%*	*0.08%*		*2.82%*	***1.23%***
Sr corr. only	4.21E-04	6.93E-04	8.87E-04	1.90E-04	1.12E-04	**2.30E-03**
Sr-90	4.52E-05	7.87E-05	5.15E-04	1.69E-04	6.94E-05	**8.77E-04**
	3.36%	*0.89%*	*2.96%*	*1.53%*	*1.63%*	***1.78%***
Mo-100	8.37E-05	4.63E-05	3.46E-05	4.75E-05	2.88E-05	**2.41E-04**
	0.48%	*1.03%*	*1.83%*	*1.23%*	*3.84%*	***0.64%***
Tc-99	5.72E-05	2.53E-05	2.00E-05	3.29E-05	1.92E-05	**1.55E-04**
	0.11%	*1.55%*	*0.55%*	*1.05%*	*2.23%*	***0.44%***
Cs-133	2.27E-03	3.44E-03	3.43E-03	1.03E-03	3.03E-04	**1.05E-02**
	0.74%	*1.08%*	*2.18%*	*1.12%*	*2.03%*	***0.82%***
Cs-135	2.22E-03	3.40E-03	3.27E-03	1.03E-03	2.89E-04	**1.02E-02**
	0.29%	*1.45%*	*1.52%*	*1.84%*	*2.11%*	***0.72%***
Cs-137	2.33E-03	3.56E-03	3.46E-03	8.83E-04	3.18E-04	**1.05E-02**
	0.94%	*0.06%*	*1.23%*	*0.11%*	*0.07%*	***0.45%***
Ba-138	2.07E-05	3.03E-05	3.33E-04	2.21E-04	1.45E-04	**7.50E-04**
	3.68%	*20.98%*	*3.88%*	*0.60%*	*2.16%*	***1.98%***
La-139	4.82E-07	3.10E-07	1.26E-06	3.30E-07	1.31E-06	**3.69E-06**
	3.71%	*22.59%*	*7.72%*	*1.98%*	*4.07%*	***3.59%***
Ce-140	1.41E-07	1.12E-07	1.06E-07	1.20E-07	8.24E-08	**5.62E-07**
	2.80%	*55.67%*	*23.36%*	*17.15%*	*23.23%*	***12.95%***
Pr-141	5.15E-07	2.53E-07	1.01E-06	2.73E-07	1.03E-06	**3.08E-06**
	4.34%	*7.82%*	*5.35%*	*4.69%*	*1.89%*	***2.14%***
Nd-144	4.72E-07	2.82E-07	1.15E-06	3.19E-07	1.35E-06	**3.58E-06**
	3.86%	*0.12%*	*2.89%*	*3.33%*	*0.32%*	***1.11%***
Eu-153	8.13E-07	8.03E-07	5.69E-06	6.73E-06	3.91E-06	**1.79E-05**
	7.53%	*1.71%*	*2.16%*	*1.94%*	*6.15%*	***1.71%***
U-238	1.90E-05	1.19E-05	1.57E-05	1.24E-05	1.10E-05	**6.99E-05**
	2.67%	*2.42%*	*1.61%*	*1.46%*	*0.79%*	***0.95%***
Np-237	2.37E-05	1.20E-05	1.84E-05	7.35E-06	8.07E-06	**6.94E-05**
	3.93%	*1.95%*	*0.73%*	*2.08%*	*0.49%*	***1.41%***
Pu-239	2.92E-06	2.18E-06	1.27E-06	5.25E-07	9.18E-07	**7.82E-06**
	0.01%	*0.84%*	*3.16%*	*1.51%*	*1.15%*	***0.59%***
Cm-244	5.44E-07	4.47E-07	1.27E-06	2.10E-07	1.35E-06	**3.83E-06**
	26.91%	*7.86%*	*17.01%*	*13.97%*	*19.67%*	***9.82%***
I-129	1.08E-03	4.93E-04	1.62E-03	4.76E-04	2.48E-04	**3.92E-03**
	1.16%	*1.14%*	*11.48%*	*0.63%*	*0.23%*	***4.77%***

Italic: relative standard deviation.

Table A-6. Release fractions, sample SUT3-00477, strip solution.

	Contact Period					
Nuclide	**1**	**2**	**3**	**4**	**5**	**Cumulative**
Rb-85	5.67E-06	2.14E-06	7.57E-06	4.26E-04	1.68E-06	**4.43E-04**
	2.13%	*3.66%*	*0.34%*	*2.74%*	*3.37%*	***2.63%***
uncorrected	3.92E-05	3.36E-05	2.72E-05	4.05E-04	4.92E-06	**5.10E-04**
Rb-87	5.20E-06	1.98E-06	6.96E-06	3.91E-04	1.53E-06	**4.06E-04**
	2.13%	*3.66%*	*0.34%*	*2.74%*	*3.37%*	***2.63%***
Sr corr. only	1.08E-05	7.20E-06	1.02E-05	3.87E-04	2.07E-06	**4.18E-04**
Sr-90	6.36E-06	9.42E-07	6.96E-06	3.88E-04	1.42E-06	**4.04E-04**
	4.66%	*30.53%*	*7.34%*	*13.35%*	*0.00%*	***12.83%***
Mo-100	2.92E-06	5.31E-07	1.63E-06	2.80E-04	2.85E-07	**2.86E-04**
	1.56%	*5.58%*	*4.51%*	*2.17%*	*131.36%*	***2.14%***
Tc-99	2.35E-06	3.95E-07	1.24E-06	2.30E-04	2.02E-07	**2.34E-04**
	0.79%	*0.30%*	*1.56%*	*2.20%*	*6.84%*	***2.16%***
Cs-133	7.10E-05	5.21E-05	4.51E-05	3.76E-04	1.19E-05	**5.56E-04**
	0.18%	*0.02%*	*0.88%*	*2.19%*	*0.59%*	***1.48%***
Cs-135	6.74E-05	5.10E-05	4.42E-05	3.58E-04	1.14E-05	**5.32E-04**
	0.49%	*0.98%*	*0.57%*	*1.15%*	*2.88%*	***0.78%***
Cs-137	6.23E-05	5.62E-05	4.60E-05	3.89E-04	1.15E-05	**5.65E-04**
	0.14%	*0.09%*	*0.48%*	*0.24%*	*0.17%*	***0.17%***
Ba-138	6.14E-06	1.59E-06	9.28E-06	3.83E-04	6.40E-06	**4.07E-04**
	0.56%	*7.84%*	*0.74%*	*3.04%*	*2.94%*	***2.86%***
La-139	5.49E-06	1.19E-06	4.95E-06	3.83E-04	1.47E-06	**3.97E-04**
	0.49%	*1.22%*	*1.31%*	*1.71%*	*0.11%*	***1.65%***
Ce-140	5.53E-06	8.83E-07	4.26E-06	3.96E-04	8.50E-07	**4.07E-04**
	0.34%	*1.51%*	*1.54%*	*1.07%*	*1.12%*	***1.04%***
Pr-141	5.80E-06	9.12E-07	4.78E-06	4.16E-04	1.09E-06	**4.29E-04**
	0.06%	*0.67%*	*0.59%*	*2.79%*	*1.27%*	***2.71%***
Nd-144	5.21E-06	7.86E-07	3.87E-06	3.76E-04	9.84E-07	**3.87E-04**
	0.08%	*0.49%*	*1.10%*	*2.54%*	*0.01%*	***2.47%***
Eu-153	6.57E-06	8.96E-07	5.39E-06	4.31E-04	1.47E-06	**4.45E-04**
	2.48%	*4.34%*	*1.55%*	*3.51%*	*1.36%*	***3.40%***
U-238	3.64E-06	7.52E-07	2.47E-06	3.11E-04	3.89E-07	**3.18E-04**
	0.10%	*0.84%*	*0.92%*	*1.88%*	*0.15%*	***1.84%***
Np-237	3.69E-06	7.13E-07	2.62E-06	3.00E-04	3.59E-07	**3.07E-04**
	0.31%	*4.13%*	*0.68%*	*2.53%*	*3.41%*	***2.47%***
Pu-239	5.60E-06	9.72E-07	4.84E-06	3.50E-04	5.87E-07	**3.62E-04**
	0.13%	*0.70%*	*1.17%*	*2.61%*	*0.06%*	***2.53%***
Cm-244	1.30E-05	1.76E-06	1.16E-05	7.57E-04	1.78E-06	**7.85E-04**
	0.01%	*6.51%*	*0.55%*	*0.90%*	*1.62%*	***0.87%***

Italic: relative standard deviation.

Table A-7. Release fractions, sample AM2-K12, centrifugate.

Nuclide	Contact Period 1	2	3	4	5	6	Cumulative
Rb-85	2.98E-04	5.52E-05	1.26E-04	1.28E-04	1.58E-04	1.88E-03	**2.64E-03**
	0.31%	*2.91%*	*3.52%*	*2.58%*	*1.46%*	*0.90%*	***0.68%***
Uncorr.	1.14E-03	1.69E-04	3.94E-04	5.26E-04	7.54E-04	1.93E-02	**2.23E-02**
Rb-87	2.77E-04	5.13E-05	1.17E-04	1.19E-04	1.47E-04	1.73E-03	**2.44E-03**
	0.31%	*2.91%*	*3.52%*	*2.58%*	*1.46%*	*0.90%*	***0.68%***
Sr corr. only	4.27E-04	7.15E-05	1.65E-04	1.90E-04	2.53E-04	4.86E-03	**5.97E-03**
Sr-90	2.52E-04	5.69E-05	1.01E-04	8.55E-05	9.54E-05	3.10E-04	**9.00E-04**
	1.36%	*5.74%*	*3.61%*	*3.03%*	*2.44%*	*0.69%*	***0.80%***
Mo-100	1.57E-05	8.03E-06	1.11E-05	8.07E-06	1.37E-05	2.65E-05	**8.30E-05**
	2.04%	*3.12%*	*3.55%*	*2.12%*	*7.38%*	*0.30%*	***1.42%***
Tc-99	1.36E-05	6.17E-06	6.89E-06	3.94E-06	5.48E-06	1.00E-05	**4.61E-05**
	2.51%	*1.12%*	*1.37%*	*1.36%*	*3.88%*	*0.88%*	***0.94%***
Cs-133	2.17E-03	2.27E-04	4.57E-04	5.82E-04	9.06E-04	2.61E-02	**3.04E-02**
	0.28%	*0.21%*	*1.01%*	*0.48%*	*4.29%*	*0.49%*	***0.44%***
Cs-135	2.15E-03	2.24E-04	4.56E-04	5.81E-04	9.05E-04	2.56E-02	**2.99E-02**
	0.19%	*0.50%*	*0.73%*	*0.37%*	*3.61%*	*0.20%*	***0.20%***
Cs-137	2.18E-03	2.24E-04	4.68E-04	5.96E-04	8.93E-04	2.62E-02	**3.06E-02**
	0.22%	*0.31%*	*0.35%*	*0.31%*	*0.14%*	*0.44%*	***0.38%***
Ba-138	4.65E-04	8.17E-05	1.07E-04	8.85E-05	1.02E-04	1.21E-03	**2.06E-03**
	0.71%	*1.01%*	*1.40%*	*0.15%*	*3.29%*	*0.10%*	***0.25%***
La-139	1.06E-05	8.23E-06	9.71E-06	5.13E-06	4.75E-06	5.21E-06	**4.36E-05**
	5.99%	*2.51%*	*0.91%*	*3.82%*	*0.58%*	*2.39%*	***1.63%***
Ce-140	1.66E-06	4.90E-07	4.55E-07	1.99E-07	2.02E-07	1.65E-07	**3.17E-06**
	18.55%	*9.57%*	*4.03%*	*9.00%*	*26.36%*	*8.17%*	***10.01%***
Pr-141	1.06E-05	8.69E-06	1.07E-05	5.69E-06	5.17E-06	5.14E-06	**4.60E-05**
	7.07%	*2.11%*	*0.41%*	*1.17%*	*2.31%*	*3.29%*	***1.75%***
Nd-144	8.95E-06	7.75E-06	9.51E-06	5.37E-06	5.03E-06	5.45E-06	**4.21E-05**
	5.93%	*1.72%*	*0.78%*	*0.52%*	*0.96%*	*0.95%*	***1.33%***
Eu-153	2.08E-05	1.32E-05	1.61E-05	9.87E-06	9.94E-06	3.15E-05	**1.01E-04**
	5.47%	*4.17%*	*0.99%*	*0.14%*	*1.70%*	*0.26%*	***1.27%***
U-238	1.07E-05	1.11E-05	1.66E-05	6.92E-06	9.15E-06	1.87E-05	**7.32E-05**
	0.47%	*0.60%*	*0.16%*	*0.05%*	*4.94%*	*0.03%*	***0.63%***
Np-237	2.74E-06	1.56E-06	2.09E-06	2.36E-06	4.91E-06	1.04E-05	**2.41E-05**
	1.08%	*0.90%*	*0.95%*	*2.93%*	*1.52%*	*1.63%*	***0.84%***
Pu-239	5.78E-06	4.50E-06	5.30E-06	4.37E-06	5.69E-06	6.44E-06	**3.21E-05**
	0.91%	*1.73%*	*0.85%*	*0.19%*	*5.87%*	*0.42%*	***1.09%***
Cm-244	1.69E-05	1.43E-05	1.77E-05	9.29E-06	8.36E-06	8.08E-06	**7.47E-05**
	10.36%	*5.21%*	*0.76%*	*1.57%*	*4.18%*	*0.24%*	***2.61%***
I-129	1.42E-02	3.21E-03	3.66E-03	5.31E-04	2.05E-04	3.21E-04	**2.21E-02**
	2.69%	*0.46%*	*9.38%*	*2.53%*	*4.61%*	*3.65%*	***2.32%***

Italic: relative standard deviation.

Table A-8. Release fractions, sample AM2-K12, strip solution.

Nuclide	Contact Period 1	2	3	4	5	6	Cumulative
Rb-85	5.51E-06	5.17E-06	6.12E-06	1.61E-06	7.45E-05	2.49E-05	**1.18E-04**
	4.62%	*1.19%*	*2.50%*	*1.02%*	*1.01%*	*4.39%*	***1.16%***
uncorrected	5.63E-06	7.97E-06	1.09E-05	8.99E-06	6.89E-05	1.83E-04	**2.86E-04**
Rb-87	5.11E-06	4.80E-06	5.69E-06	1.50E-06	6.92E-05	2.30E-05	**1.09E-04**
	4.62%	*1.19%*	*2.50%*	*1.02%*	*1.01%*	*4.39%*	***1.15%***
Sr corr. only	5.14E-06	5.30E-06	6.54E-06	2.82E-06	6.82E-05	5.14E-05	**1.39E-04**
Sr-90	8.08E-06	7.43E-06	6.64E-06	2.30E-07	1.15E-04	1.37E-05	**1.51E-04**
	1.16%	*2.63%*	*8.52%*	*106.10%*	*3.71%*	*9.48%*	***2.98%***
Mo-100	2.33E-06	2.39E-06	2.17E-06	6.04E-08	2.87E-05	3.19E-06	**3.88E-05**
	4.42%	*6.95%*	*26.86%*	*25.00%*	*0.76%*	*1.36%*	***1.68%***
Tc-99	1.65E-06	1.33E-06	1.70E-06	5.65E-08	1.90E-05	2.51E-06	**2.62E-05**
	8.72%	*7.04%*	*8.87%*	*17.36%*	*0.33%*	*0.23%*	***0.91%***
Cs-133	6.90E-06	7.08E-06	1.69E-05	1.42E-05	7.06E-05	3.06E-04	**4.21E-04**
	0.13%	*0.64%*	*0.27%*	*0.74%*	*0.33%*	*0.34%*	***0.25%***
Cs-135	6.94E-06	7.05E-06	1.69E-05	1.45E-05	7.12E-05	2.99E-04	**4.16E-04**
	1.26%	*1.87%*	*0.32%*	*1.41%*	*1.41%*	*0.98%*	***0.74%***
Cs-137	3.34E-05	6.89E-06	1.63E-05	1.40E-05	7.14E-05	6.16E-04	**7.58E-04**
	0.22%	*0.72%*	*0.03%*	*0.20%*	*0.31%*	*0.61%*	***0.50%***
Ba-138	6.07E-06	6.68E-06	8.66E-06	2.29E-06	7.87E-05	3.47E-05	**1.37E-04**
	0.43%	*3.71%*	*1.43%*	*1.01%*	*0.72%*	*0.03%*	***0.46%***
La-139	5.41E-06	5.88E-06	5.68E-06	1.68E-06	7.39E-05	1.00E-05	**1.03E-04**
	0.42%	*0.24%*	*0.81%*	*0.81%*	*0.36%*	*0.19%*	***0.26%***
Ce-140	5.59E-06	5.30E-06	4.59E-06	6.08E-07	7.36E-05	8.86E-06	**9.86E-05**
	0.30%	*0.96%*	*0.95%*	*1.03%*	*0.53%*	*0.25%*	***0.41%***
Pr-141	6.53E-06	6.53E-06	6.10E-06	8.78E-07	8.54E-05	1.08E-05	**1.16E-04**
	0.24%	*1.29%*	*0.44%*	*1.10%*	*1.41%*	*0.46%*	***1.04%***
Nd-144	5.10E-06	5.10E-06	4.93E-06	6.86E-07	6.99E-05	9.13E-06	**9.48E-05**
	0.33%	*0.72%*	*0.14%*	*1.55%*	*1.08%*	*0.64%*	***0.80%***
Eu-153	6.59E-06	6.97E-06	6.95E-06	1.33E-06	8.65E-05	1.28E-05	**1.21E-04**
	0.81%	*0.84%*	*5.28%*	*2.32%*	*2.84%*	*1.46%*	***2.06%***
U-238	1.68E-06	3.05E-06	3.06E-06	1.27E-07	4.70E-05	6.27E-06	**6.12E-05**
	139.56%	*0.26%*	*1.27%*	*0.31%*	*0.66%*	*1.53%*	***3.86%***
Np-237	3.52E-06	3.27E-06	3.17E-06	9.72E-08	4.84E-05	5.96E-06	**6.44E-05**
	0.17%	*0.41%*	*0.70%*	*3.65%*	*1.34%*	*1.69%*	***1.02%***
Pu-239	6.55E-06	6.90E-06	5.51E-06	2.38E-07	8.68E-05	9.71E-06	**1.16E-04**
	0.12%	*0.78%*	*0.09%*	*1.44%*	*0.80%*	*0.97%*	***0.61%***
Cm-244	1.31E-05	1.50E-05	1.32E-05	2.25E-06	1.65E-04	2.22E-05	**2.31E-04**
	0.05%	*1.26%*	*0.89%*	*4.48%*	*0.32%*	*0.40%*	***0.26%***

Italic: relative standard deviation.